Characterization of a qubit in presence of dissipation and external driving

Dissertation
zur Erlangung des Doktorgrades der Naturwissenschaften
(Dr. rer. nat.)
der naturwissenschaftlichen Fakultät II – Physik
der Universität Regensburg

vorgelegt von
Dipl.-Phys. Francesco Nesi
aus Tavarnelle Val di Pesa (Firenze, Italien)

Juli 2007

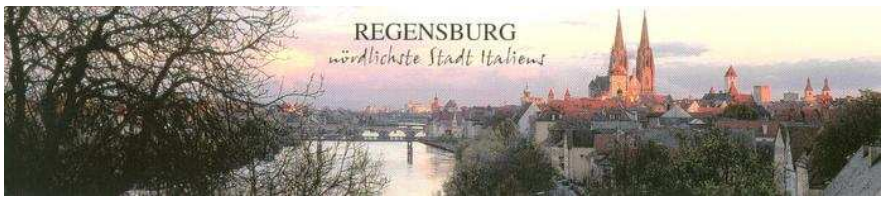

Die Arbeit wurde von Prof. Dr. M. Grifoni angeleitet.
Das Kolloquium fand am 20.07.2007 statt.

Prüfungsausschuß:

Vorsitzender:	Prof. Dr. C. Schüller
1. Gutachter:	Prof. Dr. M. Grifoni
2. Gutachter:	Prof. Dr. J. Sievert
weiterer Prüfer:	Prof. Dr. G. Bali

Contents

Acknowledgments

This Section intends to be a short and of course not fully comprehensive list of thoughts and thanks to the people who made me love Regensburg. Of course, I hope I will not forget to mention anyone. If this was the case, I apologize and thank him/her.

First of all I want to sincerely thank Milena Grifoni, my supervisor during this 3.5 years PhD. A PhD can be really hard, sometimes you don't get the expected results and you are stuck for weeks or months at the same stupid point. Milena gave me the adequate motivation to go on and not giving up, a situation which continuously repeated from time to time during these years. I appreciated a lot her kindness, her way of leading a group, her positive attitude and last but not least her physical intuition. She is great.

The next thank goes to Maddalena, with whom I had a beautiful time here in Regensburg. Her constant support and comprehension helped me a lot, expecially when she assisted me after the operation. A hard time was when she left for coming back to Italy, since we then had really few time to see each other. But things have started becoming better and better and I am really looking forward to finally stay together. Thanks for always being there.

I also wish to remember here my Bürokolleg Leo. As he came, I had never thought we would have understood us so well. We had such a nice time together and with our respective partners as well. I will never forget his patience in teaching me German at the beginning and the beautiful excursions we organized and realized! I hope we will keep always in contact, but I guess so, since for two mountaineers like us Südtirol (where I am going to settle down soon) is really our homeland! Also, wir sehen uns bald dort!

My parents, grandparents and relatives were also always present for supporting me during the hard times of my PhD. Most of the quotes present in this PhD thesis are dedicated to them. With their discrete presence, they contributed a lot not to make me miss home. They also appreciated Regensburg very much and our Lehrstuhl as well. Thank you so much for your encouragement.

Finally I would like to mention my friends, whose group has enlarged during these more

than three years... As first I want to remember Chris, with whom we created a band called *Baraonda*. I never found such a musician like him. We understand us so well: As soon as I asked him for a riff, he always found the right chords and arrangements, unbelievable! Besides the music, we also shared a lot of Italian and Bavarian culture. Thank you and thanks also to your family, that really treated me like a child. Then, my friends Christoph, Michael, Alex, Frank tought me the German language and culture, e.g. Schafkopf. I missed some of them recently, since they began the Referendariat and are therefore always busy. But if someone raises the proposal of playing darts, then Felix, Kada, Kerstin, Christian, Alexa and others will of course join us! We spent so many playing evenings and we had such nice trips together! Ich sag euch wirklich herzlichen Dank! My Lehrstuhl also was great. The people with whom I spent each single day by working side by side, going to the (ugly) mensa and enjoying the parties were really so friendly. They contributed a lot in making me amuse and happier in general. Our after-lunch discussion in the coffee-room were insuperable. In the end my Italian friends from Tuscany are to be acknowledged, even though most of them promised to visit me in Regensburg and never did it. Just a couple of them enjoyed the Bavarian beer in the very country (and not for the Oktoberfest!). Emiliano became my roommate here and we spent evenings discussing about life, relationships and Schafkopf. We also entered the Bavarian culture more deeply by meeting other guys around a Kicker table-football. He is definitely my Kicker-partner. I apologize for some discussions we of course had, but I still appreciate his understanding very much and how silent he has been every single morning in waking up! The other Tuscan friends were so nice in waiting for me most of the times they organized trips and dinners. We had such a nice time when Italy was world champion!! Po-poropo-po po-po po... Finally the Italians who recently came here in Regensburg, Andrea, Pino, Fabio and Giuseppe, really gave me so much. We spent days and days together, they let me again taste a flavour of student life. We went so deep in knowing us, their presence has been really important for me during last months. Music performances in the streets of Regensburg and at home, playing evenings somewhere and infinite strolling through the city are a minimal part of what we experienced together. Grazie di cuore.

In order to give the reader a flavour of the atmosphere I experienced in Regensburg and an idea of the places around me, I wish to show some pictures of our group trips. In the end, a picture of the Universität Regensburg and the Dome of Regensburg are attached.

Figure 1: In early 2004, a canoo-trip (left). A birthday in 2006 (right).

Figure 2: Two other beautiful trips: In Karwendeltal (left) and on the Hirschenstein (right).

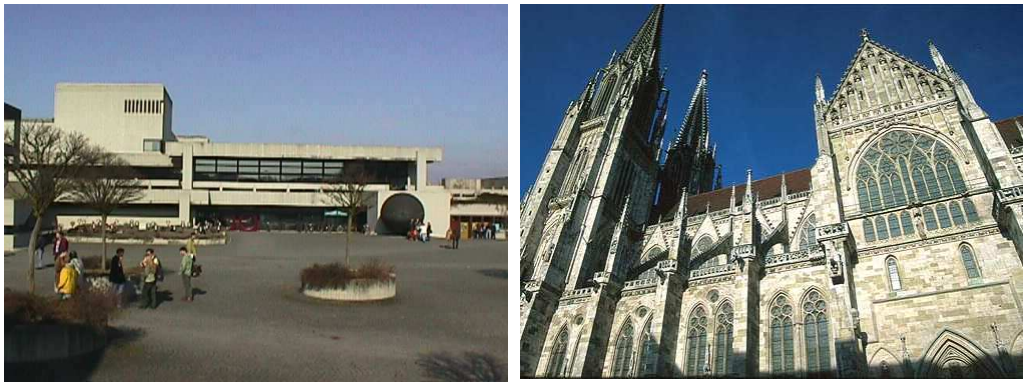

Figure 3: To conclude, the ugly buildings of our University of Regensburg (left) and the beauty of the Dom of Regensburg (right).

This work is dedicated to my future wife Maddalena
who so patiently waited for me . . .

Your heart knows in silence the secrets of the days and the nights.
But your ears thirst for the sound of your heart's knowledge.
You would know in words that which you have always known in thought.
You would touch with your fingers the naked body of your dreams.
And it is well you should.
The hidden well-spring of your soul must need rise and run murmuring to the sea;
And the treasure of your infinite depths would be revealed to your eyes.
But let there be no scales to weigh your unknown treasure;
And seek not the depths of your knowledge with staff or sounding line.
For self is a sea boundless and measureless.
Say not, "I have found the truth," but rather, "I have found a truth."
Say not, "I have found the path of the soul."
Say rather, "I have met the soul walking upon my path."
For the soul walks upon all paths.
The soul walks not upon a line, neither does it grow like a reed.
The soul unfolds itself, like a lotus of countless petals.

Gibran Khalil Gibran

Muere lentamente quien no voltea la mesa
cuando está infeliz en el trabajo,
quien no arriesga lo cierto por lo incierto
para ir detrás de un sueño,
quien no se permite por lo menos una vez en la vida,
huir de los consejos sensatos.

Pablo Neruda

Chapter 1

Introduction

The understanding of the appearance of classical behavior in quantum mechanics is an issue of fundamental relevance. In particular, in the beginning of the 80's, many questions arose about fundamental quantum-mechanical arguments concerning the reconciliation between the microscopic level description of nature and the macroscopically observed phenomena [1, 2, 3]. It has become clear that dissipation plays an important role on quantum phenomena, which could be seen in observables describing macroscopic states like macroscopic quantum tunneling and quantum coherence.

Dissipation is the consequence of an interaction between the system upon analysis and an environment which can be thought of as consisting of infinitely many degrees of freedom. In a wide sense, the coupling to an environment can be thought as a continuous measuring process leading to a destruction of phase correlations. Dissipation processes are to be understood first, in order to provide, if required, further decoherence control schemes. An important footstep to allow experimental investigation of decoherence mechanisms was the realization of micrometer-sized objects like the radio-frequency superconducting quantum interference device (rf-SQUID) [4]. Recently, due to their scalability and to the ease to experimentally control their parameters, other superconducting devices as the flux-qubit [5] or the Cooper-pair box [6, 7] have become attractive systems to explore quantum coherence on a fundamental basis and as possible basic unit (*quantum*-bit or *qubit*), for future quantum computers [8]. A short overview about quantum computation is addressed in the following Section, where the fundamental issues of this new promising research field are reviewed.

A widely used model to describe environmental effects is the so-called Ullersma-Zwanzig-Caldeira-Leggett model [2, 9, 10], which treats the reservoir as composed by harmonic oscillators. An ubiquitous system where to explore the effects of the environment on tunneling

consists of a particle in a double-well potential with an energy barrier which separates two energetically degenerate minima. In an idealized system, the barrier can be coherently traversed by the quantum mechanical particle (*coherent tunneling*). The situation is however different in the real case, where the system experiences the influence of the external thermal bath, which causes decoherence and dissipation in the quantum system.

In this work we consider a bilinear coupling between the bistable system of interest and the bath, modeled as an ensemble of harmonic oscillators. Then the bath degrees of freedom can be exactly traced out by making use of the real-time path integral technique which uses the Feynman-Vernon formulation as a starting basis [11]. In the so obtained *reduced density matrix* (RDM) the environmental influence enters through non-local in time correlations among tunneling transitions between two wells or *vibrational relaxation* processes within one well. This procedure is illustrated in Chapter 2 of this work.

The spectrum of a symmetric double-well potential consists, for energies below the barrier, of a ladder of tunneling doublets. The doublets are well separated by large interdoublet energy gaps with magnitude of the order of the characteristic classical oscillation frequency in a well, typical of a *vibrational relaxation* process, and usually much larger than the tunneling splittings.

In order to investigate the influence of an environment on quantum coherence, a commonly used approximation is to consider low enough temperatures, such that the spatially continuous bistable potential can be restricted to the lowest energy doublet, i.e. to a simple two-state system. This is the situation considered in the Chapters 3 and 4 of this work, where the bistable potential is approximated as a two-level system (TLS) interacting with a harmonic reservoir, resulting in the so-called *spin-boson* problem [1, 12]. Common approximations to describe the spin-boson dynamics are either perturbative in the tunneling splitting or in the coupling to the bath. Such schemes are known as *Non-Interacting Blip Approximation* (NIBA) [12, 13] and *Weak-Coupling Approximation* (WCA) [14, 15, 16], respectively. The limit of validity of these approximation schemes, however, is not clearly defined. In Chapter 3, we develop a novel interpolating scheme which we call *Weakly-Interacting Blip Approximation* (WIBA), being able to describe the spin-boson dynamics over the whole range of parameters for a wide class of spectral densities. In particular, a good agreement between the WIBA predictions and those of the *ab-initio* Quasi-Adiabatic Path-Integral Propagator method (QUAPI) [17] is found for an Ohmic environment.

In Chapter 4, we consider the case of bosonic environments with internal resonances. This turns out to be necessary to predict the dynamics of a realistic flux-qubit, where a TLS is read-out by a dc-SQUID used for detection which itself experiences a harmonic

bath [5, 18, 19, 20, 21]. By performing a weak-damping approximation (WDA) on the NIBA kernels for a symmetric two-state system, we obtain an analytical solution for the populations difference being able to describe the effects of the entanglement between the qubit and its detector.

When increasing the temperature, however, approximating the bistable potential as a two-state system is invalid since higher lying energy levels can become thermally populated [22, 23, 24, 25, 26, 27, 28, 29], and therefore in the regimes of temperatures and coupling strengths where their population is not negligible [22, 23, 24, 30, 31, 32] a *leakage* (i.e. loss of population) occurs in the two lowest-lying states.

In Chapter 5 we generalize the results of Refs. [28, 29], where the so-called *generalized Non Interacting Cluster Approximation* (gNICA) was performed, being able to reproduce the fully incoherent dynamics for large enough damping and/or temperatures. However, where the typical vibrational relaxation frequency, i.e. the transition between the doublets, is larger than the temperature, gNICA fails and a new theory is needed. In the mentioned Chapter, we develop an analytical analysis for the dynamics in a bistable potential in the presence of a static external bias interacting with a thermal dissipative environment. In the regime where the temperature is still larger than the typical tunneling frequency, the bath induced correlations among tunneling path elements can still be treated within the gNICA, whereas we retain bath-induced correlation among vibrational relaxation events. We finally obtain a generalized master equation for the diagonal elements of the reduced density matrix, where the dynamics *intra*-well is separated by the *inter*-well transitions.

In the remaining of this Chapter, we present some overview of quantum computing, followed by a short review of experimental works on dissipative bistable systems which constitute the motivation for this work.

1.1 Overview on quantum computation

Quantum computers offer the wonderful promise of solving certain problems which are beyond the reach of any classical machine. However, the experimental realization of a quantum computer represents a big challenge, because it requires the ability to initialize, coherently manipulate and measure individual quantum systems.

In classical computers, information is stored and processed in the processors, usually realized with silicon, which work on binary code in order to reach high-speed performances. Information is stored in bit sequences, which are constituted by 0's and 1's. As a consequence, any physical system with two possible states can be used to represent a bit. For

example, we can encode information into the spin of an electron (up/down), the polarization of a photon (horizontal/vertical), two energy levels of an atom (ground/excited state), and so on.

If these two-level systems behave quantum-mechanically, information can also be stored in a "superposition" of the two basis states,

$$|\Psi\rangle = \cos\theta|0\rangle + e^{i\varphi}\sin\theta|1\rangle\,, \tag{1.1}$$

yielding additional computation channels. In some sense, this means that such a *quantum bit* or *qubit* can assume the values 0 and 1 at the same time. Therefore, we cannot describe the state of n qubits via n complex numbers only, but we need to specify $2^n - 1$ of them. This means that the description of quantum systems becomes exponentially complex in the number of particles.

A special feature of quantum computers arises from the superposition property. In fact, applying a logic gate to the state vector describing a collection of n qubits amounts to apply in one single process the gate to *each* qubit simultaneously. In other terms, if the gate acts on the j-th qubit as $g(|j\rangle)$, the result of the application of the gate to a generic superposition of n states

$$|\Psi\rangle = \sum_{i_k=\{|0\rangle,|1\rangle\}} \alpha_{i_1,\ldots,i_k,\ldots,i_n}|i_1,\ldots,i_k,\ldots,i_n\rangle \tag{1.2}$$

is $g(|\Psi\rangle)$, namely

$$g(|\Psi\rangle) = \sum_{i_k=\{|0\rangle,|1\rangle\}} \alpha_{i_1,\ldots,i_k,\ldots,i_n} g\left(|i_1,\ldots,i_k,\ldots,i_n\rangle\right). \tag{1.3}$$

Thus, in the end a n-qubit computer can perform 2^n computations at the same time (*quantum parallelism*). This suggests that the computational capability of a quantum computer increases exponentially with its size, as David Deutsch already stated in 1985, unlike a classical computer which scales only linearly.

However, once the qubits states are measured, the results will always be either 0 or 1 for each qubit, even if it was a superposition of 0 and 1 before the measurement. Thus, although 2^n parallel computations are performed, only one of the corresponding output values will be in fact measured. Moreover, most measurement processes are destructive, which means that the state of the qubits, once projected onto one of the possible eigenvalues and therefore read out, is lost. A further measurement would require the qubit to be again initialized. This

affects of course the efficiency of the quantum computer. There are, however, measurement processes which are made in a nondestructive way (*non-demolition* measurements).

Although after the measurements only *one* result is obtained, special quantum algorithms are able to solve relevant problems in exponentially fewer steps than is possible classically. The best-known quantum algorithm is Peter Shor's 1994 algorithm for efficiently finding the prime factors of large integer numbers. The time needed on a classical computer to decompose a large number into its prime factors is thought to increase exponentially with the length of the number. This statement underlies actual cryptographic codes. On a quantum computer, in contrast, the time needed for factoring increases only polynomially. An algorithm, invented by Lov Grover in 1996, offers a quadratic speed-up for unsorted search problems. Another basic application is efficient simulation of quantum system, which can only be performed on another quantum system like for instance a quantum computer.

Quantum superpositions survive only for a short time (from μs of optical devices to ms/s for molecular NMR systems) after they have been prepared: due to interactions with the environment, a qubit in the state $(|0\rangle+|1\rangle)/\sqrt{2}$ will quickly degrade into either $|0\rangle$ or $|1\rangle$. Quantum coherence is in fact a fundamental requirement for a usable quantum computer. Fortunately, Andrew Steane and Peter Shor in 1996 discovered that it is possible to correct even the truly random errors caused by decoherence and restore the previous qubit state by using quantum error correction. Of course, error correction involves some overhead in the number of operations and the number of qubits, and this overhead also introduces more errors. It has been shown that we can correct the errors present in the computation if the probability of error per operation is below some threshold, currently estimated at roughly 1 over 10000. There are so-called *protected subspaces*, i.e. decoherence-free subspaces of the total Hilbert space where computations can be performed without dissipation-caused losses [33, 34, 35, 36, 37, 38]. However, for realizing a performant quantum computer it remains crucial to understand and control decoherence processes. Thus, minimizing decoherence effects is an aspect which has to be fully implemented in order to avoid using a redundant amount of qubits and to improve the efficiency of a quantum computer. This is the goal of the present PhD thesis.

In order to fix a universal prescription for the realization of a working quantum computer, several statements have been proposed by DiVincenzo [39], see Tab. 1.1. Satisfying these criteria represents a formidable challenge, as it requires to reconcile two conflicting requirements: On the one hand, we need access to the qubits in order to initialize, manipulate and read out their state, but on the other hand the qubits must be highly isolated from the environment, such that they remain coherent for a long time. Hence, understanding and

1. Scalability of physical systems with well-characterized qubits;
2. Initialization of the qubits to a well-known state;
3. A universal set of quantum logic gates;
4. Read-out of the qubits;
5. Coherence times long compared to the typical gate duration.

Table 1.1: DiVincenzo criteria for realization of a working quantum computer.

control of dissipation in *realistic* qubit systems, been object of this work, is of outermost importance.

In the beginning of the following Section, qubits realizations will be presented in an of course non-exhaustive list, due to the always increasing number of experiments. There, a major emphasis is put on the flux-qubits which can be described as bistable systems and are promising candidates for becoming the future building-blocks of quantum computing due to their great scalability. In the last part of the Section, we will also review some of the recent developments and experiments on multilevel systems which, together with the two-state systems, constitute the basic motivation for my PhD.

1.2 Challenges and recent achievements for two- and multi-level systems

1.2.1 Qubits experimental realizations

The different systems used to realize the quantum units may have different advantages or technical problems. The possible experimental qubits realizations can be classified in two main categories : Those which involve atomic systems, e.g. atoms in ion traps, atoms in optical lattices, ensemble of nuclear spins in liquids, and those based on solid-state systems. In the latter case, qubits are e.g. spins of electrons in semiconductor quantum dots, nuclear spins of donor atoms in a semiconductor, or the persistent currents in superconducting loops containing Josephson junctions. NMR techniques have also been widely used to address, manipulate and control the molecular angular momentum or the nuclear spins of molecules, although such systems are not very well scalable. To mention another important class of experiments among others, optical manipulation of photons has also performed several important footsteps in quantum computing.

We intend here not to present a comprehensive review of qubits realizations, but to list some beautiful experiments with different kinds of conceived qubits, in order to obtain a final picture of the state-of-the-art of the modern techniques. A more informative collections of proposals and experimental realizations can be found in [40].

In particular, we focus our attention on solid-state systems, which are supposed to be scalable like conventional solid-state integrated circuits. In contrast, atomic systems suffer the problem of scalability, though coherent on longer times. The existing and proposed solid-state qubits can be roughly grouped into two categories, being distinguishable in their *microscopic* or *macroscopic* nature [41]. The microscopic category entails qubits based on quantum objects of atomic scale, like electron-spin based qubits in semiconductor quantum dots. The macroscopic class includes all those systems whose state can be characterized by the measurement of a macroscopic observable, such as the supercurrent carried by Cooper pairs in flux qubits or charge states in a Cooper pair box, see Fig. 1.1.

Specifically, in the following we restrict our attention to the flux qubits, being mesoscopic systems (of typical size $1\mu m$) with superconducting islands connected via some tunnel junctions. The charge on each island and the current flowing through the junctions exhibit a quantum mechanical behavior when the sample is cooled at a sufficiently low temperature (about 30 mK). The charge and the magnetic flux threading the circuit, the latter being related to the currents through the junctions, are conjugate variables [42]. Incoherent

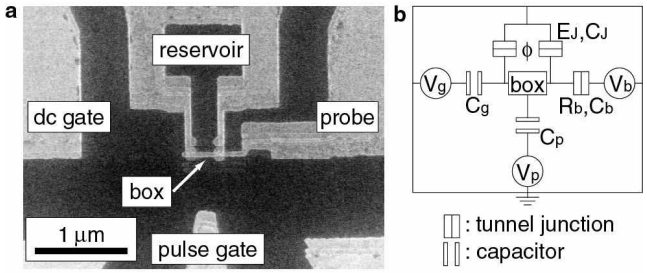

Figure 1.1: The single-Coooper-pair-box used for demonstrating the coherent superposition of two charge states [6].

tunneling of the flux variable through an energy barrier was also observed [43]. Microwave spectroscopy experiments performed on such structures show quantized energy levels [43].

We notice that big interest in these systems arose already after Leggett's early proposal in 1984 [1]. There, the challenge was posed on the experimental demonstration of a superposition of macroscopic quantum states (macroscopic quantum coherence). From the experimental point of view, suitable candidates to explore the macroscopic quantum

coherence, for their scalability and control, are the superconducting quantum interference devices, i.e. SQUIDs [44, 45, 46, 47, 48, 49, 50, 51, 52]. The flux Φ threading the SQUID (or the phase difference across the Josephson junctions in the SQUID) describes the collective motion of a macroscopic number of quasiparticles and hence exhibits quantum behavior at accessible temperatures. The equations of motion for the flux dynamics map onto that of a particle moving (dissipatively) in a bistable potential, the lowest energy states corresponding to the two fluxoid states of the SQUID. Transitions between them occur only via tunneling through the potential barrier, when the temperature is low enough. Incoherent tunneling in a macroscopic two-state system [45] between two quasi degenerate energy states localized in different fluxoid wells have been demonstrated. In 1999 Mooji and coworkers

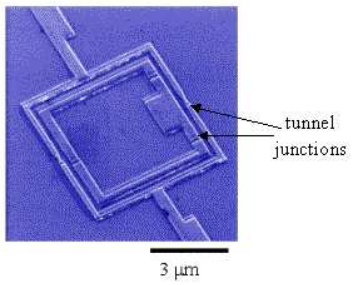

Figure 1.2: The flux qubit used for detecting the superposition of macroscopic quantum states [51, 52].

[51, 52] realized a circuit made of one superconducting loop containing three junctions, the "persistent-current flux qubit", in order to minimize the effects of environment. The small size of the circuit, i.e. of the order $1\ \mu\text{m} \times 1\ \mu\text{m}$, allow the qubit to be insensitive to background charges in the substrate and effectively decoupled from their electrostatic environment. The decoherence time, estimated for this qubit to be more than 1 ms [51], can be made substantially longer than the minimum decoherence time for an individual junction circuit. When biased at a flux Φ around $\Phi_0/2$ (half a flux quantum, being defined as $\Phi_0 \equiv h/2e$), the qubit's two lowest energy levels correspond to two classical states of opposite circulating dc-current. If the external flux is far from $\Phi_0/2$, the two energy eigenstates carry a mesoscopic supercurrent (typically 300 nA) which flows either clockwise or anticlockwise. If on the other hand $\Phi = \Phi_0/2$, the energy eigenstates are coherent superpositions of the two current-carrying states and microwave transitions between those two levels can be induced, the qubit's state being finally detected by an inductively coupled dc-SQUID. Further proof that a coherent superposition of current states was achieved was performed one year later by means of spectroscopic measurements on the system [52].

In another beautiful experiment, the coherent dynamics of a persistent-current qubit has been observed [5]. In this sample, the three-junction loop and the detection SQUID

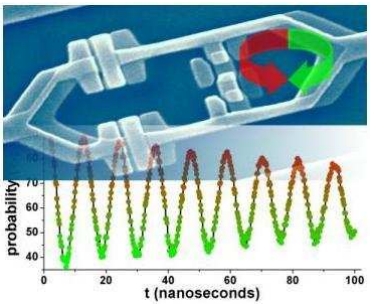

Figure 1.3: The three-junction loop and the detection SQUID share a common branch. By means of microwave pulses, the quantum state of the qubit can be easily manipulated [5].

share a common branch as it can be seen in Fig. 1.3. In the experiment, microwave pulses of variable length and amplitude were used to coherently manipulate the quantum state of the loop. The readout by the SQUID was also pulsed and revealed quantum-state oscillations with high fidelity. Under strong microwave driving, it was possible to induce hundreds of coherent oscillations. Relaxation times of 900 ns and a free-induction dephasing time of 20 ns were measured.

Friedman *et al.* [50] analogously reported on the realization of a quantum superposition of macroscopic states in an rf-SQUID.

Finally, we wish to recall some achievements in the experimental fulfillement of the third DiVincenzo criterium, i.e. the requirement of a universal set of quantum logic gates. A quantum logics can be built using single-qubit operations ('rotations') and two-qubit

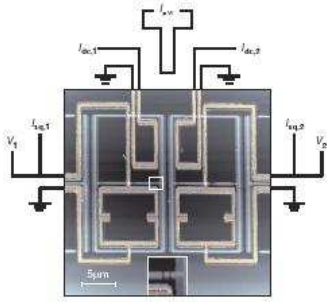

Figure 1.4: Two three-junction superconducting loops are magnetically coupled. A resonant microwave pulse induces a quantum cNOT gate [56].

cNOT gates, since any computation can be decomposed into a sequence of these basic gate operations [53]. This goal has been realized in many physical systems as, among

others, trapped-ions with individual addressing [54], photons by using linear optics [55] and superconducting flux qubits [56]. In the latter case, two superconducting loops containing three Josephson junctions are magnetically coupled. By operating the qubits far from their degeneracy points, resonances between the two qubits are induced that change the state of either the first or second qubit. The "control" and the "target" qubits can be freely chosen, due to the circuital simmetry. A resonant microwave pulse induces rotations on the qubits states and realizes a quantum cNOT gate.

1.2.2 Multilevel experimental achievements

There have been several experiments on different dissipative multilevel systems.

As already noticed, the flux dynamics in the SQUIDs can be mapped onto that of a particle dissipatively moving in a bistable potential. When the temperature is high enough, higher levels cannot be neglected and therefore an M-level system is to be taken into account. Macroscopic quantum tunneling of the flux between quantized energy levels in differ-

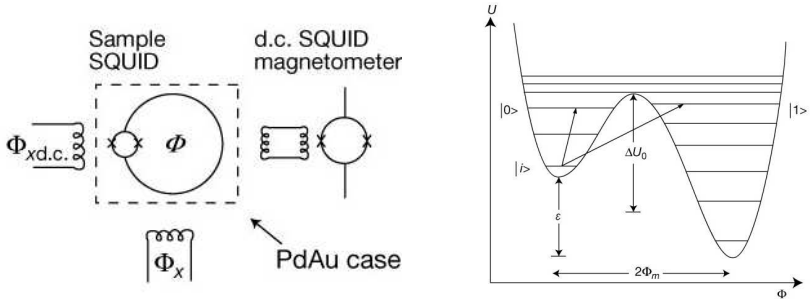

Figure 1.5: Here the experimental setup (left) and the corresponding SQUID potential (right) for demonstrating the evidence of macroscopic quantum tunneling are shown [46, 50].

ent fluxoid states of a SQUID has been demonstrated [46]. These states are macroscopically distinct, differing in mean loop current by about 6 μA. Five years later, by using the same experimental setup of Ref. [46], Friedman and coworkers [50] were able to experimentally demonstrate a quantum superposition of truly macroscopically distinct states, namely the two fluxoid states of the SQUID. They produced microwave photon-assisted tunneling from the lowest state in the left well (see Fig. 1.5) to one resonant excited state and subsequently to a right well fluxoid state, the transition between the wells being detected as a change in flux by an external magnometer.

Quantum tunneling of magnetization in nanomagnets has also been demonstrated [57]. A macroscopic sample of molecular magnets consists of a large number ($10^4 - 10^{11}$) of chemically identical magnetic clusters, regularly arranged on a crystal lattice. The single

molecules have generally a large spin, typically $S \approx 10$. Experimentally detected anisotropy of such systems produces a double-well potential with doubly degenerate excited states [58]. If the temperature is low enough, the spins can tunnel through the anisotropy barrier. Two kinds of materials have been investigated by different groups: Mn_{12}-acetate [22] and Fe_8 [23, 24]. The iron sample has the advantage that the barrier is about three times smaller than in the manganese, and this enhances the observed effects of resonant quantum tunneling of magnetization.

Why should we be in such desperate haste to succeed,
and in such desperate enterprises?
If a man does not keep pace with his companions,
perhaps it is because he hears a different drummer.
Let him step to the music which he hears,
however measured or far away...

Henry David Thoreau

Chapter 2

Real-time path-integral approach for dissipative bistable systems

In this Chapter, we present the model and we introduce the so-called DVR basis, being the eigenbasis of the discrete position operator. Then, we are able to get an exact as well as untractable analytical expression for the reduced density matrix, being the starting point for the approximations we will develop in the course of the next Chapters of this PhD thesis.

The system under analysis is such that the observed variable (i.e. flux through a superconducting ring) can be described by a Hamiltonian which can be mapped onto the one of a quantum particle with mass $\mathcal{M}$, position operator $\mathbf{q}$ and momentum operator $\mathbf{p}$ in a one-dimensional double-well potential $V_0(\mathbf{q})$. An external driving bias causes an asymmetry ε. The corresponding Hamiltonian reads

$$\mathbf{H}_0 = \frac{\mathbf{p}^2}{2\mathcal{M}} + V_0(\mathbf{q}), \tag{2.1}$$

with

$$V_0(\mathbf{q}) = \frac{\mathcal{M}^2\omega_0^4}{64\Delta U}\mathbf{q}^4 - \frac{\mathcal{M}\omega_0^2}{4}\mathbf{q}^2 - \mathbf{q}\,\varepsilon \tag{2.2}$$

being the asymmetric double-well potential. In the absence of asymmetry ($\varepsilon = 0$), ΔU denotes the barrier height and ω_0 the angular frequency of classical oscillations around each well minimum, located at $q_0/2 = \pm\sqrt{8\Delta U/\mathcal{M}\omega_0^2}/2$.

The energy spectrum is obtained by solving the time-independent Schrödinger equation $\mathbf{H}_0|n\rangle = \mathcal{E}_n|n\rangle, n = 1, 2, \ldots, \infty$.

In the case of a symmetric potential ($\varepsilon = 0$), the energy spectrum below the barrier

consists of a ladder of pairs of energy eigenstates (*doublets*). The energy gaps within each doublet, $\Delta_i^{\mathcal{E}}$'s, are usually some orders of magnitude smaller than the inter-doublet energy gaps and are responsible for the *tunneling dynamics* between the two wells. The large energy gaps are of the order of $\hbar\omega_0$, where ω_0 is the harmonic oscillation frequency around the well minima. Any transition which occurs among those largely separated energy eigenstates is called *vibrational relaxation*. In the presence of a static tilt smaller or comparable with the doublets' splittings ($\varepsilon \sim \Delta_i^{\mathcal{E}}$), the situation of well separated doublets still applies.

We choose to model the environment as an ensemble of harmonic oscillators [3, 11, 12, 59, 60] which linearly couple to the system position coordinate $\mathbf{q}$, ending up with a bath Hamiltonian $\mathbf{H}_{\mathrm{B}}$ of the form (including also the interaction between bath and system)

$$\mathbf{H}_{\mathrm{B}} = \sum_{j=1}^{\mathcal{N}} \frac{1}{2}\Big[\frac{\mathbf{p}_j^2}{m_j} + m_j\omega_j^2\Big(\mathbf{x}_j - \frac{c_j}{m_j\omega_j^2}\mathbf{q}\Big)^2\Big]. \tag{2.3}$$

The whole system is thus described by the Hamiltonian $\mathbf{H} = \mathbf{H}_0 + \mathbf{H}_{\mathrm{B}}$. In the case of a thermal equilibrium bath, its influence on the system is fully characterized by the spectral density [12]

$$J(\omega) = \frac{\pi}{2}\sum_{j=1}^{\mathcal{N}} \frac{c_j^2}{m_j\omega_j}\delta(\omega - \omega_j), \tag{2.4}$$

which reduces to a continuous spectral density once the number $\mathcal{N}$ of harmonic oscillators approaches infinity. Throughout this work, we choose different spectral densities which, case by case, are able to better model the system under analysis.

In order to describe the system's dynamics, we focus on the time evolution of the *reduced density matrix* (RDM) $\rho(t) = \mathrm{tr}_{\mathrm{B}}\,\mathbf{W}(t)$, which we obtain after tracing out all bath degrees of freedom from the total density matrix $\mathbf{W}(t)$. The RDM reads in position representation:

$$\begin{aligned}
\rho_{\sigma_f,\sigma_f'}(t) &= \langle\sigma_f|\boldsymbol{\rho}(t)|\sigma_f'\rangle \\
&= \mathrm{tr}_{\mathrm{B}}\langle\sigma_f|\mathbf{U}_{t,0}\,\mathbf{W}(0)\,\mathbf{U}_{t,0}^{-1}|\sigma_f'\rangle \qquad (2.5)\\
&= \int d\mathbf{x}_f\langle\sigma_f\mathbf{x}_f|\mathbf{U}_{t,0}\,\mathbf{W}(0)\,\mathbf{U}_{t,0}^{-1}|\sigma_f'\mathbf{x}_f\rangle, \qquad (2.6)
\end{aligned}$$

with $\mathbf{U}_{t,0} = \mathcal{T}\exp\left[-\frac{i}{\hbar}\int_0^t dt'\,\mathbf{H}(t')\right]$ the time evolution operator and $\mathcal{T}$ the time ordering operator; $\mathbf{W}(0)$ is the full density operator at the initial time $t = 0$ and tr_{B} indicates the partial trace over the harmonic bath coordinates x_j (here we use the shorthand notation $\mathbf{x} \equiv \{x_j\}$). The diagonal elements of the RDM are called *populations*, whereas the off-diagonal terms *coherences*. We choose a factorizing initial condition, namely at time $t = 0$

the full density operator $\mathbf{W}(0)$ is expressed as a product of the initial system density operator $\rho^{(\mathrm{S})}(0)$ and the canonical bath density operator at temperature T.

The dynamical quantity of interest is then the probability

$$P_R(t) = \int_0^\infty dq_f \, \rho_{q_f q_f}(t) \tag{2.7}$$

of finding the system in the right well at time t if it was prepared in some state localized in the right well at time $t = 0$ as well (with P_L we denote the analogue quantity for the left well).

The regime of high temperatures ($\hbar\Delta_i^{\mathcal{E}} < k_{\mathrm{B}}T \lesssim \hbar\omega_0$) and strong damping ($\Delta_i^{\mathcal{E}} \ll \gamma < \omega_0$) has been already discussed in [28, 29]. The first condition is consistent with a multilevel approach, since the higher states populations cannot be neglected; the second one accounts for the fact that the frictional level broadening due to the bath must not exceed the bare interdoublet spacing, otherwise a quantum treatment is no more required. In this range of parameters one cannot observe quantum coherent oscillations in the occupation probability of the right well, since the damping is sufficiently strong to suppress them.

We are here mainly interested in the *intermediate* temperatures regime $\hbar\Delta_i^{\mathcal{E}} \lesssim k_{\mathrm{B}}T$ where one clearly sees the presence of damped oscillations at short times in the population behavior. We will discuss further the limits of validity of this theory later on.

2.1 The reduced density matrix in the *Discrete Variable Representation* (DVR)

2.1.1 The DVR-basis

Given a particle in a double-well potential, a quantum-mechanical description would be inappropriate if the temperature is very large with respect to the energy scale of the system ($k_{\mathrm{B}}T \gg \hbar\omega_0$). Here, we consider the opposite regime $k_{\mathrm{B}}T \lesssim \hbar\omega_0$ and $\hbar\Delta_i^{\mathcal{E}} \lesssim k_{\mathrm{B}}T$ where energy doublets can still be resolved and the lowest M-lying energy eigenstates are largely populated.

Then, it appears convenient to truncate the Hilbert space to the space spanned by the M lowest-lying energy eigenstates $\{|m\rangle\}$ of the potential. The problem of a spatially continuous double-well potential is then reduced to a problem of a finite M-dimensional system. In this minor Hilbert space, also the position operator, being the coordinate that couples the bare system to the thermal bath, is discretized. Due to the bilinear coupling between system's and oscillators' coordinates (see Eq. (2.3)), it is useful to introduce a

basis termed DVR (*Discrete Variable Representation*) [61], which is defined as the basis which diagonalizes the system position operator:

$$\langle q_\mu|\mathbf{q}|q_\nu\rangle = q_\mu\delta_{\mu\nu}\,, \quad \mu,\nu = 1,\ldots,M\,. \tag{2.8}$$

Starting from the energy eigenbasis $\{|m\rangle\}$, the DVR states follow from the identity $\mathbb{I} = \sum_{m=1}^{M}|m\rangle\langle m|$ as $|q_\mu\rangle = \sum_{m=1}^{M}\langle m|q_\mu\rangle|m\rangle$.

We notice that with $M = 2$ the well-known *spin-boson* model is recovered. There, the DVR-basis coincides with the localized basis $\{|L\rangle, |R\rangle\}$, which can be expressed in terms of the energy eigenstates $|m = 1\rangle \equiv |g\rangle$ and $|m = 2\rangle \equiv |e\rangle$ as follows:

$$\begin{cases} |L\rangle = +\cos\frac{\theta}{2}|e\rangle + \sin\frac{\theta}{2}|g\rangle\,, \\ |R\rangle = +\cos\frac{\theta}{2}|g\rangle - \sin\frac{\theta}{2}|e\rangle\,, \end{cases} \tag{2.9}$$

where $\tan\theta = \frac{\Delta}{\varepsilon}$, and $\hbar\Delta$ being the energy separation of the two levels at zero bias ($\varepsilon = 0$). For $M > 2$ we introduce analogously the transition amplitudes ($q_\mu \neq q_\nu$)

$$\Delta_{\mu\nu} \equiv \frac{2}{\hbar}\langle q_\mu|\mathrm{H}_0|q_\nu\rangle \tag{2.10}$$

and the on-site energies

$$E_\mu \equiv \frac{1}{\hbar}\langle q_\mu|\mathrm{H}_0|q_\mu\rangle. \tag{2.11}$$

The frequencies $\Delta_{\mu\nu}$'s can take very different values, depending on whether they connect DVR-states which lie in different wells or within the same well. For example, we call Δ_{intra} the characteristic frequency scale associated to *vibrational relaxation* processes, i.e. to transitions occurring between DVR-states lying in the same well. Δ_{intra} is related to the classical oscillation frequency around the minima, ω_0, and is proportional to the separation between the doublets under the potential barrier.

On the other side, a generic *DVR-tunneling* event takes place at a rate Δ_{inter} which can be expressed as a linear combination of the splittings between energy states within the doublets, i.e. the tunneling splittings. This frequency accounts in fact for tunneling transitions which connect any DVR-state of one well with another lying in the other well.

In general, the *tunneling* frequencies are much smaller than the *vibrational relaxation* ones, since the events of tunneling are quantum processes, which are much less frequent than the intra-well transitions.

For the *spin-boson* problem ($M = 2$), it is common to evaluate the dynamics of the

expectation value of the position operator $\langle \mathbf{q}(t) \rangle$ which is related to the quantity

$$P(t) := P_R(t) - P_L(t), \tag{2.12}$$

namely the difference of populations in the reduced density matrix in the DVR-basis, since this is the quantity of interest in the experiments. In analogy, for a generic M-level system, we investigate the decay of the whole population of one well of the bistable potential, for example the right well. Hence, we define the quantity of interest to be the sum of the populations of those DVR-states $|q_\mu\rangle$ which belong to the *positive position eigenvalues* q_μ, i.e., those which are located at the right hand-side with respect to the origin, where we assume the potential is 0. In other terms, the integral in Eq. (2.7) is replaced by a sum over the diagonal elements of the RDM (populations) corresponding to the DVR-states lying in the right well:

$$P_R(t) = \sum_{\{\mu \in \mathrm{R}\}} \rho_{\mu\mu}(t)\,. \tag{2.13}$$

In the case of a symmetric potential, i.e. $\varepsilon = 0$ in the potential Eq. (2.2), the energy eigenfunctions occur in pairs of symmetric and antisymmetric wave functions. This means that the number of states in the system is even and hence half of the position eigenvalues lies on the left side and the other half on the right side of the origin. As a consequence, only $M/2$ DVR-states are relevant for the population $P_R(t)$ of the right well. However, in the case of a finite static asymmetry, nothing general can be said.

2.1.2 Formally exact expression for the reduced density matrix

Our assumption of a factorizing initial condition and the choice of the DVR basis allows us to perform the partial trace over the bath coordinates exactly, see also [29]. In the end, we can recast the reduced density operator according to Feynman and Vernon [11] as

$$\rho_{q_f,q'_f}(t) = \sum_{q_i} \sum_{q'_i} \rho^{(\mathrm{S})}_{q_i,q'_i}(t_0) \int_{q(t_0)=q_i}^{q(t)=q_f} \mathcal{D}q \int_{q'(t_0)=q'_i}^{q'(t)=q'_\mathrm{f}} \mathcal{D}q' \mathcal{A}[q]\mathcal{A}^*[q']\mathcal{F}_{\mathrm{FV}}[q,q']\ , \tag{2.14}$$

where the forward (backward) path integral is over piecewise constant trajectories $q(t)(q'(t))$ in which the system is in the DVR state $|q_{\mu_j}\rangle$ ($|q'_{\nu_j}\rangle$) at time t_j. A sketch of these paths is shown in Fig. 2.1 for a $M = 6$ level system. In Eq. (2.14), $\mathcal{F}_{\mathrm{FV}}[q,q'] = \exp(-\phi_{\mathrm{FV}}[q,q']/\hbar)$ is the Feynman-Vernon influence functional. Unlike the two-level system, for a generic continuous bistable potential the bare system amplitude $\mathcal{A}[q]$ can no longer be expressed in terms of the classical action functional of the system variable q. For our purpose, it is

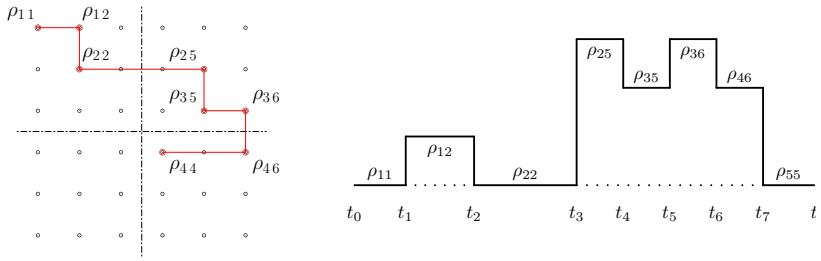

(a) (b)

Figure 2.1: (Left panel) Schematic representation of the RDM for a $M = 6$ level system in the DVR-basis. The two dot-dashed lines delimit the right- and the left-lying DVR-states in the double well as it would be the case e.g. for $\varepsilon = 0$. In red a generic path is shown, the bolded dot denoting the visited states in the RDM space. (Right panel) The same path is sketched by means of *theta*-functions, the jumps happening at subsequent times $t_1, \ldots, t_7$. It is characterized by three *sojourns* (time-intervals spent in diagonal states of the RDM), and two *clusters* (time-intervals spent between two successive visits to diagonal states of the RDM). A cluster is denoted *blip* when the path returns to a diagonal state only after two VR- or tunneling-transitions.

convenient to write the influence phase $\phi_{\rm FV}[q, q']$ in terms of relative coordinates $\xi(t') = q(t') - q'(t')$ and center of mass coordinates $\chi(t') = q(t') + q'(t')$, yielding

$$\begin{aligned}\phi_{\rm FV}[\xi,\chi] = &\int_{t_0}^{t} dt' \int_{t_0}^{t'} dt'' \{\dot\xi(t') S(t'-t'') \dot\xi(t'') + i\dot\xi(t') R(t'-t'') \dot\chi(t'')\} \\ &+ \xi(t) \int_{t_0}^{t} dt' \{\dot\xi(t') S(t-t') + i\dot\chi(t') R(t-t')\} \\ &+ \xi(t_0)\{\xi(t) S(t-t_0) - \int_{t_0}^{t} dt' \dot\xi(t') S(t'-t_0)\} \\ &+ i\chi(t_0)\{\xi(t) R(t-t_0) - \int_{t_0}^{t} dt' \dot\xi(t') R(t'-t_0)\}\,. \end{aligned} \tag{2.15}$$

As one notices, the influence of the environment is in the functions $S(t)$ and $R(t)$, which denote the real and imaginary part, respectively, of the bath correlation function $Q(t)$, i.e. [12]

$$Q(t) = S(t) + iR(t) = \frac{1}{\pi\hbar} \int_0^\infty d\omega \frac{J(\omega)}{\omega^2} \left\{ \coth \frac{\hbar\omega\beta}{2} (1 - \cos\omega t) + i \sin\omega t \right\}. \tag{2.16}$$

In our truncated Hilbert space, the position eigenvalues are discrete values q_{μ_j} on the q-axis and generate a grid of states among which the system performs quantum jumps at

subsequent times t_j.

We need to introduce some symbols and notations. The coordinate (μ, ν) from now on indicates a generic matrix element corresponding to a generic choice of q and q', respectively (μ holds for the rows and ν for the columns). The coordinate sequence for a discrete path is given by a collection of indexes $\{\mu_j, \nu_j\}$, where for example for a horizontal transition in the RDM the first index remains constant, i.e. $\mu_j\nu_j \rightarrow \mu_j\nu_{j+1}$, and for a vertical one it is the opposite, i.e. $\mu_j\nu_j \rightarrow \mu_{j+1}\nu_j$. The corresponding amplitudes are proportional to the frequencies Δ_j, which are defined as

$$\Delta_j = \Delta_{\nu_{j+1}\nu_j} \equiv \frac{2}{\hbar}\langle q_{\nu_{j+1}}|\mathrm{H}_0|q_{\nu_j}\rangle \tag{2.17}$$

for a horizontal transition, and as

$$\Delta_j = \Delta_{\mu_{j+1}\mu_j} \equiv \frac{2}{\hbar}\langle q_{\mu_{j+1}}|\mathrm{H}_0|q_{\mu_j}\rangle \tag{2.18}$$

for a vertical jump. The factor 2 has been extracted in order to have the same convention as in the spin-boson problem [12]. The amplitude to stay in the j-th off-diagonal state from the time t_j to t_{j+1} reads $\mathrm{e}^{-\mathrm{i}\epsilon_{\mu_j\nu_j}(t_{j+1}-t_j)}$, where

$$\epsilon_{\mu_j\nu_j} \equiv E_{\mu_j} - E_{\nu_j}, \quad E_{\mu_j} \equiv \frac{1}{\hbar}\langle q_{\mu_j}|\mathrm{H}_0|q_{\mu_j}\rangle, \tag{2.19}$$

are the on-site energies in the DVR representation (also called *bias factors*).

Upon taking the derivatives of the paths with respect to the time variable, the relative and center of mass coordinates read

$$\dot{\xi}(t') = \sum_{j=1}^{N} \xi_j \delta(t' - t_j)\,, \tag{2.20a}$$

$$\dot{\chi}(t') = \sum_{j=1}^{N} \chi_j \delta(t' - t_j)\,, \tag{2.20b}$$

where we introduced paths weights $\xi_j \equiv \xi_{\mu_j\nu_j} - \xi_{\mu_{j-1}\nu_{j-1}}$ and $\chi_j \equiv \chi_{\mu_j\nu_j} - \chi_{\mu_{j-1}\nu_{j-1}}$, with $\xi_{\mu_j\nu_j} \equiv q_{\mu_j} - q'_{\nu_j}$ and $\chi_{\mu_j\nu_j} \equiv q_{\mu_j} + q'_{\nu_j}$, $j = 1, ..., N$. For $j = 0$, we define $\xi_0 \equiv \xi_{\mu_0\nu_0}$ and $\chi_0 \equiv \chi_{\mu_0\nu_0}$.

The time intervals spent by the system in a diagonal state of the reduced density matrix are called *sojourns*. They are characterized by $\xi(t) = 0$ and $\chi(t) \neq 0$. On the other side, the time intervals when the system is in an off-diagonal state are termed *clusters* and are such

that in general $\xi(t) \neq 0$ and $\chi(t) \neq 0$. This is a main difference from the spin-boson problem [3, 12, 62] where the off-diagonal states (*blips*) are in general characterized by $\xi(t') \neq 0$ and $\chi(t') = 0$. By inserting Eq. (2.20) in Eq. (2.15), the influence phase becomes

$$\phi_{\rm FV}[\xi,\chi] = -\sum_{l=1}^{N}\sum_{j=0}^{l-1}\xi_l S(t_l - t_j)\xi_j - i\sum_{l=1}^{N}\sum_{j=0}^{l-1}\xi_l R(t_l - t_j)\chi_j\,. \tag{2.21}$$

After introducing center of mass and relative coordinates, the double path integral in Eq.(2.14) transforms into a discrete summation over all possible path configurations $\{\mu_j, \nu_j\}$ in the DVR-basis and an integration over all intermediate times $\{t_j\}$. Formally,

$$\int \mathcal{D}q \int \mathcal{D}q' \Longrightarrow \int \mathcal{D}\xi \int \mathcal{D}\chi \Longrightarrow \int \mathcal{D}\{t_j\} \sum_{\{\mu_j\nu_j\}}\,, \tag{2.22}$$

where we have introduced a compact notation according to

$$\int_{t_0}^{t} \mathcal{D}\{t_j\} \equiv \int_{t_0}^{t} dt_N \int_{t_0}^{t_N} dt_{N-1} \ldots \int_{t_0}^{t_3} dt_2 \int_{t_0}^{t_2} dt_1 \tag{2.23}$$

for the time ordered integration over the N transition times t_j in the chosen paths.

Thus, collecting all terms we can obtain the dissipative real-time path integral expression for the diagonal elements of the RDM of an M-level system in the DVR-basis (for $t > t_0$)

$$\rho_{\mu_N\mu_N}(t) = \langle q_{\mu_N}|\boldsymbol{\rho}(t)|q_{\mu_N}\rangle \tag{2.24}$$

$$= \sum_{\mu_0=1}^{M} \rho_{\mu_0\mu_0} \left[\delta_{\mu_N\mu_0} + \sum_{N=1}^{\infty}\int_{t_0}^{t}\mathcal{D}\{t_j\}\sum_{\{\mu_j\nu_j\}} \mathrm{e}^{-\mathrm{i}\sum_{j=1}^{n}\epsilon_{\mu_{2j-1}\nu_{2j-1}}\tau_j}\right.$$
$$\left. i^N \prod_{j=0}^{N-1}(-1)^{\delta_j}\frac{\Delta_j}{2}\exp\left\{\sum_{l=1}^{N}\sum_{j=0}^{l-1}\xi_l S(t_l - t_j)\xi_j + i\sum_{l=1}^{N}\sum_{j=0}^{l-1}\xi_l R(t_l - t_j)\chi_j\right\}\right]\,, \tag{2.25}$$

where we define $\tau_j \equiv t_{2j} - t_{2j-1}$ and indicate with μ_0 and μ_N the initial (which we assume diagonal) and the final RDM state, respectively. Moreover, it holds $\delta_j = 0(1)$ for a horizontal (vertical) jump [29] (we can easily define its contribution as $(-1)^{\delta_j} \equiv \delta_{\mu_{j+1},\mu_j} - \delta_{\nu_{j+1},\nu_j}$).

The path integral in Eq. (2.25) is given in its most general form and is formally *exact*. It constitutes the expression from which to start in order to derive the generalized master equation and hence the full dynamics as well as the decay rates.

In the case of a two-level system ($M = 2$), Eq. (2.25) reduces to the well-known ex-

pression for the (driven) *spin-boson* problem [3, 12, 62]. There, the problem simplifies since the path weights during the time evolution can only assume two values, corresponding to the two states localized in the left and in the right well of the potential. This means that the path flips between a sojourn and a blip at each jump, and hence the spin-boson path integral assumes the form of a power series in the tunneling splitting $\Delta \equiv \mathcal{E}_2 - \mathcal{E}_1$ of the two lowest levels. This is not necessarily the case for a generic M-level system where a path can visit many off-diagonal states before ending in a diagonal state. Such a path becomes however less likely the longer it remains off-diagonal as a consequence of damping.

In the following two Chapters, we will restrict our analysis to a two-level system interacting with an unstructured and a structured bath, respectively. In Chapter 5, the M-level dynamics is finally considered. Though exact, the expression (2.25) is too intricate to allow for a closed form solution. Hence, approximation schemes are developed in order to get rid of negligible interactions upon specific regimes of parameters, which can allow us to analytically describe the dynamics.

Do not follow where the path may lead.
Go instead where there is no path
and leave a trail.

Ralph Waldo Emerson

Chapter 3

Spin-boson dynamics: An interpolating approach for weak to strong dissipation

Many physical and chemical two-level systems (TLSs) suffer the influence of external environments which cause decoherence effects [12, 13, 63]. Electron and proton transfer reaction in condensed phases [64, 65], tunneling phenomena in condensed matter physics [4, 66], or two-level atoms in an optical cavity [67] are some very well known situations susceptible to lack of coherence.

The spin-boson model, where the TLS is bilinearly coupled to a bath of harmonic oscillators, is commonly used to quantitatively describe some aspects of the dissipative dynamics of the above mentioned systems.

To date, the spin-boson model has been mostly described within two main approximation schemes, each describing different regimes of temperature and coupling strength to the thermal bath. One main road of approximation is based on an expansion to leading order in the tunneling frequency Δ (see (3.2) below), yielding the so-called noninteracting-blip approximation (NIBA) [12, 13, 68]. Equations of motion for the dynamical quantity $P(t)$ defined in Eq. (2.12) equivalent to the NIBA were also obtained using projection operator techniques [69, 70, 71]. The NIBA equations are easily solved numerically and yield analytical solutions in special cases [12, 13, 63]. However, for a biased TLS they can be only used in the regime of high temperatures and/or strong friction. An improvement to the NIBA has been performed for a super-Ohmic bath, in the regime of strong coupling [72]. A more refined model, which yields nonconvolutive dynamical equations, is the so-called

interacting-blip chain approximation IBCA [73], which retains the nearest-neighbour blip-blip and blip-sojourn correlations. This model is known to give better results than NIBA in the moderate-to-strong damping regime.

In the range of weak coupling and low-temperature, however, the above mentioned schemes fail to properly describe the dynamics of a biased TLS, e.g. a symmetry breaking at zero temperature even for vanishing asymmetries is predicted. In this regime, path-integral methods [14, 15, 74] as well as the Bloch-Redfield formalism [16] are used, where an expansion to lowest order in the coupling strength between system and bath is performed. Both methods have been shown to yield the same dynamics for weak Ohmic damping [75].

Recently, the spin-boson dynamics at low temperatures and very weak coupling for Ohmic damping within the lowest-order Born approximation and its next-order corrections has been explored [39].

To date, only numerical theories [17, 76, 77, 78, 79] can provide a description of the TLS dynamics, being capable to smoothly match between the high and the weak-coupling regimes. However, ab-initio calculations can become costly if the regime of low temperatures or the long time dynamics are investigated.

In this Chapter we propose a novel approximation scheme, which we call *weakly-interacting blip approximation* (WIBA), capable to bridge between the weak-coupling and strong-coupling theories. It is based on the observation that bath-induced correlations among "blips" and between "blips" and "sojourns" are intrinsically weak. Thus, in the WIBA, those correlations are included up to first order only. As in the NIBA, the time evolution of the population difference $P(t)$ is given by the general master equation (GME) ($t \geq 0$)

$$\dot{P}(t) = -\int_0^t dt' [K^a(t-t') - W(t-t') + K^s(t-t')P(t')] \,, \tag{3.1}$$

where the irreducible WIBA kernels K^s and K^a are, respectively, symmetric and antisymmetric with respect to an external bias ε. The kernel W accounts for the initial preparation. As discussed below, such kernels are neither perturbative in the tunneling matrix Δ nor in the TLS-bath coupling, see Eqs. (3.66), (3.64) and (3.67).

Since the inter-blip and blip-sojourn correlations become negligible at high temperatures or large system-bath coupling, the WIBA well matches the NIBA predictions in this regime. On the other hand, at low temperatures and couplings such correlations, neglected in the NIBA, become essential to properly describe the dynamics. In this limit, WIBA perfectly agrees with the predictions of the weak-coupling theories. Finally, in the intermediate coupling and temperature regime where the perturbative approaches fail, the WIBA yields

a good agreement with predictions of *ab-initio* calculations.

The Chapter is organized as follows: In Sec. 3.1 we introduce the well-known spin-boson model. Then, in Sec. 3.2, starting from the path-integral expression for the RDM derived in Chapter 2, we discuss an exact series expression for the expectation value of the system "coordinate" $P(t)$. Since the exact expression is very nontrivial, the following Sections are dedicated to some approximation schemes. In Sec. 3.3, an extended version of the familiar non-interacting blip approximation (*extended*-NIBA) is presented. There we derive a prescription to calculate the kernels entering an equation of the form (3.1). Sec. 3.4 finally contains a major findings of this Chapter. There we introduce the WIBA, which is able to bridge between the weak and strong coupling regimes within the same theory. The WIBA kernels entering (3.1) are found in analytical form. A comparison with predictions of *ab-initio* Quasi-Adiabatic Path-Integral (QUAPI) calculations [17] shows that the WIBA covers a wide spectrum of parameters and constitutes an interpolation between the NIBA and weak-coupling approximation schemes.

3.1 The spin-boson model

In this Section, the spin-boson model is shortly reviewed, and the dynamical variables of interest are defined. To start, we consider the pseudo-spin Hamiltonian in the "localized basis" $\{|L\rangle, |R\rangle\}$,

$$\hat{\mathbf{H}}_0 = \frac{\hbar}{2}[\varepsilon\hat{\sigma}_z - \Delta\hat{\sigma}_x]\,, \tag{3.2}$$

with $\hat{\sigma}_z$ and $\hat{\sigma}_x$ the Pauli matrices and $\hbar\Delta$ the energy separation of the two levels at zero bias ($\varepsilon = 0$) which accounts for the *tunneling* dynamics. Thus, we can interpret $\hat{\sigma}_z$ as a "position" operator such that $\langle L|\sigma_z|L\rangle = -1$ and $\langle R|\sigma_z|R\rangle = +1$. The localized representation $\{|L\rangle, |R\rangle\}$ and the energy representation $\{|g\rangle, |e\rangle\}$, with $|g\rangle, |e\rangle$ ground and excited states, respectively, are related by Eq. (2.9).

We choose to model the environment as an ensemble of harmonic oscillators [13, 12, 3] which linearly couple to the system "position coordinate" σ_z, ending up with a bath Hamiltonian $\mathbf{H}_\mathrm{B}$ of the form, including also the interaction between bath and system, given in Eq. (2.3). The whole system is thus described by the well known spin-boson Hamiltonian $\mathbf{H} = \mathbf{H}_0 + \mathbf{H}_\mathrm{B}$. In the case of a thermal equilibrium bath, its influence on the system is fully characterized by the spectral density, which becomes a continuous function once the number $\mathcal{N}$ of harmonic oscillators approaches infinity. Throughout this Chapter, we choose

spectral densities with power-law behavior at low frequencies, i.e. ($s > 0$)

$$G(\omega) = 2\delta_s \omega_{\rm ph}^{1-s} \omega^s e^{-|\omega|/\omega_c} \,, \tag{3.3}$$

with δ_s being a dimensionless coupling parameter, $\omega_{\rm ph}$ a characteristic phonon frequency, and ω_c the bath cut-off frequency which is taken to be the largest frequency in the model. Thus, this class encompasses the commonly considered Ohmic spectrum with exponential cutoff $G(\omega) = 2\alpha\omega e^{-|\omega|/\omega_c}$, with $\alpha = \delta_1$ being the so called Kondo parameter of the TLS.

The spin-boson spectral density $G(\omega)$ defined here is related to the spectral density of the continuous model $J(\omega)$ defined in Eq. (5.1) through the relation

$$G(\omega) = \frac{q_0^2}{\pi\hbar} J(\omega) \,, \tag{3.4}$$

and has dimension frequency now.

As already seen in the Chapter 2, in order to describe the system's dynamics, we focus on the time evolution of the reduced density matrix $\rho(t) = {\rm tr}_{\rm B}\, \mathbf{W}(t)$. The initial preparation requires some attention [12]. One could distinguish two different preparations, according to the time when the coupling between system and bath is switched on, which we assume to happen at a time $t_0 \leq 0$. In the first one, which we refer as "class A", the bath is in canonical equilibrium and the system is being prepared at time $t_0 = 0$ in a certain state, e.g. corresponding to $\sigma_z = +1$. Then, the system evolves out of the state before the environment has relaxed to the shifted equilibrium distribution. This initial preparation is the typical situation in electron transfer reactions when a specific electronic donor is suddenly prepared by photoinjection [80]. The other situation, "class B", is when the system has been held for a long time in a certain state, e.g. $\sigma_z = +1$, so that the bath had time enough to thermalize with the system. It corresponds to choose $t_0 \to -\infty$. Then, at time $t = 0$, the constraint is released and the system evolves with the spin-boson Hamiltonian. This initial preparation is performed, e.g. in rf-SQUID devices by a suitable choice of an external magnetic field. We shall refer ourselves to the latter initial preparation throughout the work.

In the spin-boson model, the sum over the populations in Eq. (2.13) just reduces to the simple expression

$$P_R(t) = \rho_{\sigma_f=1,\sigma'_f=1}(t) \equiv \rho_{RR}(t) \,. \tag{3.5}$$

Hence, the dynamical quantity of interest measured in the experiments, i.e. the expectation value of the pseudo-spin operator $\langle\sigma_z(t)\rangle$, becomes $P(t) = \rho_{RR}(t) - \rho_{LL}(t)$.

3.2 Real-time path-integral approach to the dynamics

In this Section we recall the main steps yielding an exact series expression for $P(t)$, obtained within the path-integral approach.

3.2.1 Influence functional and bath correlation function

As we already anticipated, we assume a factorized initial condition at time $t = 0$. For such initial condition, the exact formal solution for the RDM can be expressed in terms of a real time double path integral over piecewise constant forward $\sigma(\tau)$ and backward $\sigma'(\tau)$ spin paths [12, 13, 63] with values ± 1, in analogy to Eq. (2.14). Notice that for the two-state system $\mathbf{q} = (q_0/2)\hat{\sigma}_z$, the distance between the minima of the two wells being reabsorbed in the coupling constant, which is therefore dimensionless. The effects of the environment are in an influence functional inducing non-local in time correlations between different path segments. Upon introducing the linear combinations $\chi(\tau) = [\sigma(\tau) + \sigma'(\tau)]/2$, and $\xi(\tau) = [\sigma(\tau) - \sigma'(\tau)]/2$, the population difference reads

$$P(t) = \int \mathcal{D}\xi \mathcal{D}\chi \mathcal{A}[\xi, \chi] \exp\{\Phi[\xi, \chi]\} , \tag{3.6}$$

where $\mathcal{A}$ is the path weight in the absence of coupling with the bath. A generic double path

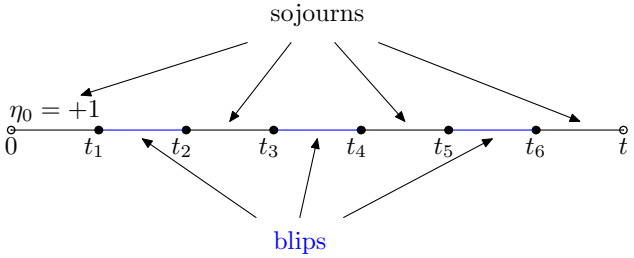

Figure 3.1: Generic path with $2n = 6$ transitions at flip times $t_1, t_2, \ldots, t_{2n}$. The system is in an off-diagonal state (blip) of the reduced density matrix (RDM) in the time intervals $t_{2j} - t_{2j-1}$ (blue online) and in a diagonal state (sojourn) during the intervals $t_{2j+1} - t_{2j}$. Due to the initial preparation, the initial sojourn obeys the constraint $\chi_0 = +1$.

can now be visualized as a single path over the four-states of the reduced density matrix, i.e. the sojourns ($\chi(\tau) = \pm 1, \xi(\tau) = 0$) and the blips ($\chi(\tau) = 0, \xi(\tau) = \pm 1$) [13], see Fig. (3.1). Due to the initial condition, the path sum runs over all paths with boundary conditions $\xi(0) = \xi(t) = 0$ and $\chi(0) = 1$, $\chi(t) = \pm 1$. Environmental effects are included in the influence functional (2.15), with the bath correlation function $Q = S + iR$ being

$$Q(t) = \int_0^\infty d\omega \frac{G(\omega)}{\omega^2} \Big[\coth\Big(\frac{\hbar\omega}{2k_{\rm B}T}\Big)(1-\cos\omega t) + i\sin\omega t \Big] \tag{3.7}$$

and $Q_{j,k} := Q(t_j - t_k)$. For the class of spectral densities considered in Eq. (3.3), the functions S and R read [74]

$$\begin{aligned} S(t) = 2\delta_s \Gamma(s-1) \Bigg\{ \Big(\frac{\omega_c}{\omega_{\rm ph}}\Big)^{s-1} \Big[1 - \big(1+(\omega_c t)^2\big)^{\frac{1-s}{2}} \\ \times \cos\big[(s-1)\arctan(\omega_c t)\big] \Big] + (\hbar\beta\omega_{\rm ph})^{1-s} \Big[2\zeta(s-1, 1+\kappa) \\ - \zeta\Big(s-1, 1+\kappa+i\frac{t}{\hbar\beta}\Big) - \zeta\Big(s-1, 1+\kappa-i\frac{t}{\hbar\beta}\Big) \Big] \Bigg\}, \end{aligned} \tag{3.8}$$

and

$$\begin{aligned} R(t) = 2\delta_s \Gamma(s-1) \Big(\frac{\omega_c}{\omega_{\rm ph}}\Big)^{s-1} \\ \times \big(1+(\omega_c t)^2\big)^{\frac{1-s}{2}} \sin\big[(s-1)\arctan(\omega_c t)\big], \end{aligned} \tag{3.9}$$

where $\Gamma(z)$ is the Euler's gamma function and $\zeta(q,z)$ is the Riemann's generalized zeta function [81]. Moreover, $\kappa = 1/\hbar\beta\omega_c$ becomes important as the ratio $k_{\rm B}T/\hbar\omega_c$ becomes large.

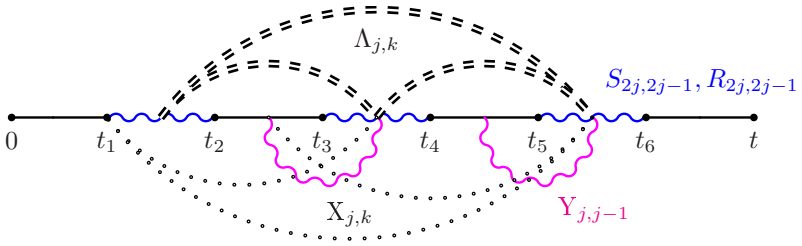

Figure 3.2: Bath-induced non-local in time correlations among tunneling transitions. The interactions $S_{2j,2j-1}$, $R_{2j,2j-1}$ and $Y_{j,j-1}$ (intra-dipole and blip-preceeding-sojourn interactions) which appear in the influence phase $\Phi_{\rm intra,bps}$, cf. Eq. (3.10), are symbolized by the wiggled lines (blue and magenta online, respectively). The double-dashed lines denote the inter-dipole interactions $\Lambda_{j,k}$, while the bold-dotted lines are the remaining blip-sojourn interactions $X_{j,k}$ contained in the influence phase $\Phi_{\rm inter}$, cf. Eq. (3.14).

For a generic path with $2n$ transitions at times t_j, $j = 1, 2, ..., 2n$, one finds $\dot{\xi}(\tau) = \sum_{j=1}^{2n} \xi_j \delta(\tau - t_j)$ and $\dot{\chi}(\tau) = \sum_{j=0}^{2n} \chi_j \delta(t - t_j)$. Here is $\chi_0 = 1$ due to the initial preparation

and $\xi_j = \pm 1$, $\chi_j = \pm 1$ for $j > 0$. Because $\xi_{2j} = -\xi_{2j-1}$, the influence function in (2.15) becomes $\Phi^{(n)} = \Phi^{(n)}_{\rm intra,bps} + \Phi^{(n)}_{\rm inter}$ (Fig. 3.2). The function $\Phi^{(n)}_{\rm intra,bps}$ describes intra-blip and blip-preceeding sojourn correlations, and reads

$$\begin{aligned} \Phi^{(n)}_{\rm intra,bps} &= -\sum_{j=1}^{n}\Big[S_{2j,2j-1} - i\xi_j\chi_{j-1}X_{j,j-1}\Big] \\ &= \Phi^{(n)}_{\rm intra} + \Phi^{(n)}_{\rm bps}\,, \end{aligned} \tag{3.10}$$

$$\Phi^{(n)}_{\rm intra} = -\sum_{j=1}^{n}\Big[S_{2j,2j-1} - i\xi_j\chi_{j-1}R_{2j,2j-1}\Big]\,, \tag{3.11}$$

$$\Phi^{(n)}_{\rm bps} = i\sum_{j=1}^{n}\xi_j\chi_{j-1}Y_{j,j-1}\,, \tag{3.12}$$

where we split $X_{j,j-1} = R_{2j,2j-1} + Y_{j,j-1}$, with

$$Y_{j,j-1} = R_{2j-1,2j-2} - R_{2j,2j-2}\,. \tag{3.13}$$

Moreover, the functional $\Phi^{(n)}_{\rm inter}$ accounts for inter-blip and blip-sojourns interactions [13, 12]

$$\Phi^{(n)}_{\rm inter} = -\sum_{j=2}^{n}\sum_{k=1}^{j-1}\xi_j\xi_k\Lambda_{j,k} + i\sum_{j=2}^{n}\sum_{k=0}^{j-2}\xi_j\chi_k X_{j,k}\,. \tag{3.14}$$

The function $\Lambda_{j,k}$ contains the blip-blip interactions between the flip pairs $\{j,k\}$, while the blip-sojourn interaction $X_{j,k}$ yields a phase factor. To be definite, for $k > 0$,

$$\Lambda_{j,k} = S_{2j,2k-1} + S_{2j-1,2k} - S_{2j,2k} - S_{2j-1,2k-1}, \tag{3.15a}$$

$$X_{j,k} = R_{2j,2k+1} + R_{2j-1,2k} - R_{2j,2k} - R_{2j-1,2k+1}, \tag{3.15b}$$

The correlations $X_{j,0}$ depend on the initial preparation, being of class A or B [12].

3.2.2 Exact series expression for $P(t)$

The summation over the path histories reduces to an expansion in the number of tunneling transitions yielding a formally exact series expression for the population difference

$P(t)$ [12, 13]. It reads (here we identify χ_{2n} with χ_f)

$$P(t) = \sum_{\chi_f=\pm 1} \chi_f J(\chi_f, t; \chi_0 = 1, 0)\,, \tag{3.16}$$

with the conditional propagating function being

$$\begin{aligned} J(\chi_f, t; \chi_0 = 1, 0) = \delta_{\chi_f,\chi_0} + \sum_{n=1}^{\infty} \int_0^t \mathcal{D}\{t_j\} \left(-\frac{\Delta^2}{2^2}\right)^n \\ \times \sum_{\{\xi_j=\pm 1\}} B_n \sum_{\{\chi_j=\pm 1\}'} \exp\{\Phi^{(n)}\} \Bigg]\,, \end{aligned} \tag{3.17}$$

with $B_n \equiv \exp\left\{-\mathrm{i}\varepsilon \sum_{j=1}^n \xi_j \tau_j\right\}$, and where we defined $\tau_j \equiv t_{2j} - t_{2j-1}$. In (3.17), n counts the number of blips and the prime in $\{\chi_j = \pm 1\}'$ means that the sum does not run over the initial and final sojourns, since they are fixed. Moreover,

$$\int_0^t \mathcal{D}\{t_j\} \equiv \int_0^t dt_{2n} \int_0^{t_{2n}} dt_{2n-1} \ldots \int_0^{t_2} dt_1\,. \tag{3.18}$$

Performing the summation over the intermediate sojourns, one gets for the population difference [12, 13]:

$$\begin{aligned} P(t) = 1 + \sum_{n=1}^{\infty} \int_0^t \mathcal{D}\{t_j\} \left(-\frac{\Delta^2}{2}\right)^n \\ \times \sum_{\{\xi_j=\pm 1\}} \left(F_n^{(+)} B_n^{(s)} + F_n^{(-)} B_n^{(a)}\right)\,, \end{aligned} \tag{3.19}$$

where $B_n^{(s)} \equiv \cos\left(\varepsilon \sum_{j=1}^n \xi_j \tau_j\right)$, $B_n^{(a)} \equiv \sin\left(\varepsilon \sum_{j=1}^n \xi_j \tau_j\right)$ and

$$F_n^{(+)} \equiv G_n \prod_{k=0}^{n-1} \cos(\phi_{k,n}), \tag{3.20a}$$

$$F_n^{(-)} \equiv G_n \sin(\phi_{0,n}) \prod_{k=1}^{n-1} \cos(\phi_{k,n})\,, \tag{3.20b}$$

with $\phi_{k,n} \equiv \sum_{j=k+1}^n \xi_j X_{j,k}$ and

$$G_n \equiv \exp\left\{\mathfrak{Re}\left[\Phi^{(n)}\right]\right\} \tag{3.21}$$

$$= \exp\left\{ -\sum_{j=1}^{n} S_{2j,2j-1} - \sum_{j=2}^{n}\sum_{k=1}^{j-1} \xi_j \xi_k \Lambda_{j,k} \right\}. \tag{3.22}$$

The expression (3.19) is still practically untractable. Thus, it is necessary to perform some approximations to describe the TLS dynamics. Two novel approximation schemes are discussed in the coming Sections 3.3 and 3.4.

3.3 The extended Non-Interacting Blip Approximation

In this section we want to discuss an improvement to the familiar non-interacting blip approximation (NIBA) [12, 13], which better treats the blip-preceeding sojourns interactions. We call our more refined approximation scheme "*extended*-NIBA" (see Fig. 3.3). As we shall see, as the NIBA, the *extended*-NIBA enables to recast the series expression for $P(t)$ into a generalized master equation (GME) of the form (3.1) with kernels of second order in the level splitting Δ.

The advantage of the NIBA relies on its extreme simplicity and on its non-perturbative in the coupling to the bath character. Hence, the non-interacting blip approximation is a popular approximation scheme. Nevertheless, although it works in the whole regime of coupling strength and temperatures for a symmetric system, it has some intrinsic weaknesses in the asymmetric case (i.e. $\varepsilon \neq 0$) for low temperature and weak coupling. For example, NIBA predicts the unphysical asymptotic limit $\sigma_{z,\mathrm{N}}^{\infty} = -\tanh(\frac{\hbar\beta\varepsilon}{2})$, implying a localization of the TLS ($\sigma_{z,\mathrm{N}}^{\infty} = -1$) at zero temperature even for vanishing asymmetries.

The limits of validity of the theory are still dim, this approximation holding whenever the average time spent in a diagonal state (sojourn) $\langle s \rangle$ is very large compared to the average time spent in an off-diagonal state (blip) $\langle \tau \rangle$. Within the NIBA, the full inter-blip correlations $\Lambda_{j,k}$ and the blip-sojourn interactions $X_{j,k}$ with $j \neq k+1$ are neglected ($\Phi_{\mathrm{inter}}^{(n)} \approx 0$). The blip-preceeding-sojourn interactions $Y_{j,j-1}$ in Eq. (3.13) are neglected as well (see Fig. 3.3a). Hence, $G_n \approx \exp\left\{ \mathfrak{Re}\left[\Phi_{\mathrm{intra}}^{(n)} \right] \right\}$. The explicit form of the NIBA kernel is given in App. A.

In the following Sec. 3.4, we shall introduce a novel approximation scheme, the weakly-interacting blip approximation (WIBA), capable to overcome these drawbacks. Before doing this, however, we need to introduce the *extended*-NIBA where, as in NIBA, is $\Phi_{\mathrm{inter}}^{(n)} \approx 0$, but the blip-preceeding-sojourn correlations $Y_{j,j-1}$ are retained, despite in approximate form.

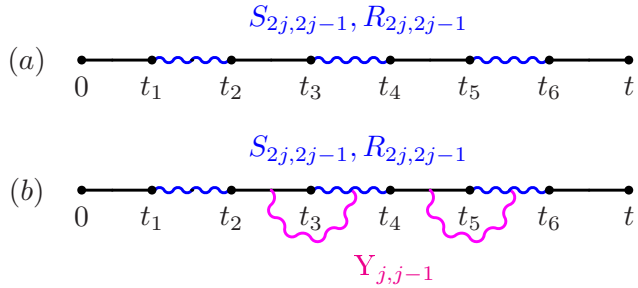

Figure 3.3: Generic path and bath-induced correlations retained in the NIBA (a) and in the *extended*-NIBA (b). In both approximations the inter-blip and blip-sojourns correlations $\Lambda_{j,k}$ and $X_{j,k}$, respectively, which appear in the influence phase $\Phi_{\rm inter}$ (see Eq. (3.10)), are neglected. Within the *extended*-NIBA the blip-preceeding-sojourn interaction $Y_{j,j-1}$ (magenta online), which contributes to the influence phase $\Phi_{\rm bps}$ (see Eq. (3.12)) and is being neglected in the NIBA, is retained. The first sojourn is treated differently, according to the initial preparation (here we choose the preparation of "class B").

3.3.1 Series expression within the *extended*-NIBA

After performing the sum over the blip indices $\xi_j = \pm 1$ in Eq. (3.19), the *extended*-NIBA prescription $\Phi^{(n)}_{\rm inter} = 0$ yields for the probability difference $P_{\rm eN}(t)$:

$$\begin{aligned} P_{\rm eN}(t) = 1 + \sum_{n=1}^{\infty} (-1)^n \int_0^t \mathcal{D}\{t_j\}[g(\tau_1, s_0) \\ + h(\tau_1, s_0)] \prod_{j=2}^{n} g(\tau_j, s_{j-1}) \,, \end{aligned} \tag{3.23}$$

where $\tau_j := t_{2j} - t_{2j-1}$ and $s_j := t_{2j+1} - t_{2j}$ denote the blip and the sojourn lengths, respectively. The *extended*-NIBA kernels are defined as

$$\begin{aligned} g(\tau_j, s_{j-1}) &= \Delta^2 \mathrm{e}^{-S(\tau_j)} \cos(\varepsilon\tau_j) \cos[X_{j,j-1}] \,, \\ h(\tau_j, s_{j-1}) &= \Delta^2 \mathrm{e}^{-S(\tau_j)} \sin(\varepsilon\tau_j) \sin[X_{j,j-1}] \,. \end{aligned} \tag{3.24}$$

Remember that $X_{j,j-1} = R(\tau_j) - R(\tau_j + s_{j-1}) + R(s_{j-1})$. The functions $g(\tau_1, s_0)$ and $h(\tau_1, s_0)$ explicitly depend on the length s_0 of the initial sojourn, and assume a different form for preparation class A and B.

In the following, we choose a factorized initial condition at time $t = 0$ with the particle being held at the site $|R\rangle$ ($\sigma_z = +1$) from time $t_0 = -\infty$ till $t = 0$ (class B), which amounts

to consider $s_0 \to \infty$. Hence, Eq. (3.24) for $j = 1$ reads

$$\begin{aligned} g(\tau_1, s_0 \to \infty) &= \Delta^2 \mathrm{e}^{-S(\tau_1)} \cos(\varepsilon\tau_1) \cos[R(\tau_1)] \equiv g_{\mathrm{N}}(\tau_1) \,, \\ h(\tau_1, s_0 \to \infty) &= \Delta^2 \mathrm{e}^{-S(\tau_1)} \sin(\varepsilon\tau_1) \sin[R(\tau_1)] \equiv h_{\mathrm{N}}(\tau_1) \,, \end{aligned} \tag{3.25}$$

being independent of s_0. Notice that $g_{\mathrm{N}}(\tau_1)$ and $h_{\mathrm{N}}(\tau_1)$ coincide with the symmetric and antisymmetric NIBA kernels, respectively (cf. Eq. (A.1)).

Due to the convolutive structure of Eq. (3.23), it is easier to evaluate the probability difference upon Laplace transformation. By exchanging the integration order and performing some change of variables, one gets

$$\begin{aligned} \hat{P}_{\mathrm{eN}}(\lambda) = \frac{1}{\lambda} + \sum_{n=1}^{\infty} (-1)^n \int_0^{\infty} \mathcal{D}_{\infty}\{\tau_j, s_{j-1}\} \\ \times [g(\tau_1, s_0) + h(\tau_1, s_0)] \prod_{j=2}^{n} g(\tau_j, s_{j-1}) \,, \end{aligned} \tag{3.26}$$

where $\hat{P}(\lambda) \equiv \int_0^{\infty} dt \, \exp[-\lambda t] P(t) = \mathcal{L}_t\{P(t)\}$ and

$$\begin{aligned} &\int_0^{\infty} \mathcal{D}_{\infty}\{\tau_j, s_{j-1}\} \equiv \int_0^{\infty} ds_n \int_0^{\infty} d\tau_n \int_0^{\infty} ds_{n-1} \\ &\times \ldots \int_0^{\infty} ds_1 \int_0^{\infty} d\tau_1 \int_0^{\infty} ds_0 \, \mathrm{e}^{-\lambda(\sum_{j=1}^{n}(\tau_j + s_{j-1}) + s_n)} \\ &= \int_0^{\infty} ds_n \mathrm{e}^{-\lambda s_n} \\ &\times \int_0^{\infty} d\xi_n \mathrm{e}^{-\lambda\xi_n} \int_0^{\xi_n} d\tau_n \ldots \int_0^{\infty} d\xi_1 \mathrm{e}^{-\lambda\xi_1} \int_0^{\xi_1} d\tau_1 \,, \end{aligned} \tag{3.27}$$

with $\xi_j \equiv \tau_j + s_{j-1}$ the length of each blip plus its preceeding sojourn. Let us introduce the functions

$$F(\xi_j) \equiv \int_0^{\xi_j} d\tau_j \, g(\tau_j, \xi_j - \tau_j) \,, \quad j > 1, \tag{3.28a}$$

$$F_0(\xi_1) \equiv \int_0^{\xi_1} d\tau_1 \, g_{\mathrm{N}}(\tau_1) \,, \tag{3.28b}$$

$$A_0(\xi_1) \equiv \int_0^{\xi_1} d\tau_1 \, h_{\mathrm{N}}(\tau_1) \,, \tag{3.28c}$$

noticing that $X_{j,j-1} = R(\tau_j) - R(\xi_j) + R(\xi_j - \tau_j)$. Then $\hat{P}(\lambda)$ assumes the form

$$\begin{aligned}\hat{P}_{\rm eN}(\lambda) = \frac{1}{\lambda} + \frac{1}{\lambda}\sum_{n=1}^{\infty}\prod_{j=2}^{n}\left[-\mathcal{L}_{\xi_j}F(\xi_j)\right](\lambda) \\ \times\left\{-\mathcal{L}_{\xi_1}\left[F_0(\xi_1)+A_0(\xi_1)\right]\right\}(\lambda),\end{aligned} \tag{3.29}$$

where the $1/\lambda$ comes from the free last sojourn s_n, or equivalently

$$\hat{P}_{\rm eN}(\lambda) = \frac{1}{\lambda} - \frac{1}{\lambda}\sum_{n=1}^{\infty}[-\hat{F}(\lambda)]^{n-1}[\hat{F}_0(\lambda)+\hat{A}_0(\lambda)] \tag{3.30}$$

$$= \frac{1}{\lambda} - \frac{1}{\lambda}\frac{\hat{F}_0(\lambda)+\hat{A}_0(\lambda)}{1+\hat{F}(\lambda)}. \tag{3.31}$$

It is convenient to introduce the functions $\hat{K}^a_{\rm eN}(\lambda) \equiv \lambda\hat{A}_0(\lambda)$, $\hat{K}^s_{\rm eN}(\lambda) \equiv \lambda\hat{F}(\lambda)$ and $\hat{W}_{\rm eN}(\lambda) \equiv \lambda\left[\hat{F}(\lambda) - \hat{F}_0(\lambda)\right]$. Then Eq. (3.31) becomes

$$\hat{P}_{\rm eN}(\lambda) = \frac{1 - \dfrac{\hat{K}^a_{\rm eN}(\lambda) - \hat{W}_{\rm eN}(\lambda)}{\lambda}}{\lambda + \hat{K}^s_{\rm eN}(\lambda)}\,. \tag{3.32}$$

3.3.2 Generalized master equation (GME) for the *extended*-NIBA

Eq. (3.32) can be easily transformed back to the time domain. We find

$$\dot{P}_{\rm eN}(t) = -\int_0^t dt'[K^a_{\rm eN}(t-t') - W_{\rm eN}(t-t') + K^s_{\rm eN}(t-t')P_{\rm eN}(t')]\,, \tag{3.33}$$

with *extended*-NIBA kernels defined as

$$K^s_{\rm eN}(t) \equiv \frac{d}{dt}F(t) := \dot{F}(t), \tag{3.34a}$$

$$K^a_{\rm eN}(t) \equiv \frac{d}{dt}A_0(t) := \dot{A}_0(t), \tag{3.34b}$$

$$K^s_{0,\rm eN}(t) \equiv \frac{d}{dt}F_0(t) := \dot{F}_0(t), \tag{3.34c}$$

$$W_{\rm eN}(t) \equiv K^s_{\rm eN}(t) - K^s_{0,\rm eN}(t)\,. \tag{3.34d}$$

Although the time derivatives (3.34) can be straightforwardly calculated from Eqs. (3.28), the explicit dependence of the function $g(\tau_j, \xi_j - \tau_j)$ on ξ_j still implies an integral form for the function $\dot{F}(\xi_j)$. An approximate form of $\dot{F}(\xi_j)$ can be obtained if we

observe that the blip length $\langle\tau\rangle$ is suppressed by the intra-blip interaction $\exp[-S(\tau)]$ in the integrands of Eq. (3.28) and that the imaginary part of the bath correlation function $R(\tau)$, Eq. (3.9), slightly deviates from a constant. Hence, we approximate

$$-R(\xi_j) + R(\xi_j - \tau_j) \approx -\tau_j \dot{R}(\xi_j) + \mathcal{O}[\tau_j^2 \ddot{R}(\xi_j)] \,. \tag{3.35}$$

Corrections proportional to the second derivative of $R(t)$ have been neglected. The functions $g(\tau_j, s_j)$ and $h(\tau_j, s_j)$ defined in Eq. (3.24) become ($j > 1$)

$$\begin{aligned} g(\tau_j, \xi_j - \tau_j) &\approx \tilde{g}(\tau_j, \xi_j) \\ &:= \Delta^2 \mathrm{e}^{-S(\tau_j)} \cos(\varepsilon\tau_j) \cos[R(\tau_j) - \tau_j \dot{R}(\xi_j)] \,, \\ h(\tau_j, \xi_j - \tau_j) &\approx \tilde{h}(\tau_j, \xi_j) \\ &:= \Delta^2 \mathrm{e}^{-S(\tau_j)} \sin(\varepsilon\tau_j) \sin[R(\tau_j) - \tau_j \dot{R}(\xi_j)] \,, \end{aligned} \tag{3.36}$$

the corrections being of order $\mathcal{O}[\tau_j^2 \ddot{R}(\xi_j)]$. In particular, we define $g_{\mathrm{eN}}(\xi_j)$ and $h_{\mathrm{eN}}(\xi_j)$ as

$$\begin{aligned} g_{\mathrm{eN}}(\xi_j) &\equiv \tilde{g}(\xi_j, \xi_j) = \Delta^2 \mathrm{e}^{-S(\xi_j)} \cos(\varepsilon\xi_j) \cos[\tilde{R}(\xi_j)] \,, \\ h_{\mathrm{eN}}(\xi_j) &\equiv \tilde{h}(\xi_j, \xi_j) = \Delta^2 \mathrm{e}^{-S(\xi_j)} \sin(\varepsilon\xi_j) \sin[\tilde{R}(\xi_j)] \,, \end{aligned} \tag{3.37}$$

where $\tilde{R}(t) \equiv R(t) - t\dot{R}(t)$. The extended-NIBA kernels, obtained as prescribed by Eqs. (3.34) and (3.35), then read

$$K^s_{\mathrm{eN}}(t) := g_{\mathrm{eN}}(t) \,, \tag{3.38a}$$

$$K^a_{\mathrm{eN}}(t) := h_{\mathrm{eN}}(t) \,, \tag{3.38b}$$

$$K^s_{0,\mathrm{eN}}(t) := g_{\mathrm{N}}(t) \,, \tag{3.38c}$$

$$W_{\mathrm{eN}}(t) := g_{\mathrm{eN}}(t) - g_{\mathrm{N}}(t) \,. \tag{3.38d}$$

The irreducible kernel $K^s_{\mathrm{eN}}(t)$ entering the *extended*-NIBA master equation (3.33) is shown in Fig. 3.4b. The irreducible NIBA kernel $K^s_{\mathrm{N}}(t)$, Eq. (A.1a), is depicted in Fig.

Figure 3.4: Irreducible kernel $K^{(s)}(t)$ in the NIBA (a) and in the *extended*-NIBA (blue online) (b). The *extended*-NIBA kernel is obtained from the NIBA one by replacing the function $R(t)$ with $\tilde{R}(t) \equiv R(t) - t\dot{R}(t)$. Hence, the blip becomes "dressed".

3.4a. As discussed in App. A, within the NIBA an analogous GME as in (3.33) is obtained where, due to the approximation $\Phi^{(n)}_{\rm bps} = 0$, is $W_{\rm N}(t) = 0$.

The extended-NIBA kernels $K^s_{\rm eN}$ and $K^a_{\rm eN}$ differ from the conventional NIBA ones, $K^s_{\rm N}$ and $K^a_{\rm N}$, by the replacing of the imaginary part of the bath correlation function $R(t)$ with the "dressed" one $\tilde{R}(t) \equiv R(t) - t\dot{R}(t)$ (see Fig. 3.4b). At small coupling strength, the NIBA is recovered, since blip-preceeding-sojourn correlations become negligible. Despite its simplicity, however, the *extended*-NIBA already yields an improvement to the NIBA in the intermediate coupling regime (see Fig. 3.5).

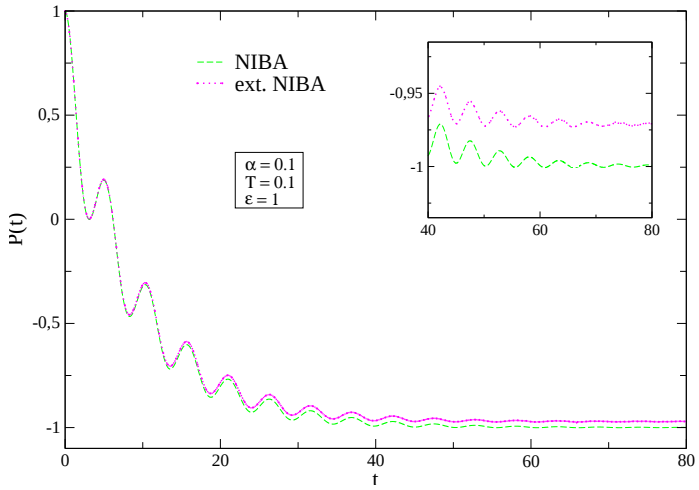

Figure 3.5: A comparison between the standard NIBA and the *extended*-NIBA for an Ohmic bath ($s = 1$) is shown. The parameters are: $\alpha = 0.1$ (dimensionless), $T = 0.1$, $\varepsilon = 1$ (in units of the tunneling frequency Δ). One can see that in the chosen intermediate parameter regime the *extended*-NIBA coincides with the conventional one at short times. However, it predicts a different asymptote from the NIBA one (see inset). Hence, at moderate damping and temperatures, the blip-preceeding-sojourn correlations retained in the *extended*-NIBA become important.

3.4 The Weakly-Interacting Blip Approximation (WIBA)

To bridge between the strong damping situation described by the NIBA and the extremely underdamped case we observe that, for spectral densities of the form (3.3), the blip-blip interaction terms $\Lambda_{j,k}$ as well as the blip-sojourn terms $X_{j,k}$ ($k \neq j-1$) are intrinsically small. Therefore, we propose a novel approximation scheme, which we call weakly-interacting blip approximation (WIBA). Within the WIBA, the full $\Phi^{(n)}_{\rm intra,bps}$ is retained as in the *extended*-NIBA and one expands the influence functional $\exp\{\Phi^{(n)}_{\rm inter}\}$ up

to linear order in the blip-blip and blip-preceeding sojourns interactions $\Lambda_{j,k}$ and $X_{j,k}$ (see Fig. 3.6). Hence,

$$\exp\{\Phi^{(n)}\} \approx \exp\{\Phi^{(n)}_{\rm intra,bps}\}\left(1+\Phi^{(n)}_{\rm inter}\right). \tag{3.39}$$

In other terms, all contributions which involve $\phi_{k,n}$ (cf. Eq. (3.20)) must be expanded up to first order in $X_{j,k}$, $j > k+2$, and $G_n \approx \exp\left\{\mathfrak{Re}\left[\Phi^{(n)}_{\rm intra,bps}\right]\right\}\left(1+\mathfrak{Re}\left[\Phi^{(n)}_{\rm inter}\right]\right)$ (cf. Eq. (3.21)). All terms of the order ΛX or higher are neglected. As usual, the first sojourn and blip must be treated differently from the others, according to the initial preparation.

The inter-blip and blip-sojourns correlations $\Lambda_{j,k}$ and $X_{j,k}$ are known to become essential to properly describe the dynamics of a *biased* TLS at low temperatures [74, 14, 15]. Specifically, in [15] a systematic weak-coupling approximation (WCA) was developed where *all* bath-induced correlations were linearized: $\exp\{\Phi^{(n)}\} \approx 1+\Phi^{(n)}$. It was shown in [75] that the WCA exactly matches results obtained within the lowest-order Born approximation for weak-coupling to an Ohmic bath.

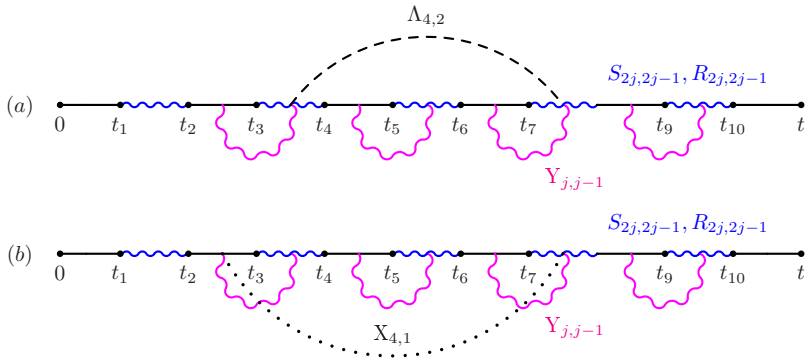

Figure 3.6: Generic paths and bath-induced correlations retained in the WIBA. The linearized influence functional $\Phi^{(n)}_{\rm inter}$ yields one single blip-blip correlation (a) or blip-sojourns interaction (b) for each path.

Hence, the WIBA constitutes an improvement of the *extended*-NIBA on one side and of the WCA on the other. At high temperatures, where the dipole-dipole interactions are negligible, the WIBA kernels reduce to the *extended*-NIBA ones. By expanding the WIBA kernels to first order in δ_s, the weak damping kernels in [14, 15] are recovered.

In contrast to the *extended*-NIBA or the weak-coupling approximation, the WIBA has no small parameter in a strict sense, and it is based on the consideration that the correlations $\Phi^{(n)}_{\rm inter}$ are intrinsically weak over the whole parameter regime. As we show below, the WIBA indeed well describes the TLS dynamics over a wide parameter range.

3.4.1 Series expression within the WIBA

Let us again start from Eq. (3.19) and apply the WIBA prescription. After performing the sum over the indices $\xi_j = \pm 1$ we then find

$$\begin{aligned} P_{\rm WIBA}(t) = 1 &+ \int_0^t dt_2 \int_0^{t_2} dt_1 [-(g_1 + h_1)] \\ &+ \sum_{n=2}^{\infty} (-1)^n \int_0^t \mathcal{D}\{t_j\} \Bigg\{ (g_1 + h_1) \left(\prod_{j=2}^{n} g_j \right) \\ &+ \sum_{l=2}^{n} \left(\prod_{j=l+1}^{n} g_j \right) \Bigg[-\bar{h}_l \left(\prod_{j=2}^{l-1} g_j \right) (\bar{g}_1 - \bar{h}_1) \Lambda_{l,1} \\ &+ \bar{h}_l \left(\prod_{j=2}^{l-1} g_j \right) (g_1 + h_1) X_{l,0} \Bigg] \\ &+ \sum_{l=3}^{n} \sum_{k=2}^{l-1} \left(\prod_{j=l+1}^{n} g_j \right) \Bigg[\bar{h}_l \left(\prod_{j=k+1}^{l-1} g_j \right) \bar{h}_k \Lambda_{l,k} \\ &+ \bar{h}_l \left(\prod_{j=k+1}^{l-1} g_j \right) h_k X_{l,k-1} \Bigg] \left(\prod_{j=2}^{k-1} g_j \right) (g_1 + h_1) \Bigg\}, \end{aligned} \tag{3.40}$$

$$= P_{\rm eN}(t) + P_{\rm inter}(t)\,, \tag{3.41}$$

where $P_{\rm eN}(t)$ is the *extended*-NIBA expression (3.23), while $P_{\rm inter}(t)$ contains the contributions coming from the linearized influence functional $\exp\{\Phi^{(n)}_{\rm inter}\}$, cf. (3.39). In (3.40), g_j and h_j are the functions already occurring in (3.23):

$$\begin{aligned} g_j &\equiv g(\tau_j, s_{j-1}) = \Delta^2 \mathrm{e}^{-S(\tau_j)} \cos(\varepsilon\tau_j) \cos[X_{j,j-1}]\,, \\ h_j &\equiv h(\tau_j, s_{j-1}) = \Delta^2 \mathrm{e}^{-S(\tau_j)} \sin(\varepsilon\tau_j) \sin[X_{j,j-1}]\,. \end{aligned} \tag{3.42}$$

The functions $\bar{g}_j$ and $\bar{h}_j$ are analogously defined as

$$\begin{aligned} \bar{g}_j &\equiv \Delta^2 \mathrm{e}^{-S(\tau_j)} \cos(\varepsilon\tau_j) \sin[X_{j,j-1}]\,, \\ \bar{h}_j &\equiv \Delta^2 \mathrm{e}^{-S(\tau_j)} \sin(\varepsilon\tau_j) \cos[X_{j,j-1}]\,. \end{aligned} \tag{3.43}$$

Notice that g_j and $\bar{g}_j$ are symmetric in the bias, while h_j and $\bar{h}_j$ are antisymmetric. In particular,

$$g_1 \equiv g(\tau_1, s_0 \to \infty) = g_{\rm N}(\tau_1)\ , \tag{3.44}$$

$$h_1 \equiv h(\tau_1, s_0 \to \infty) = h_{\rm N}(\tau_1)\ , \tag{3.45}$$

cf. Eq. (3.25), and analogously for $\bar{g}_1$ and $\bar{h}_1$. To proceed, let us consider the function (for $k > 1$)

$$\Sigma_s^{(l-k+1)}(t_{2l} - t_{2k-2}) \equiv \int_{t_{2k-2}}^{t_{2l}} dt_{2l-1} \ldots \int_{t_{2k-2}}^{t_{2k}} dt_{2k-1}\, \bar{h}_l \left(\prod_{j=k+1}^{l-1} g_j \right) \left[\bar{h}_k \Lambda_{l,k} + h_k X_{l,k-1} \right] \tag{3.46}$$

entering (3.40), where $2(l-k+1)$ denotes the number of tunneling transitions. Upon introducing the variables $\xi \equiv t_{2l} - t_{2k-2}$ and $\xi_j \equiv \tau_j + s_{j-1}$, Eq. (3.46) assumes the form

$$\begin{aligned} \Sigma_s^{(l-k+1)}(\xi) = \int_0^{\xi} d\xi_k \int_0^{\xi-\xi_k} d\xi_l \gamma_{\bar{h}_l}(\xi_l) f(\xi - \xi_k - \xi_l) \\ \times \left[\gamma_{h_k}(\xi_k) X_{l,k-1} + \gamma_{\bar{h}_k}(\xi_k) \Lambda_{l,k} \right]\ , \end{aligned} \tag{3.47}$$

where $\gamma_{h_j/\bar{h}_j}(\xi_j)$ is an operator which acts on a generic function $w(\tau_j)$ as (e.g. let us consider the operator $\gamma_{h_j}(\xi_j)$)

$$\gamma_{h_j}(\xi_j) w := \int_0^{\xi_j} d\tau_j\, h\left(\tau_j, \xi_j - \tau_j\right) w(\tau_j)\,. \tag{3.48}$$

In (3.47), the function $f(s)$ is given by the expression

$$\begin{aligned} f(t_{2l-2} - t_{2k}) &= \delta(t_{2l-2} - t_{2k}) \\ &+ \int_{t_{2k}}^{t_{2l-2}} dt_{2l-3} \ldots \int_{t_{2k}}^{t_{2k+2}} dt_{2k+1} \left(\prod_{j=k+1}^{l-1} -g_j \right)\ . \end{aligned} \tag{3.49}$$

Upon introducing $s \equiv t_{2l-2} - t_{2k}$ and $\xi_j \equiv \tau_j + s_{j-1}$ as in Eq. (3.47), we find

$$\begin{aligned} f(s) &= \delta(s) \\ &+ \int_0^{s} d\xi_{k+1} \int_0^{\xi_{k+1}} d\tau_{k+1} \left[-g(\tau_{k+1}, \xi_{k+1} - \tau_{k+1}) \right] \\ &\times \ldots \int_0^{s-\sum_{j=k+1}^{l-3} \xi_j} d\xi_{l-2} \int_0^{\xi_{l-2}} d\tau_{l-2} \left[-g(\tau_{l-2}, \xi_{l-2} - \tau_{l-2}) \right] \end{aligned}$$

$$\times \int_0^{s-\sum_{j=k+1}^{l-2}\xi_j} d\tau_{l-1}\left[-g\left(\tau_{l-1}, s-\sum_{j=k+1}^{l-2}\xi_j-\tau_{l-1}\right)\right] \tag{3.50}$$

$$= \delta(s)+\dot{p}_{\rm eN}^{(l-k-1)}(s)\,, \tag{3.51}$$

where the first derivative of the conditional probability $p_{\rm eN}$ has been introduced. It satisfies the symmetric master equation for the *extended*-NIBA:

$$\dot{p}_{\rm eN}(t) = -\int_0^t dt' K_{\rm eN}^s(t-t')p_{\rm eN}(t')\,. \tag{3.52}$$

Analogously we can treat the contributions to $P_{\rm inter}(t)$ which depend on the initial preparation. Specifically, we introduce for the case $k=1$ (here $\xi \equiv t_{2l}-0$)

$$\begin{aligned}\Sigma_{0,a}^{(l)}(\xi) \equiv \int_0^{\xi} d\xi_1 \int_0^{\xi-\xi_1} d\xi_l \gamma_{\bar{h}_l}(\xi_l) f(\xi-\xi_1-\xi_l) \\ \times\left[\gamma_{g_1}(\xi_1)X_{l,0}-\gamma_{\bar{g}_1}(\xi_1)\Lambda_{l,1}\right]\,,\end{aligned} \tag{3.53}$$

$$\begin{aligned}\Sigma_{0,s}^{(l)}(\xi) \equiv \int_0^{\xi} d\xi_1 \int_0^{\xi-\xi_1} d\xi_l \gamma_{\bar{h}_l}(\xi_l) f(\xi-\xi_1-\xi_l) \\ \times\left[\gamma_{h_1}(\xi_1)X_{l,0}+\gamma_{\bar{h}_1}(\xi_1)\Lambda_{l,1}\right]\,,\end{aligned} \tag{3.54}$$

where the operators $\gamma_{g_j/\bar{g}_j}(\xi_j)$ act analogously as in (3.48), and $f(s)=\delta(s)+\dot{p}_{\rm eN}^{(l-2)}(s)$.

As discussed in the Sec. 3.3.2, we choose a factorized initial condition at time $t=0$, which corresponds to set $s_0 \to \infty$. This means that in Eqs. (3.53) and (3.54), $X_{l,0} = R(t_{2l}-t_1)-R(t_{2l-1}-t_1) = R(\xi-\xi_1+\tau_1)-R(\xi-\xi_1+\tau_1-\tau_l)$. Moreover, $\Lambda_{l,1} = S(\xi-\xi_1+\tau_1)+S(\xi-\xi_1-\tau_l)-S(\xi-\xi_1)-S(\xi-\xi_1+\tau_1-\tau_l)$.

As done before for the (*extended*)-NIBA case, it is more convenient to work now in the Laplace space, where many terms factorize. In fact, one can identify (see e.g. Fig. 3.6) products of *one* or several irreducible *extended*-NIBA kernels ($\hat{F}(\lambda)$, $\hat{A}_0(\lambda)$ and $\hat{F}_0(\lambda)$) with one of the irreducible kernels containing inter-blip and blip-sojourns interactions ($\hat{\Sigma}_s^{(n)}(\lambda)$, $\hat{\Sigma}_{0,a}^{(n)}(\lambda)$ and $\hat{\Sigma}_{0,s}^{(n)}(\lambda)$). After exchanging the integration order as done in Eq. (3.27), the probability difference reads in the Laplace space

$$\begin{aligned}\hat{P}_{\rm WIBA}(\lambda) &= \hat{P}_{\rm eN}(\lambda) \\ &+\frac{1}{\lambda}\sum_{n=2}^{\infty}\left\{\sum_{l=2}^{n}\left[\prod_{j=l+1}^{n}-\hat{F}(\lambda)\right]\left[\hat{\Sigma}_{0,a}+\hat{\Sigma}_{0,s}\right]^{(l)}\right.\end{aligned}$$

$$+\sum_{l=3}^{n}\sum_{k=2}^{l-1}\left[\prod_{j=l+1}^{n}-\hat{F}(\lambda)\right]\left[\hat{\Sigma}_s\right]^{(l-k+1)} \times\left[\prod_{j=2}^{k-1}-\hat{F}(\lambda)\right]\left[-\left(\hat{F}_0(\lambda)+\hat{A}_0(\lambda)\right)\right]\Bigg\}. \tag{3.55}$$

After some changes of variables, Eq. (3.55) can be recast in the form

$$\begin{aligned}\hat{P}_{\rm WIBA}(\lambda) &= \hat{P}_{\rm eN}(\lambda)\\ &+\frac{1}{\lambda}\sum_{m=0}^{\infty}\sum_{\gamma=0}^{m}\Bigg\{\left[\hat{\Sigma}_{0,a}+\hat{\Sigma}_{0,s}\right]^{(\gamma+2)}\left[-\hat{F}(\lambda)\right]^{m-\gamma}\\ &+\left[\hat{\Sigma}_s\right]^{(\gamma+2)}\left[-\hat{F}(\lambda)\right]^{m-\gamma}(m-\gamma+1)\\ &\times\left[-\left(\hat{F}_0(\lambda)+\hat{A}_0(\lambda)\right)\right]\Bigg\},\end{aligned} \tag{3.56}$$

which becomes, after noticing that $\sum_{m=0}^{\infty}\sum_{\gamma=0}^{m}=\sum_{\gamma=0}^{\infty}\sum_{m=\gamma}^{\infty}$:

$$\begin{aligned}\hat{P}_{\rm WIBA}(\lambda) &= \hat{P}_{\rm eN}(\lambda)\\ &+\frac{1}{\lambda}\sum_{m=0}^{\infty}\Bigg\{\left[\hat{\Sigma}_{0,a}+\hat{\Sigma}_{0,s}\right]^{(m+2)}\sum_{p=0}^{\infty}\left[-\hat{F}(\lambda)\right]^{p}\\ &+\left[\hat{\Sigma}_s\right]^{(m+2)}\sum_{p=0}^{\infty}\left[-\hat{F}(\lambda)\right]^{p}(p+1)\left[-\left(\hat{F}_0(\lambda)+\hat{A}_0(\lambda)\right)\right]\Bigg\}.\end{aligned} \tag{3.57}$$

It is convenient to introduce the irreducible kernels $\Sigma_s\equiv\sum_{m=0}^{\infty}\Sigma_s^{(m+2)}$ and $\Sigma_{0,a/s}\equiv\sum_{m=0}^{\infty}\Sigma_{0,a/s}^{(m+2)}$ obtained upon summing over the number of tunneling transitions. Thus, recalling the *extended*-NIBA expression (3.26), we find

$$\begin{aligned}\hat{P}_{\rm WIBA}(\lambda) &= \frac{1}{\lambda}+\frac{1}{\lambda}\left[-\left(\hat{F}_0(\lambda)+\hat{A}_0(\lambda)\right)\right]\\ &\times\sum_{m=0}^{\infty}\left[-\hat{F}(\lambda)\right]^{m-1}\left[-\hat{F}(\lambda)+m\hat{\Sigma}_s(\lambda)\right]\\ &+\frac{1}{\lambda}\left[\hat{\Sigma}_{0,a}(\lambda)+\hat{\Sigma}_{0,s}(\lambda)\right]\sum_{m=0}^{\infty}\left[-\hat{F}(\lambda)\right]^{m}.\end{aligned} \tag{3.58}$$

Keeping in mind that we should always retain the interactions Λ and X up to the first

order, Eq. (3.58) can be rearranged in a more compact form as

$$\begin{aligned}\hat{P}_{\mathrm{WIBA}}(\lambda) \approx \frac{1}{\lambda} + \frac{1}{\lambda}\Big[&-\Big(\hat{F}_0(\lambda)+\hat{A}_0(\lambda)\Big) \\ &+ \hat{\Sigma}_{0,a}(\lambda)+\hat{\Sigma}_{0,s}(\lambda)\Big]\sum_{m=0}^{\infty}\Big[-\hat{F}(\lambda)+\hat{\Sigma}_s(\lambda)\Big]^m,\end{aligned} \tag{3.59}$$

yielding

$$\begin{aligned}&\hat{P}_{\mathrm{WIBA}}(\lambda) \\ &= \frac{1}{\lambda}\left[1+\frac{-\Big(\hat{F}_0(\lambda)+\hat{A}_0(\lambda)\Big)+\hat{\Sigma}_{0,a}(\lambda)+\hat{\Sigma}_{0,s}(\lambda)}{1+\hat{F}(\lambda)-\hat{\Sigma}_s(\lambda)}\right] &(3.60)\\ &= \frac{1+\hat{W}_{\mathrm{WIBA}}/\lambda-\hat{K}^a_{\mathrm{WIBA}}/\lambda}{\lambda+\hat{K}^s_{\mathrm{WIBA}}}, &(3.61)\end{aligned}$$

where we introduced the functions

$$\hat{K}^s_{\mathrm{WIBA}}(\lambda) = \lambda\left[\hat{F}(\lambda)-\hat{\Sigma}_s(\lambda)\right], \tag{3.62a}$$

$$\hat{K}^a_{\mathrm{WIBA}}(\lambda) = \lambda\left[\hat{A}_0(\lambda)-\hat{\Sigma}_{0,a}(\lambda)\right], \tag{3.62b}$$

$$\hat{K}^s_{0,\mathrm{WIBA}}(\lambda) = \lambda\left[\hat{F}_0(\lambda)-\hat{\Sigma}_{0,s}(\lambda)\right], \tag{3.62c}$$

$$\hat{W}_{\mathrm{WIBA}}(\lambda) = \hat{K}^s_{\mathrm{WIBA}}(\lambda)-\hat{K}^s_{0,\mathrm{WIBA}}(\lambda). \tag{3.62d}$$

3.4.2 Generalized master equation (GME) for the WIBA

After multiplying both sides of Eq. (3.61) by $\lambda+\hat{K}^s_{\mathrm{WIBA}}$, one can recognize the Laplace transform of the generalized master equation Eq. (3.1), where from Eq. (3.62) the WIBA kernels in the time domain are

$$\begin{aligned}K^s_{\mathrm{WIBA}}(t) &\equiv \dot{F}(t)-\dot{\Sigma}_s(t),\\ K^s_{0,\mathrm{WIBA}}(t) &\equiv \dot{F}_0(t)-\dot{\Sigma}_{0,s}(t),\\ K^a_{\mathrm{WIBA}}(t) &\equiv \dot{A}_0(t)-\dot{\Sigma}_{0,a}(t),\\ W_{\mathrm{WIBA}}(t) &\equiv K^s_{\mathrm{WIBA}}(t)-K^s_{0,\mathrm{WIBA}}(t).\end{aligned} \tag{3.63}$$

The prescription (3.63) allows the explicit evaluation of the irreducible kernels. This

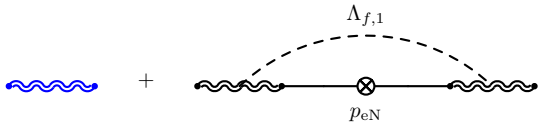

Figure 3.7: Irreducible symmetric WIBA kernel. Notice that the lowest order reproduces the *extended*-NIBA case, see Fig. 3.4b. The inner bubble represents the contribution coming from the sum of all orders in Δ^2 which coincides with the symmetric part of the solution of the master equation for $P(t)$ in the *extended*-NIBA case.

procedure is illustrated in App. B. Explicitly, the antisymmetric WIBA kernel reads

$$\begin{aligned} K^a_{\rm WIBA}(\xi) = & K^a_{\rm eN}(\xi) \\ & - \int_0^{\xi} d\xi_1 \int_0^{\xi-\xi_1} d\xi_f \, \bar{h}_{\rm eN}(\xi_f)\, p_{\rm eN}(\xi-\xi_1-\xi_f) \\ & \times \left[g_{\rm N}(\xi_1) X_{f,0} - \bar{g}_{\rm N}(\xi_1)\Lambda_{f,1} \right] , \end{aligned} \tag{3.64}$$

where, as in the *extended*-NIBA case, cf. (3.35), corrections of order $\ddot{R}(\xi_f)\xi_f^2$ have been neglected. The functions $g_{\rm eN}$, $h_{\rm eN}$ have been defined in (3.37). Analogously, we also introduced here the functions

$$\begin{aligned} \bar{g}_{\rm eN}(\xi_j) &= \Delta^2 \mathrm{e}^{-S(\xi_j)} \cos(\varepsilon\xi_j) \sin[\tilde{R}(\xi_j)] , \\ \bar{h}_{\rm eN}(\xi_j) &= \Delta^2 \mathrm{e}^{-S(\xi_j)} \sin(\varepsilon\xi_j) \cos[\tilde{R}(\xi_j)] , \end{aligned} \tag{3.65}$$

with $\tilde{R}(t) \equiv R(t) - t\dot{R}(t)$. The symmetric WIBA kernel becomes

$$\begin{aligned} K^s_{\rm WIBA}(\xi) = & K^s_{\rm eN}(\xi) \\ & - \int_0^{\xi} d\xi_1 \int_0^{\xi-\xi_1} d\xi_f \, \bar{h}_{\rm eN}(\xi_f)\, p_{\rm eN}(\xi-\xi_1-\xi_f) \\ & \times \left[\bar{h}_{\rm eN}(\xi_1)\Lambda_{f,1} \right] . \end{aligned} \tag{3.66}$$

The irreducible symmetric kernel is shown in Fig. 3.7. Moreover, the function $W_{\rm WIBA}$ is now given by

$$W_{\rm WIBA}(\xi) \equiv K^s_{\rm WIBA}(\xi) - K^s_{0,\rm WIBA}(\xi) , \tag{3.67}$$

where

$$K^s_{0,\rm WIBA}(\xi) = K^s_{0,\rm eN}(\xi)$$

$$- \int_0^{\xi} d\xi_1 \int_0^{\xi-\xi_1} d\xi_f \, \bar{h}_{\rm eN}(\xi_f)\, p_{\rm eN}(\xi - \xi_1 - \xi_f)$$
$$\times \left[h_{\rm N}(\xi_1) X_{f,0} + \bar{h}_{\rm N}(\xi_1) \Lambda_{f,1} \right] . \qquad (3.68)$$

In the Eqs. (3.64) and (3.68), is $X_{f,0} = R(\xi) - R(\xi - \xi_f)$, and for all the three kernels $\Lambda_{f,1} = S(\xi) - S(\xi - \xi_1) + S(\xi - \xi_1 - \xi_f) - S(\xi - \xi_f)$.

3.4.3 Dynamics within the WIBA

Let us now come to the WIBA predictions. In this Section we will be showing the comparison of all the theories previously discussed, namely the NIBA, its extended version, the weak-coupling approximation (WCA) and our WIBA, for different choices of the parameters. In the following subsections we examine the behavior of the dynamical quantity $P(t)$, being the expectation value of σ_z at time t, in the case of Ohmic bath ($s = 1$ in the spectral density (3.3)), with cutoff frequency $\omega_c = 50\Delta$, and of super-Ohmic dissipative environment (we choose $s = 3$), for different choices of the frequencies ω_c and $\omega_{\rm ph}$.

Ohmic case ($s = 1$)

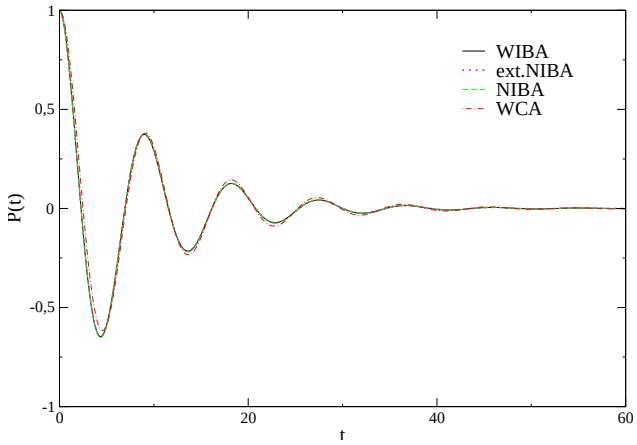

Figure 3.8: Time evolution of $P(t)$ for an Ohmic *symmetric* two-state system. The WIBA (full lines) coincides with the NIBA (dashed lines) and the *extended*-NIBA (dotted lines) over the whole range of parameters. Here $\alpha = 0.1$, $T = 0.1$ (expressed in units of Δ) have been chosen. For such a choice, the WCA (dot-dashed lines) slightly deviates from all other predictions.

We expect WIBA to work particularly well in the Ohmic case due to $S(t) \sim t$ at long times. This has the simultaneous effect of suppressing the blip lengths and to yield a

vanishing interblip interaction at large blip separation.

We first present (Fig. 3.8) the results for an Ohmic symmetric two-state system ($\varepsilon = 0$) for a generic choice of the parameters. For the symmetric case, the NIBA is expected to predict the correct time evolution over the whole range of coupling strengths and temperatures. One sees a complete agreement of the WIBA with the (*extended*-) NIBA. For the chosen parameters, also WCA well agrees with the WIBA predictions.

The situation becomes more intricate for the case of finite bias ($\varepsilon \neq 0$), since on the one hand NIBA is expected to fail at low temperatures and damping, while the WCA becomes inappropriate at large temperatures and/or damping. In the following, we fix the external bias as $\varepsilon = \Delta$.

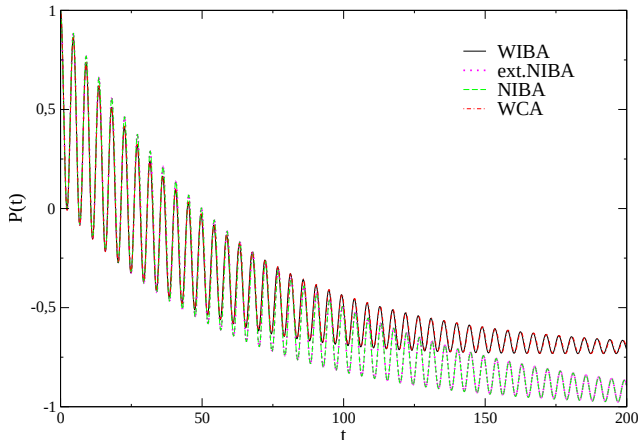

Figure 3.9: Time evolution of $P(t)$ for Ohmic damping and finite bias. The chosen parameters are $\alpha = 0.01$, $T = 0.1$ and $\varepsilon = 1$ (in units of Δ). The WIBA (full lines) coincides with the WCA (dot-dashed lines) for low temperatures and small coupling, while the NIBA (dashed lines) and the *extended*-NIBA (dotted lines) predict an unphysical asymptote, for an asymmetric system.

Fig. 3.9 shows a case of low temperature $k_{\mathrm{B}}T \leq E = \sqrt{\varepsilon^2 + \Delta^2}$ (with respect to the tunneling matrix element Δ) and small damping α, namely $\alpha = 0.01$, $T = 0.1$ (in units of Δ). One can see that the agreement between WIBA e WCA is striking, whereas both NIBA and *extended*-NIBA fail to reach the correct asymptotic value, predicting an unphysical symmetry breaking.

In Figs. 3.10, 3.11 and 3.12, a comparison between WIBA and a numerical *ab-initio* path-integral approach (QUAPI [17]) is made, in order to proof the validity of our theory in an intermediate-to-high regime of temperatures and coupling strength. As the coupling strength is raised, $\alpha = 0.1$ (Fig. 3.10), while keeping the temperature constant, one sees

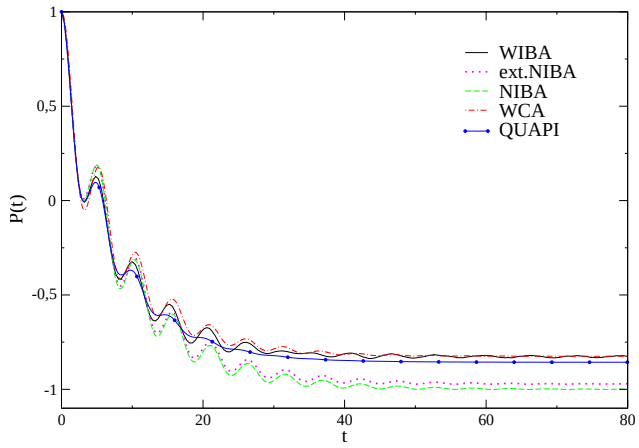

Figure 3.10: Time evolution of $P(t)$ for $\alpha = 0.1$, $T = 0.1$ and finite bias $\varepsilon = 1$ (in units of Δ). The WIBA (full lines) exhibits more coherence than the QUAPI (lines with bullets), being however its predictions closer to the QUAPI than the WCA (dot-dashed lines). The *extended*-NIBA (dotted lines) is also getting closer to the QUAPI predictions, the NIBA (dashed lines) still predicting a strong localization in the left well.

that the asymptote of the *extended*-NIBA is slowly moving from the NIBA one towards the QUAPI one. At the same time, the WCA also disagrees with the WIBA predictions, the

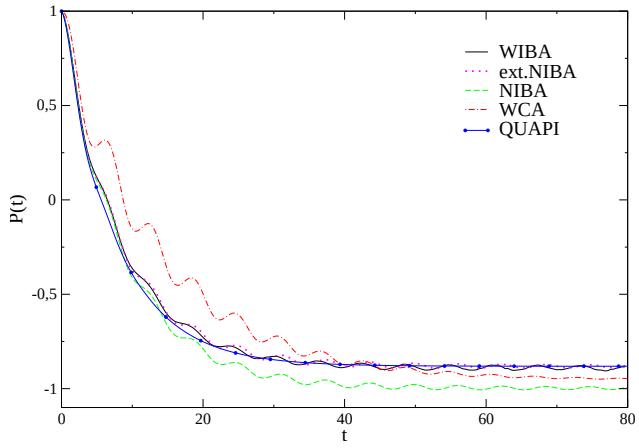

Figure 3.11: Time evolution of $P(t)$ for $\alpha = 0.25$, $T = 0.01$ and finite bias $\varepsilon = 1$ (in units of Δ). The WCA (dot-dashed lines) completely fails in describing the short-time dynamics and also predicts a wrong asymptote. The WIBA (full lines) as well as the *extended*-NIBA (dotted lines) very well agree with the QUAPI predictions (lines with bullets), despite some spurious oscillations, still contained in the theory. The disagreement with the NIBA is striking, already at this intermediate-to-high regime of parameters, although the NIBA correctly describes the short-time dynamics.

former starting to be invalid for higher coupling strength. The WIBA, however, shows the presence of some unphysical "beatings" at the onset of the long-time dynamics, whose origin is not yet well understood. Hence, some more investigations seem to be required, in order to improve the theory in this regime of parameters.

By raising the coupling strength ($\alpha = 0.25$) (Fig. 3.11) while lowering the temperature ($T = 0.01$), one can observe that the WCA completely fails in predicting the right asymptote or the intermediate dynamics. The NIBA also predicts a wrong asymptotic value, while correctly describing the short-time dynamics. For such a choice of parameters, the *extended*-NIBA very well agrees with QUAPI, although some oscillations are still present. The WIBA also smoothly oscillates close to the QUAPI predictions.

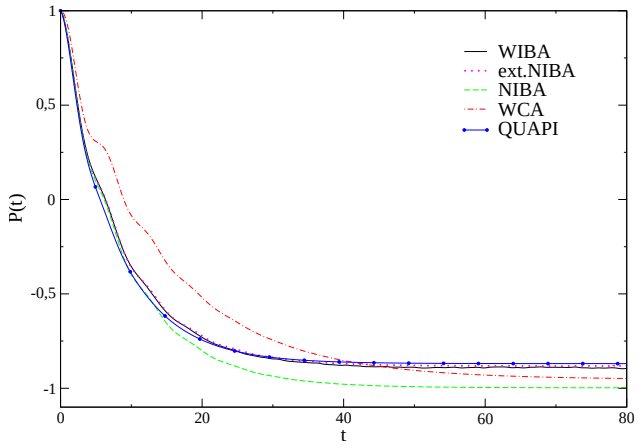

Figure 3.12: Time evolution of $P(t)$ for $\alpha = 0.25$, $T = 0.1$ and finite bias $\varepsilon = 1$ (in units of Δ). In this regime the *extended*-NIBA (dotted lines) as well as the WIBA (full lines) are almost indistinguishable from QUAPI (lines with bullets), whereas both WCA (dot-dashed lines) and NIBA (dashed lines) fail in describing the dynamics, the latter being, however, able to reproduce the short-time dynamics.

Finally, Fig. 3.12 shows that, for the parameters $\alpha = 0.25$, $T = 0.1$, the WIBA and the *extended*-NIBA are almost indistinguishable from the QUAPI predictions. The WCA and the NIBA fail to describe the dynamics, even though the NIBA correctly reproduces the short-time dynamics.

By looking at Figs. 3.10, 3.11 and 3.12, it is interesting to notice that the WIBA predicts more coherence than QUAPI. The overall agreement with QUAPI though remains very good.

Super-Ohmic case ($s = 3$)

Let us now consider the predictions of the WIBA in the presence of a super-Ohmic bath. We choose to show here a very common situation (we set $s = 3$). Since $S(t \sim \Delta^{-1})$ differs only little from its asymptotic value $S(t \to \infty)$, the interblip interactions are weak and the WCA is expected to be a good approximation in a wide regime of parameters. This also implies that $S(t)$ is *not* effective in suppressing long-blip lenghts and the NIBA as well as even the WIBA might not be justified. Notice that we expect WIBA to work in all the situations such that $1 < s < 2$.

In the following figures, we keep temperature, external bias and coupling constant fixed ($T = 0.1$, $\varepsilon = 1$ in units of Δ, $\delta_3 = 0.01$), while keeping the ratio $\omega_c/\omega_{\rm ph}$ constant ($\omega_c/\omega_{\rm ph} = 8$). This choice is reasonable and agrees with some experiments [82]. The ratio $\omega_c/\omega_{\rm ph}$

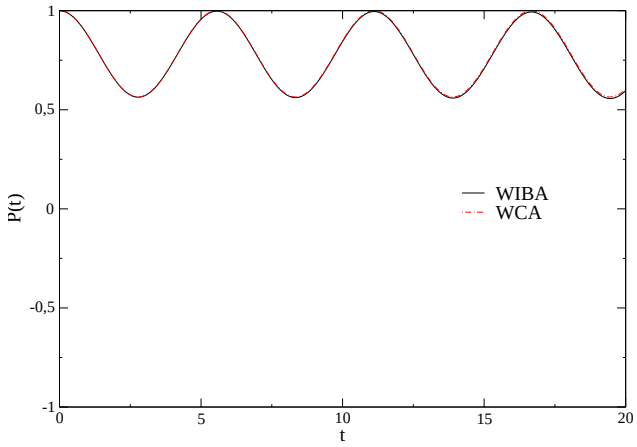

Figure 3.13: Time evolution of $P(t)$ for $\delta_s = 0.01$, $\omega_c = 200$ ($T = 0.1$, $\varepsilon = 1$). Here one sees no difference between WCA (dot-dashed lines) and WIBA (full lines), showing that the chosen parameters lie in an effective weak-coupling regime.

acts as an effective correction factor to the real coupling strength, see Eqs. (3.8) and (3.9). Moreover, since we fix the temperature, in the bath correlation function corrections proportional to the temperature ($\kappa = 1/\hbar\beta\omega_c$) become important as the cutoff frequency is decreased.

In Fig. 3.13 the cutoff frequency $\omega_c = 200$ is assumed to be very large compared to the system frequency scales. There, one sees that the WIBA well matches the WCA predictions, as expected in the regime of weak damping.

On the other hand, Fig. 3.14 shows the WIBA predictions for $P(t)$ when the cutoff frequency ω_c is of the order of the tunneling frequency Δ, namely when the bath becomes "slow", a case where the WCA and the NIBA are expected to fail. This case is the most

difficult one, since the bath is very coherent and memory effects are to be taken into account, which requires to perform a very good description of the full bath dynamics. One sees that the NIBA completely fails to reproduce the dynamics, even reaching unphysical values below -1. The *extended*-NIBA works better, approaching closer the QUAPI predictions. Nevertheless, too few correlations are taken into account, and it oscillates still too much with respect to the numerical plot of QUAPI. The WIBA shows discrepancies from the QUAPI as well, being still "too" coherent, even though its predictions are more accurate than the *extended*-NIBA ones. The WCA, despite better than WIBA in this regime, also lie apart from the numerical prediction of QUAPI. In this range of parameters, the temperature-dependent corrections in the bath correlation function Q become relevant and the perturbative weak-coupling approach begins to fail. Thus, some more analysis of the complicated super-Ohmic case is to be done, in order to better understand the different dynamical situations which take place by varying the coupling strength δ_s, the cutoff frequency ω_c and the phonon frequency $\omega_{\rm ph}$.

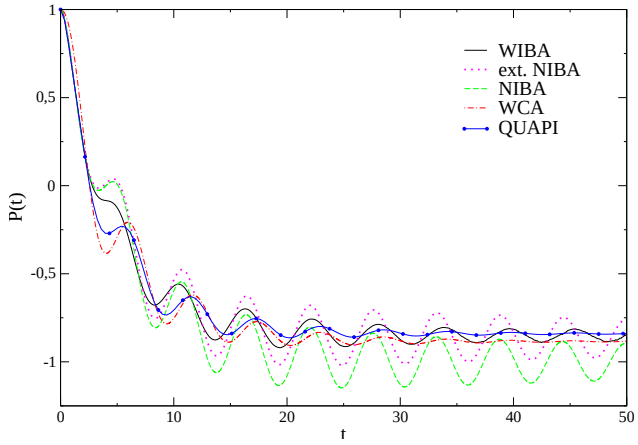

Figure 3.14: Time evolution of $P(t)$ for $\delta_s = 0.01$, $\omega_c = 1$ ($T = 0.1$, $\varepsilon = 1$). Here we notice discrepancies between WIBA (full lines) and QUAPI (full lines with bullets), since the *extended*-NIBA predictions (dotted lines) also account for too many oscillations. Nevertheless, it gives much better results than NIBA (dashed lines), predicting unphysical values for $P(t)$. Finally, the WCA (dot-dashed lines) is so far the best model in this regime, although it lies apart as well from the QUAPI predictions, since the perturbative approach for such parameters begins to fail.

3.5 Conclusions

To conclude, we presented here a novel analytical scheme dubbed WIBA (Weakly-Interacting Blip Approximation) which is able to match between diverse approximation schemes for different parameters choices. In particular, the WIBA is valid over a large regime of temperatures and coupling strength for a wide class of spectral densities (3.3). For Ohmic damping the WIBA reproduces very well weak-coupling approximation schemes for small damping and temperature and the well-known NIBA in the opposite regime of strong damping and high temperature. It yields a good, though not perfect agreement, with *ab-initio* QUAPI calculation in the regime of intermediate temperatures and damping. For super-Ohmic damping, the WIBA predicts a correct dynamical behaviour in the regime of small damping, whereas for a higher effective damping the disagreement of the NIBA with *ab-initio* numerical theories for $s \geq 2$ even affects the performances of the *extended*-NIBA and consequently of the WIBA.

The sub-Ohmic environment, i.e. such that $0 < s < 1$, suppresses the tunneling transitions between the left and the right states, which are therefore almost localized. A realization of sub-Omhic environment for electron tunneling can be e.g. a long RC line corresponding to s = 1/2. In such a regime, NIBA works for all values of bias and temperatures and WIBA agrees with it.

Hence, the WIBA overcomes the dim validity of the perturbative approaches discussed in the previous Sections which, up to now, was only possible via numerical *ab-initio* schemes. It also serves as benchmark to limiting simple analytical schemes, in order to proof their range of applicability over the various regimes, and combine weak-coupling and strong-damping approaches in one single, unified model.

Our approach is based on the consideration that bath-induced blip-blip and blip-sojourn interactions are weak in the whole regime of parameters for the spectral densities (3.3). It is expecially needed in several contexts, and we mention here few of them: i) The WIBA could be very useful when experimentally the bath temperature or the external bias are varied over a wide range: In fact, WCA and NIBA are unreliable at high temperatures and low-to-intermediate driving, respectively. ii) It should be used to investigate the situation of several TLS's interacting with a common heat bath [83], as in glasses [72], at low temperature being characterized by a broad distribution of tunneling parameters and asymmetries.

We must, however, notice, that in the case of "slow" environments with cut-off frequency of the order of the tunneling frequency, still our approximation has to be improved, since neither the WIBA nor other analytical approximation schemes are able to reproduce the correct onset of decoherence which in fact takes place. This situation occurs e.g. in non-

adiabatic electron transfer [64] or for charge qubits interacting with piezo-electric phonons [82].

May I become at all times,
both now and for ever,
a protector for the helpless,
a guide for the lost ones,
a ship for those to cross oceans,
and a bridge to cross rivers,
a sanctuary for those in danger,
a lamp for those in darkness,
a refuge for those who need shelter,
a servant to all in need.

the XIV Dalai Lama

Chapter 4

Dynamics of a qubit coupled to a broadened harmonic mode at finite detuning

A prominent physical model to study dissipative and decoherence effects in quantum mechanics is the spin-boson model [12, 13, 84]. Currently, we witness its revival since it allows a quantitative description of solid-state quantum bits (qubits) [8]. A more realistic description requires the inclusion of external control fields as well as of a detector. In the spin-boson model, the environment is characterized by a spectral density $G(\omega)$, already introduced in Eq. (3.3). If the environment is formed by a quantum detector which itself is damped by Ohmic fluctuations, the form of the spectral density can become non-trivial, as it reflects also internal resonances of the detector.

An example is provided by a flux-qubit read out by a dc-SQUID [5, 18, 19] whose plasma resonance at Ω gives rise to an effective spectral density $G_{\rm eff}(\omega)$ for the qubit with a peak at Ω [20, 21], cf. Eq. (4.2) below. Recently, the coherent coupling of a single photon mode and a superconducting charge qubit has also been studied [85]. Until now, the effects of such a structured spectral density on the decoherence properties of a qubit have been studied in [86, 87] within a perturbative approach in $G_{\rm eff}$. It was shown in [88, 89] that such a perturbative scheme breaks down for strong qubit-detector coupling, and when the qubit and detector frequencies are comparable. Hence, in [88, 90, 91] the dynamics was investigated by mapping the spin-boson problem onto the equivalent situation of a two-level system (TLS) coupled to a harmonic oscillator (HO), the latter coupled to an Ohmic bath with spectrum $G_{\rm Ohm}$. By considering the TLS and HO as the relevant system, analytic

solutions perturbative in $G_{\rm Ohm}$ were obtained.

In this Chapter we show how to investigate the dynamics of a spin-boson system with a structured environment, in the case of a strong coupling between qubit and detector. We evaluate the dynamics upon starting from the (nonperturbative in $G_{\rm eff}$) Non-Interacting Blip Approximation (NIBA) [12, 13]. Analytical results, valid also at finite detuning, are obtained by approximating the NIBA kernels up to first order in the detector-bath coupling strength. The Chapter is organized as follows: In the next Section we will introduce the model. Then, in Sec. 4.2 we discuss the well-known and widely used Non-Interacting Blip Approximation and its predictions. Analytical results for the dynamics are derived in Sec. 4.3.

4.1 The model

We consider in this Chapter the spin-boson Hamiltonian describing the interaction of a *symmetric* TLS with a structured environment. This means that we set $\varepsilon = 0$ in the already introduced Hamiltonian (3.2). By writing the bath plus interaction Hamiltonian (2.3) in second quantization, the system-bath Hamiltonian reads [13, 12]

$$\mathbf{H}_{\rm SB} = -\frac{\hbar\Delta}{2}\hat{\sigma}_x + \frac{1}{2}\hat{\sigma}_z\hbar\sum_k \tilde{\lambda}_k(\tilde{b}_k^\dagger + \tilde{b}_k) + \sum_k \hbar\tilde{\omega}_k\tilde{b}_k^\dagger\tilde{b}_k\,, \tag{4.1}$$

where $\hat{\sigma}_i$ are Pauli matrices and $\hbar\Delta$ is the tunnel splitting. Moreover, $\tilde{b}_k$ is the annihilation operator of the $k-$th bath mode with frequency $\tilde{\omega}_k$. In the spin-boson model the influence of the environment is fully characterized by the spectral function, which we assume to be of the form

$$G_{\rm eff}(\omega) = \frac{2\alpha\omega\Omega^4}{(\Omega^2-\omega^2)^2 + (\Gamma\omega)^2}. \tag{4.2}$$

It has a Lorentzian peak of width Γ at the characteristic frequency Ω, and behaves Ohmically at low frequencies with the dimensionless coupling strength $\alpha = \lim_{\omega\to 0} G_{\rm eff}(\omega)/2\omega$. As shown in [64], such spin-boson Hamiltonian can be exactly mapped onto that of a TLS coupled to a single harmonic oscillator mode of frequency Ω with coupling strength g. The HO iteslf interacts with a set of harmonic oscillators with spectral density of the continuous bath modes being $G_{\rm Ohm}(\omega) = \kappa\omega$. The mapping between the two models is completed with $\Gamma = 2\pi\kappa\Omega$ and $\alpha = 8\kappa g^2/\Omega^2$. Notice that the oscillator can e.g. represent a dc-SQUID with plasma frequency Ω which couples inductively to a

superconducting flux qubit [20, 21]. The damping of the dc-SQUID is due to its coupling to an electromagnetic environment.

If the damping of the harmonic oscillator is small ($\kappa \ll 1$), as in typical experiments where the dc-SQUIDs are typically underdamped, then it would seem more convenient to use the mapping, and consider the qubit coupled to the dc-SQUID as unique quantum system. However, since such a system has an infinite Hilbert space, the inclusion of dissipation is typically done [88, 91] upon truncation of the system's Hilbert space to a few relevant levels (which is the case e.g. if $\hbar\Omega\,, \hbar\Delta \gg k_{\rm B}T$). This led in [88] to find analytical results for the resonant case $\Delta = \Omega$ within a three-level approximation. In the present work analytical results valid at finite detuning $\Delta \neq \Omega$ are obtained by focusing on the spin-boson model (4.1). The advantage of this approach is that the reduced density matrix has rank 2. The peculiar feature of the peaked spectrum (4.2) is reflected in the form of the bath correlation functions, cf. (4.4) and (4.4b) below.

Specifically, in the spin-boson model the environmental effects are captured in the so-called bath correlation function

$$Q(\tau) \equiv S(\tau) + \mathrm{i}R(\tau) = \int_0^\infty \mathrm{d}\omega \frac{G_{\rm eff}(\omega)}{\omega^2} \left[\coth\left(\frac{\hbar\omega\beta}{2}\right)(1-\cos\omega t) + \mathrm{i}\sin\omega t \right], \tag{4.3}$$

which for the effective spectral density (4.2) reads

$$S(\tau) = X\tau + L\left(e^{-\frac{\Gamma}{2}\tau}\cos\bar{\Omega}\tau - 1\right) + Ze^{-\frac{\Gamma}{2}\tau}\sin\bar{\Omega}\tau + S_{Mats}(\tau), \tag{4.4a}$$

$$R(\tau) = \pi\alpha - e^{-\frac{\Gamma}{2}\tau}\pi\alpha\left(N\sin\bar{\Omega}\tau + \cos\bar{\Omega}\tau\right), \tag{4.4b}$$

being $\bar{\Omega} = \sqrt{\Omega^2 - \frac{\Gamma^2}{4}}$ and

$$X = \frac{2\pi\alpha}{\hbar\beta}, \tag{4.5}$$

$$L = \frac{\pi\alpha}{\Gamma\bar{\Omega}} \frac{1}{\cosh\left(\beta\bar{\Omega}\right) - \cos\left(\beta\frac{\Gamma}{2}\right)} \left[\left(\tfrac{\Gamma^2}{4} - \bar{\Omega}^2\right)\sinh\left(\beta\bar{\Omega}\right) + \Gamma\bar{\Omega}\sin\left(\beta\tfrac{\Gamma}{2}\right)\right], \tag{4.6}$$

$$Z = \frac{\pi\alpha}{\Gamma\bar{\Omega}} \frac{1}{\cosh\left(\beta\bar{\Omega}\right) - \cos\left(\beta\frac{\Gamma}{2}\right)} \left[-\Gamma\bar{\Omega}\sinh\left(\beta\bar{\Omega}\right) + \left(\tfrac{\Gamma^2}{4} - \bar{\Omega}^2\right)\sin\left(\beta\tfrac{\Gamma}{2}\right)\right], \tag{4.7}$$

$$N = \frac{1}{\Gamma\bar{\Omega}}\left(\tfrac{\Gamma^2}{4} - \bar{\Omega}^2\right). \tag{4.8}$$

$S_{Mats}(\tau)$ is a function of Matsubara frequencies and has the form

$$S_{Mats}(\tau) = -4\pi\alpha\frac{\Omega^4}{\hbar\beta}\sum_{n=1}^{+\infty}\frac{1}{(\Omega^2+\nu_n^2)^2-\Gamma^2\nu_n^2}\left[\frac{e^{-\nu_n\tau}-1}{\nu_n}\right], \tag{4.9}$$

with the Matsubara frequencies defined as $\nu_n \equiv \frac{2\pi}{\hbar\beta}n$. For temperatures high enough ($k_BT \gg \frac{\hbar\Gamma}{2\pi}$), contributions coming from the Matsubara term can be neglected, as done in the rest of this Chapter.

The qubit dynamics is described by the reduced density operator $\rho(t)$ obtained by tracing out all environmental degrees of freedom. Again, we investigate the population difference $\langle\sigma_z(t)\rangle \equiv P(t)$, see Eq. (2.12). Such a dynamical quantity $P(t)$ obeys the exact generalized master equation (GME) already introduced in Eq. (3.1), which with $\varepsilon = 0$ and consequently $K^a = 0$ and $W = 0$ becomes

$$\dot{P}(t) = -\int_0^t \mathrm{d}t' K^s(t-t')P(t'), \qquad t > 0. \tag{4.10}$$

with the kernels $K^s(t)$ being a series expression in the number of tunneling transitions. Since Eq. (4.10) involves only convolutions, it can be solved by using Laplace Transforms. Hence, the GME transforms as

$$P(\lambda) = \frac{1}{\lambda + K^s(\lambda)}, \tag{4.11}$$

where the same symbols $P(\lambda)$ and $K(\lambda)$ for the Laplace transform of $P(t)$ and $K(\tau)$ have been used, respectively. From Eq. (4.11), it follows that in order to obtain $P(t)$ it can be enough to solve the pole equation

$$\lambda + K^s(\lambda) = 0 \tag{4.12}$$

and then antitrasform back to the time space.

Due to the intricate form of the exact kernel $K^s(t)$ (or $K^s(\lambda)$), Eqs. (4.10) (or (4.11)) cannot be solved neither numerically nor analytically. We must therefore invoke the Non-Interacting Blip Approximation (NIBA) which correctly describes a symmetric system in the whole regime of coupling strength and temperatures, as already mentioned in Section 3.3.

4.2 The Non-Interacting Blip Approximation

Within the NIBA [12, 13], of the exact series expression for $K^s(\lambda)$ only the first term of second order in the tunneling frequency Δ is retained. In the undriven case, the model is justified for weak damping since the neglected correlations are of second order in the coupling α, whereas for high temperature and/or large damping extra correlations are exponentially suppressed. In the Section 3.3 and more specifically in App. A, the limits of validity of the NIBA are discussed and the kernels are given therein. For a symmetric system (i.e. $\varepsilon = 0$), the NIBA kernel reads

$$K^s(t) = \Delta^2 e^{-S(t)} \cos\left(R\left(t\right)\right), \tag{4.13}$$

or in the Laplace space

$$K^s(\lambda) = \Delta^2 \int_0^\infty \mathrm{d}\tau \, e^{-\lambda\tau} e^{-S(\tau)} \cos\left(R\left(\tau\right)\right), \tag{4.14}$$

where the .4).

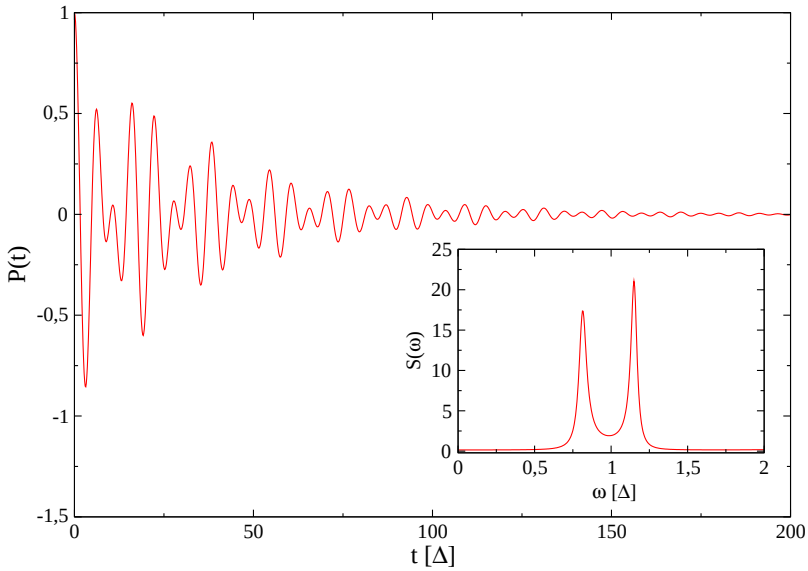

Figure 4.1: Time evolution of the population difference $P(t)$ of a symmetric TLS in the resonant case $\Omega = \Delta$. The parameters are: $\alpha = 4\,10^{-3}$, ($g = 0.18$) and $\Gamma = 0.097$, $T = 0.1$ (expressed in units of Δ). In this range of parameters, one clearly sees that the dynamics is dominated by *two* frequencies. Inset: Fourier Transform of $P(t)$. One clearly sees the appearance of two peaks, centered symmetrically around $\Omega \pm g \approx 1 \pm 0.18$.

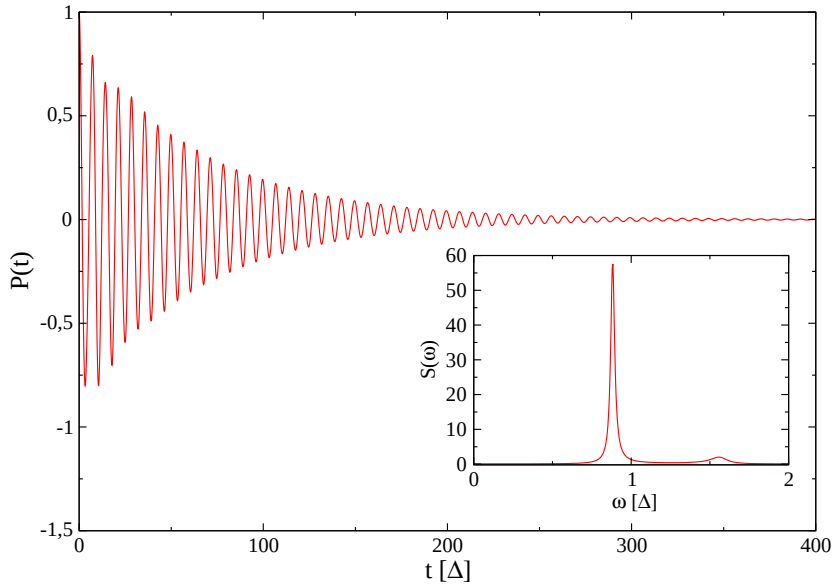

Figure 4.2: Time evolution of the population difference $P(t)$ of a symmetric TLS in the case of a finite detuning $\Omega = 1.5\Delta$. The parameters are: $\alpha = 5\,10^{-3}$, ($g = 0.3$) and $\Gamma = 0.145$, $T = 0.1$ (in units of Δ). For a TLS being off-resonance with the HO, one notices that the relative magnitude of the two peaks become larger and larger, the higher the detuning is (see the Fourier Transform in the inset).

Typical results for $P(t)$ obtained from the numerical integration of the NIBA master equation for the resonant case $\Omega = \Delta$ and at finite detuning $\Omega = 1.5\Delta$ are shown in Figs. 4.1 and 4.2, respectively. In the resonant case $P(t)$ exhibits a very pronounced beating pattern. The analysis of the corresponding spectrum

$$S(\omega) \equiv 2 \int_0^\infty \mathrm{d}t \cos(\omega t)\, P(t) \tag{4.15}$$

for the parameters choice of Fig. 4.1 (resonant case) clearly reveals the presence of two frequencies, which lie around $\Omega_\pm \approx \Omega \pm g$, where g is the coupling strength in the TLS+HO model, as discussed above. This is in agreement with predictions of a three-level system Bloch-Redfield analysis (with second-order perturbation theory in g) as well as with exact results obtained within the numerical real-time path-integral approach QUAPI [88]. The Fourier spectrum for the detuned case in Fig. 4.2 shows a more pronounced oscillation frequency, the relative magnitude of the two peaks becoming larger and larger, the higher the detuning is. As one raises the coupling strength α between TLS and effective environment, multiple resonances appear, due to the fact that higher orders in Bessel functions contribute

to the dynamics (see discussion in the next Section). This beating pattern clearly originates from the peaked nature of the environmental spectrum and it is thus absent for the more frequently investigated cases of unstructured environments [12, 13], i.e. $G(\omega) \propto \omega^s e^{-\omega/\omega_c}$, $s > 0$, see Eq. (3.3). Starting point is Eq. (4.11) and its related pole equation (4.12). The nature of the beatings as well as an analytical approximation to $P(t)$ are discussed in the following Section.

4.3 Weak-Damping Approximation (WDA) for a symmetric TLS

For a symmetric TLS, NIBA is expected to be justified in the whole regime of parameters. In particular we have seen, cf. Fig. 4.1, that in the regime of resonance, i.e. $\Omega = \Delta$, and strong coupling, i.e. $g \gg \Gamma$, it predicts the two oscillation frequencies already found in Ref. [88] within a three-level approximation. However, the analysis in Ref. [88] was restricted to the case $\Delta = \Omega \gg k_{\rm B}T$. In the following, we shall derive an analytical expression for $P(t)$ valid for *arbitrary* detuning $|\Delta - \Omega| \neq 0$ and low-to-moderate temperatures $k_{\rm B}T \lesssim \hbar\Omega$. The key idea is that, since we are looking to a sharply peaked spectral density, i.e. $\kappa = \Gamma/2\pi\Omega \ll 1$, an expansion of the NIBA symmetric kernel (4.14) up to first order in κ is justified.

Since the bath-correlation functions S and R (Eq. (4.4b)) depend in a nontrivial way on κ, this requires some attention. In the end we obtain

$$S(\tau) = \overbrace{Y\left(\cos\Omega\tau - 1\right)}^{S_0(\tau)} + \overbrace{A\tau\cos\Omega\tau + B\tau + C\sin\Omega\tau}^{S_1(\tau)} + \mathcal{O}[\kappa^2]\,, \tag{4.16a}$$

$$R(\tau) = \underbrace{W\sin\Omega\tau}_{R_0(\tau)} + \underbrace{V\left(1 - \cos\Omega\tau - \frac{\Omega}{2}\tau\sin\Omega\tau\right)}_{R_1(\tau)} + \mathcal{O}[\kappa^2], \tag{4.16b}$$

with the zero-order terms

$$Y = -\frac{4g^2}{\Omega^2}\,\frac{\sinh\beta\Omega}{\cosh\beta\Omega - 1}, \qquad W = \frac{4g^2}{\Omega^2}, \tag{4.17}$$

and first-order terms

$$A = -\Gamma\frac{Y}{2}, \tag{4.18}$$

$$B = \Gamma \frac{8g^2}{\Omega^3 \hbar \beta}, \tag{4.19}$$

$$C = -\Gamma \frac{2g^2}{\Omega^3} \frac{\beta\Omega + 2\sinh \beta\Omega}{\cosh \beta\Omega - 1}, \tag{4.20}$$

$$V = \Gamma \frac{4g^2}{\Omega^3}. \tag{4.21}$$

Notice that the contribution coming from the Matsubara frequencies (4.9) has been neglected, affecting only the short-time dynamics. We will here discuss first the simpler undamped case ($\kappa = 0$) and later perform the weak-damping approximation on the NIBA kernels.

4.3.1 Undamped case ($\kappa = 0$)

In this Subsection we discuss the case of a TLS coupled with an undamped HO initially prepared in a thermal equilibrium state. The pole equation reads now

$$\lambda_p + K_0^s(\lambda_p) = 0\,, \tag{4.22}$$

with

$$K_0^s(\lambda) = \Delta^2 \int_0^\infty \mathrm{d}\tau e^{-\lambda\tau}\, e^{-S_0(\tau)} \cos\left(R_0(\tau)\right), \tag{4.23}$$

where we denoted with λ_p the solution of the undamped pole equation. Notice that $K_0^s(\lambda)$ has the same expression as in Eq. (4.14), if one replaces S and R with S_0 and R_0, respectively. In order to evaluate Eq. (4.23) analytically, we replace $\cos\left(R_0\left(\tau\right)\right)$ with $\mathfrak{Re}\{\exp\left(\mathrm{i}R_0\left(\tau\right)\right)\}$ and we perform the Jacobi-Anger expansion [81]

$$e^{\mathrm{i}z\cos y} \equiv J_0(z) + 2\sum_{n=1}^{+\infty} \mathrm{i}^n J_n(z)\cos\left(ny\right), \tag{4.24}$$

where $J_n(z)$ are Bessel functions of a complex argument. These expansions are valid only if z is independent of y, which is the case here. We also make use of Graf's Addition Theorem

$$\sum_{k=-\infty}^{\infty} J_{n+k}(u) J_k(v) \begin{matrix}\cos\\ \sin\end{matrix}(k\alpha) = J_n(w) \begin{matrix}\cos\\ \sin\end{matrix}(n\chi), \tag{4.25}$$

where

$$w = \sqrt{u^2 + v^2 - 2\,u\,v\,\cos\alpha} \tag{4.26}$$

and

$$\begin{cases} u - v\cos\alpha = w\cos\chi, & (4.27a) \\ v\sin\alpha = w\sin\chi. & (4.27b) \end{cases}$$

We finally obtain

$$K_0^s(\lambda) = \Delta^2 e^Y \int_0^\infty \mathrm{d}\tau e^{-\lambda\tau} \mathfrak{Re}\left[J_0(u_0) + 2\sum_{n=1}^{+\infty} \mathrm{i}^n J_n(u_0)\cos\left[n(\Omega t - x)\right]\right] \tag{4.28}$$

where (see App. C)

$$u_0 = \frac{\mathrm{i}Y}{\cos x} = \mathrm{i}\sqrt{Y^2 - W^2} = \mathrm{i}\frac{4g^2}{\Omega^2}\frac{1}{\sinh\left(\frac{\beta\Omega}{2}\right)}, \tag{4.29a}$$

$$x = \pi + \mathrm{i}\frac{\beta\Omega}{2} \quad \left(\tan x = -\mathrm{i}\frac{W}{Y}\right). \tag{4.29b}$$

After expanding the cosine which appears in the Eq. (4.28) and after noticing that $J_0(u_0)$ and $\mathrm{i}^n J_n(u_0)$ are always real, the espression for the symmetric kernel in the undamped case finally reads

$$K_0^s(\lambda) = \Delta^2 e^Y \int_0^\infty \mathrm{d}\tau e^{-\lambda\tau}\left[J_0(u_0) + 2\sum_{n=1}^{+\infty}(-\mathrm{i})^n J_n(u_0)\cos\left(n\Omega\tau\right)\cosh\left(n\frac{\beta\Omega}{2}\right)\right]. \tag{4.30}$$

It is useful to introduce here some amplitudes, in order to enhance the readability of the kernel. We therefore define

$$\Delta_{n_{(c)}} \equiv \Delta e^{Y/2}\sqrt{(2-\delta_{n,0})\,(-\mathrm{i})^n J_n(u_0)\cosh\left(n\frac{\beta\Omega}{2}\right)}, \tag{4.31a}$$

such that we can rewrite Eq. (4.30) in the very compact form

$$K_0^s(\lambda) = \sum_{n=0}^{+\infty}\Delta_{n_{(c)}}^2 \int_0^\infty \mathrm{d}\tau e^{-\lambda\tau}\cos\left(n\Omega\tau\right). \tag{4.32}$$

The population difference $P_0(\lambda)$ in the undamped case becomes

$$P_0(\lambda) = \frac{1}{\lambda + K_0^s(\lambda)} \tag{4.33}$$

$$= \frac{1}{\lambda\left[1+\sum_{n=0}^{+\infty}\Delta^2_{n_{(c)}}\frac{1}{\lambda^2+n^2\Omega^2}\right]} \tag{4.34}$$

$$= \frac{\lambda^2\prod_{n=1}^{\infty}(\lambda^2+n^2\Omega^2)}{\lambda\left[\prod_{n=0}^{\infty}(\lambda^2+n^2\Omega^2)+\sum_{m=0}^{+\infty}\Delta^2_{m_{(c)}}\prod_{\substack{n=0\\n\neq m}}^{+\infty}(\lambda^2+n^2\Omega^2)\right]}, \tag{4.35}$$

and it is clear that the pole in $\lambda = 0$ is not a physical one, since $P_0(\lambda = 0)$ vanishes. This means that the dissipation-free ($\kappa = 0$) pole equation reads

$$\lambda_p + K_0^s(\lambda_p) = 0 \quad \rightarrow \quad \prod_{n=0}^{\infty}(\lambda_p^2+n^2\Omega^2)+\sum_{m=0}^{+\infty}\Delta^2_{m_{(c)}}\prod_{\substack{n=0\\n\neq m}}^{+\infty}(\lambda_p^2+n^2\Omega^2) = 0. \tag{4.36}$$

4.3.2 The weak-damping population difference $P_{\mathrm{WDA}}(t)$

The weak-damping kernel $K^s_{\mathrm{WDA}}(\lambda)$ is obtained from Eq. (4.14) by retaining only terms up to first order in the linearized in κ bath correlation functions S_1 and R_1. It reads

$$K^s_{\mathrm{WDA}}(\lambda) = \Delta^2\int_0^{\infty}\mathrm{d}\tau e^{-\lambda\tau}\, e^{-S_0(\tau)}\left\{\cos\left(R_0(\tau)\right)\left[1-S_1(\tau)\right]-\sin\left(R_0(\tau)\right)R_1(\tau)\right\}. \tag{4.37}$$

The WDA kernel will be used in Eq. (4.12) to solve the pole equation and finally obtain $P_{\mathrm{WDA}}(t)$. Consistent with the previous prescription $\kappa \ll 1$, we can expand the solutions λ^* of the pole equation around the solutions λ_p of the non-interacting pole equation up to first order in κ In other terms

$$\lambda^* = \lambda_p - \kappa\gamma_p + \mathrm{i}\kappa\varphi, \tag{4.38}$$

where λ_p satisfies the undamped pole equation (4.36). By inserting Eq. (4.16) and (4.38) in Eq. (4.37), one finds the following expressions for the kernels (to first order in κ) at the poles:

$$\begin{aligned} K^s_{\mathrm{WDA}}(\lambda^*) = \Delta^2 &\int_0^{\infty}\mathrm{d}\tau e^{-\lambda_p\tau}\, e^{-S_0(\tau)} \\ &\times\left\{\cos\left(R_0(\tau)\right)\left[1+\kappa\gamma_p\tau-\mathrm{i}\kappa\varphi\tau-S_1(\tau)\right]-\sin\left(R_0(\tau)\right)R_1(\tau)\right\}+\mathcal{O}[\kappa^2]. \end{aligned} \tag{4.39}$$

According to Eq. (4.39), the pole equation (4.12) now reads

$$-\kappa\gamma_p + \mathrm{i}\kappa\varphi + \Delta^2\int_0^{\infty}\mathrm{d}\tau e^{-\lambda_p\tau}\, e^{-S_0(\tau)}$$

$$\times \{\cos(R_0(\tau))\,[\kappa\gamma_p\tau - \mathrm{i}\kappa\varphi\tau - S_1(\tau)] - \sin(R_0(\tau))R_1(\tau)\} = 0\,, \tag{4.40}$$

where we used the pole equation for the undamped case (4.22). After isolating the real and the imaginary terms from the above equation[1], we find

$$\begin{aligned} -\kappa\gamma_p &\left[1 - \Delta^2 \int_0^\infty \mathrm{d}\tau e^{-\lambda_p\tau}\, e^{-S_0(\tau)} \cos(R_0(\tau))\,\tau\right] \\ &= \Delta^2 \int_0^\infty \mathrm{d}\tau e^{-\lambda_p\tau}\, e^{-S_0(\tau)}\,[\cos(R_0(\tau))\, S_1(\tau) + \sin(R_0(\tau))R_1(\tau)]\,, \end{aligned} \tag{4.41a}$$

$$\mathrm{i}\kappa\varphi \left[1 - \Delta^2 \int_0^\infty \mathrm{d}\tau e^{-\lambda_p\tau}\, e^{-S_0(\tau)} \cos(R_0(\tau))\,\tau\right] = 0. \tag{4.41b}$$

If the term between brackets is different from zero, one easily gets $\varphi = 0$ and

$$\gamma_p = -\frac{\Delta}{\kappa}^2 \frac{\int_0^\infty \mathrm{d}\tau e^{-\lambda_p\tau}\, e^{-S_0(\tau)}\,[\cos(R_0(\tau))\, S_1(\tau) + \sin(R_0(\tau))R_1(\tau)]}{1 - \Delta^2 \int_0^\infty \mathrm{d}\tau e^{-\lambda_p\tau}\, e^{-S_0(\tau)} \cos(R_0(\tau))\,\tau}\,, \tag{4.42}$$

which we can also rewrite as

$$\gamma_p = -\frac{\Delta}{\kappa}^2 \frac{\int_0^\infty \mathrm{d}\tau e^{-\lambda_p\tau}\, e^{-S_0(\tau)}\,[\cos(R_0(\tau))\, S_1(\tau) + \sin(R_0(\tau))R_1(\tau)]}{\left[1 + \dfrac{\partial}{\partial\lambda} K_0^s(\lambda)\right]\Big|_{\lambda=\lambda_p}}\,. \tag{4.43}$$

Once we have obtained the expression for the decay rates γ_p corresponding to each pole λ_p, we have all ingredients to get the population difference $P(t)$ with the help of the Residue Theorem. In fact, it holds

$$P(t) \equiv \sum_{\mathrm{Res}} e^{\lambda t} P(\lambda) \tag{4.44}$$

$$= \sum_{\lambda_p} e^{\lambda_p t} e^{-\kappa\gamma_p(\lambda_p)t} \lim_{\lambda=\lambda_0-\kappa\gamma\to\lambda_p-\kappa\gamma_p} [\lambda - (\lambda_p - \kappa\gamma_p)] \frac{1}{\lambda + K^s_{\mathrm{WDA}}(\lambda)}\,, \tag{4.45}$$

as follows from Eq. (4.39). Notice that here we split the damping-dependent and the damping-indipendent contributions as $\lambda = \lambda_0 - \kappa\gamma$. The limit $\lim_{\lambda=\lambda_0-\kappa\gamma\to\lambda_p-\kappa\gamma_p}$ can also be rewritten as $\lim_{\lambda_0\to\lambda_p} \lim_{\gamma\to\gamma_p(\lambda_0)}$. Hence, performing first the limit over the decay rate γ, we

[1] Note that the Laplace Transform of an odd function of τ is even in λ and vice versa. In this case, the integrand is odd in τ, thus the corresponding Laplace Transform is even in λ: For pure-imaginary values of λ, the result of the integral is real.

find

$$P(t) = \sum_{\lambda_p} e^{\lambda_p t} e^{-\kappa\gamma_p t} \lim_{\lambda_0 \to \lambda_p} (\lambda_0 - \lambda_p) \left[\lambda_0 + \Delta^2 \int_0^\infty \mathrm{d}\tau e^{-\lambda_0 \tau}\, e^{-S_0(\tau)} \cos\left(R_0(\tau)\right) \right.$$
$$\left. -\kappa \left(1 - \Delta^2 \int_0^\infty \mathrm{d}\tau e^{-\lambda_0 \tau}\, e^{-S_0(\tau)} \cos\left(R_0(\tau)\right)\tau \right) \left(\gamma_p(\lambda_0) - \gamma_p(\lambda_p)\right) \right]^{-1} \tag{4.46}$$

and performing the limit over λ_0, $P(t)$ finally reads

$$P(t) = \sum_{\lambda_p} e^{\lambda_p t} e^{-\kappa\gamma_p t} \lim_{\lambda_0 \to \lambda_p} (\lambda_0 - \lambda_p) P_0(\lambda_0)\,, \tag{4.47}$$

as it follows from Eq. (4.33). We stress that the dynamics in the (weakly) damped case is essentially determined by the correponding undamped dynamics, the damping being only responsible for pole-dependent exponentially decaying factors.

4.3.3 Series expression for the weakly-damped symmetric kernel and decay rate

Now we want to find a compact analytical form for the kernel $K^s_{\mathrm{WDA}}(\lambda)$ and the decay rate γ_p (4.37) and (4.43), respectively. To this extent, let us start from the kernel $K^s_{\mathrm{WDA}}(\lambda)$, the generalization to the decay rate being straightforward.

As in the undamped case, in Eq. (4.37) we replace $\cos\left(R_0\left(\tau\right)\right)$ with $\mathfrak{Re}\{\exp\left(\mathrm{i}R_0\left(\tau\right)\right)\}$ and $\sin\left(R_0\left(\tau\right)\right)$ with $\mathfrak{Im}\{\exp\left(\mathrm{i}R_0\left(\tau\right)\right)\}$, then we use the Jacobi-Anger expansion (4.24) and obtain

$$K^s_{\mathrm{WDA}}(\lambda) = \Delta^2 e^Y \int_0^\infty \mathrm{d}\tau e^{-\lambda\tau} \left\{ \mathfrak{Re}\left[J_0(u_0) + 2\sum_{n=1}^{+\infty} \mathrm{i}^n J_n(u_0) \cos\left[n(\Omega t - x)\right] \right] \right.$$
$$\left. \times \left[1 - S_1(\tau)\right] - \mathfrak{Im}\left[J_0(u_0) + 2\sum_{n=1}^{+\infty} \mathrm{i}^n J_n(u_0) \cos\left[n(\Omega t - x)\right] \right] R_1(\tau) \right\} \tag{4.48}$$

where u_0 and x are given by Eq. (4.29a) and Eq. (4.29b). As done before, by noticing that $J_0(u_0)$ and $\mathrm{i}^n J_n(u_0)$ are always real, the WDA kernel can be finally rewritten as

$$K^s_{\mathrm{WDA}}(\lambda) = \sum_{n=0}^{+\infty} \int_0^\infty \mathrm{d}\tau e^{-\lambda\tau} \left\{ \Delta^2_{n_{(c)}} \cos\left(n\Omega\tau\right) \left[1 - S_1(\tau)\right] + \Delta^2_{n_{(s)}} \sin\left(n\Omega\tau\right) R_1(\tau) \right\}, \tag{4.49}$$

where $\Delta_{n_{(c)}}$ have been already defined in Eq. (4.31a) and

$$\Delta_{n_{(s)}} \equiv \Delta e^{Y/2}\sqrt{(2-\delta_{n,0})\,(-\mathrm{i})^n J_n(u_0)\sinh\left(n\frac{\beta\Omega}{2}\right)}. \tag{4.50}$$

The expression for $P(\lambda)$ follows from (4.49) (see the discussion in the Section 4.3.5 below). Along similar lines, the decay rate γ_p, cf. Eq. (4.43), may also be written as

$$\gamma_p = \frac{1}{\kappa}\frac{\sum_{n=0}^{+\infty}\int_0^\infty \mathrm{d}\tau e^{-\lambda_p\tau}\left[\Delta^2_{n_{(c)}}\cos(n\Omega\tau)\,S_1(\tau)+\Delta^2_{n_{(s)}}\sin(n\Omega\tau)\,R_1(\tau)\right]}{\sum_{n=0}^{+\infty}\Delta^2_{n_{(c)}}\dfrac{2\lambda_p^2}{(\lambda_p^2+n^2\Omega^2)^2}}. \tag{4.51}$$

4.3.4 The case $n = 0,\ n = 1$

In order to obtain a more useful analytical expression for $P(t)$, we notice that the lowest orders in n give the largest contribution to the sum in Eq. (4.49), because the amplitudes Δ_n^2 depend on Bessel functions $J_n(x)$, which roughly behave as x^n as soon as the argument becomes small. Since we investigate a regime of temperatures generally smaller than Ω, i.e. $\beta\hbar\Omega/2 \gtrsim 1$, and of coupling such that in general $g \lesssim \Omega$, then the quantity u_0 is smaller than one. Hence, we just restrict our analysis to the orders $n = 0, n = 1$ in Eqs. (4.49) and (4.51). The undamped pole equation Eq. (4.36) therefore becomes (we identify here Δ_0 with $\Delta_{0_{(c)}}$ for the sake of clarity)

$$(\lambda_p^2+\Omega^2)(\lambda_p^2+\Delta_0^2)+\lambda_p^2\Delta^2_{1_{(c)}} = 0\,, \tag{4.52}$$

yielding

$$\lambda_p^2 = -\frac{\Delta_0^2+\Delta^2_{1_{(c)}}+\Omega^2}{2} \pm \sqrt{\left(\frac{\Delta_0^2-\Omega^2}{2}\right)^2+\frac{\Delta^2_{1_{(c)}}}{2}\left(\Delta_0^2+\frac{\Delta^2_{1_{(c)}}}{2}+\Omega^2\right)} \equiv \lambda_\pm^2\,. \tag{4.53}$$

We notice that only terms quadratic in λ_p appear in the formal expression of the decay rate (cf. Eq. (D.1)). Hence, it is enough to express the poles as in Eq. (4.53).

Given the poles in the undamped case, we can substitute each of them in the Eq. (4.51) for γ_p with sum restricted to $n = 0, n = 1$. We will refer to them as $\gamma_\pm = \gamma(\lambda_\pm)$, the explicit form of the decay rate being given in App. D.

4.3.5 Analytical expression for $P(t)$

In order to obtain the analytical expression for $P(t)$ in the symmetric case, let us start again from Eq. (4.47). By summing up all residues contributions, we end up with

$$\begin{aligned} P(t) = e^{-\kappa\gamma_- t}\,\frac{\lambda_-^2+\Omega^2}{\lambda_-^2+\lambda_+^2}\cos\Omega_- t + e^{-\kappa\gamma_+ t}\,\frac{\lambda_+^2+\Omega^2}{\lambda_+^2+\lambda_-^2}\cos\Omega_+ t \\ - e^{-\kappa\gamma_- t}\,\frac{\kappa\gamma_-}{\Omega_-}\,\frac{\lambda_-^2+\Omega^2}{\lambda_-^2-\lambda_+^2}\sin\Omega_- t - e^{-\kappa\gamma_+ t}\,\frac{\kappa\gamma_+}{\Omega_+}\,\frac{\lambda_+^2+\Omega^2}{\lambda_+^2-\lambda_-^2}\sin\Omega_+ t, \end{aligned} \tag{4.54}$$

where $\Omega_\pm \equiv -\mathrm{i}\lambda_\pm$, as follows from Eq. (4.53).

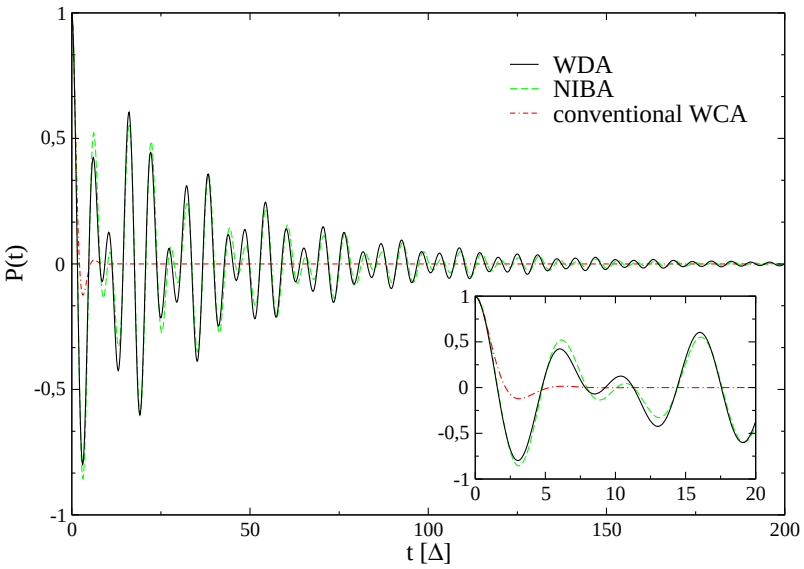

Figure 4.3: Time evolution of $P(t)$ within the NIBA as well as the analytical WDA. The parameters are as in Fig. 4.1, namely $\alpha = 4\,10^{-3}$, ($g = 0.18$), $\Omega = \Delta$ and $\Gamma = 0.097$, $T = 0.1$ (in units of Δ). Notice the perfect agreement between the numerical NIBA and the analytical WDA. A perturbative approach in $G_{\mathrm{eff}}(\omega)$, denoted here as "conventional WCA" (see (4.55)), completely fails because it does not even account for the two main oscillation frequencies. In the inset the short-time dynamics is showed in detail.

Notice that the expression for $P(t)$ is invariant upon exchanging the frequencies $\Omega_- \to \Omega_+$.

The analytical formula Eq. (4.54) for $P(t)$ is compared in Fig. 4.3 with the exact numerical NIBA and the conventional weak-coupling approximation (WCA), obtained by a linear expansion of the bath correlation function for the coupling strength α [12]. There,

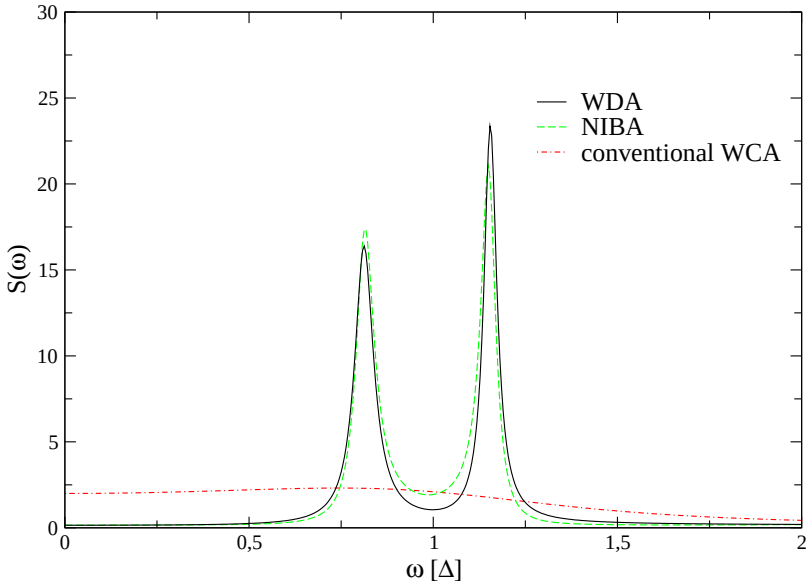

Figure 4.4: Spectral function of $P(t)$, corresponding to the same regime as in the previuos case. One clearly sees that the Fourier Transforms of NIBA and WDA exhibit a double peak structure. In contrast, the WCA predicts a single broadened oscillation peak.

the analytical form for the probability difference reads in the symmetric case

$$P(t) = \left\{\cos \Delta t + \frac{\gamma_\varphi}{\Delta} \sin \Delta t\right\} e^{-\gamma_\varphi t}, \tag{4.55}$$

where $\gamma_\phi = \frac{\pi}{4} S(\Delta)$ is the dephasing rate. Moreover, $S(\omega) \equiv G_{\text{eff}}(\omega) \coth\left(\frac{\hbar\omega}{2k_{\text{B}}T}\right)$ is a spectral contribution which represents emission and absorption of a single photon. The choice of parameters in Figs. 4.3 and 4.4 is the same as in Fig. 4.1 and as Ref. [88], under the resonance condition $\Omega = \Delta$. One can notice a very good agreement between NIBA and the analytical WDA, whereas Eq. (4.55) completely fails in describing the oscillatory behaviour of $P(t)$. In Fig. 4.4 the corresponding Fourier Transform of the probability difference is showed. There, one can see the missing oscillation frequency of the conventional WCA given by Eq. (4.55) and the excellent agreement between the numerical NIBA and our analytical solution WDA.

Finally, in Fig. 4.5 we show a comparison among the WDA and the NIBA in presence of finite detuning $|\Delta - \Omega| = 0.5$ for a higher coupling strength between qubit and HO ($g = 0.3$), keeping the coupling between detector and environment constant. Also in this case, the weak-damping approximation fully agrees with the numerical solution of the NIBA. In the

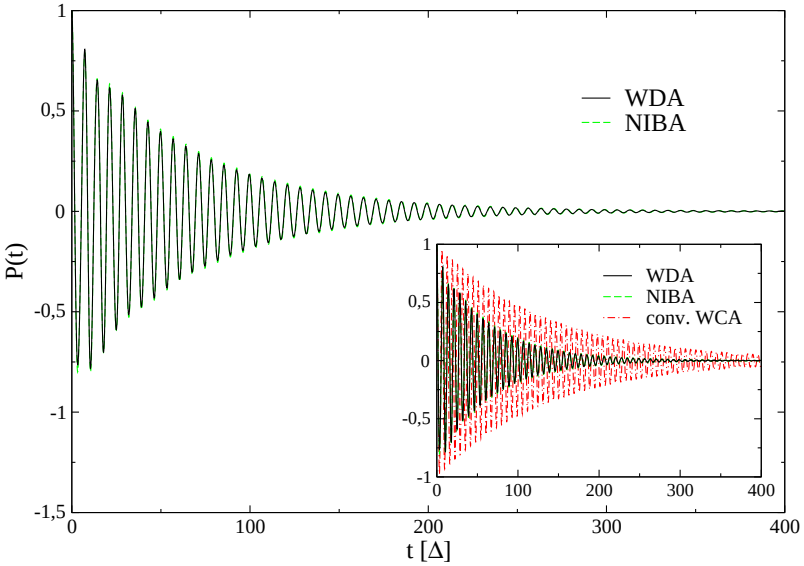

Figure 4.5: Time evolution of $P(t)$ at finite detuning within the NIBA and the analytical WDA. The parameters are as in Fig. 4.2, namely $\alpha = 5\,10^{-3}$, ($g = 0.3$), $\Omega = 1.5\Delta$ and $\Gamma = 0.145$, $T = 0.1$ (in units of Δ). Again, the agreement between the numerical NIBA and the analytical WDA is striking. The conventional WCA (4.55), see inset, also in this case fails in describing the correct dynamics, as expected.

inset one can also notice the disagreement of both models with the conventional WCA, characterized by a single oscillation frequency at $\omega = \Delta$, see in particular Fig. 4.6 which shows the Fourier Transform of $P(t)$.

4.4 Conclusions

In conclusion, we discussed the dynamics of a symmetric TLS interacting with an effective structured environment, modelling a qubit interacting with a readout dissipative detector. This case has not been so far deeply investigated within an analytical approach out of resonance, i.e. if the tunneling frequency Δ differs from the detection frequency Ω. We approximated an exact generalized master equation (GME) within a novel *weak-damping approximation* (WDA) which, in contrast to "conventional" weak-coupling approaches [12], is able to correctly reproduce the dynamics, characterized by multiple oscillation frequencies. The WDA approach is based on a first approximation of the kernel of the GME up to second order in the tunneling frequency, i.e. the Non-Interacting Blip Approximation (NIBA), which for a symmetric spin-boson model is valid over the *whole* range of param-

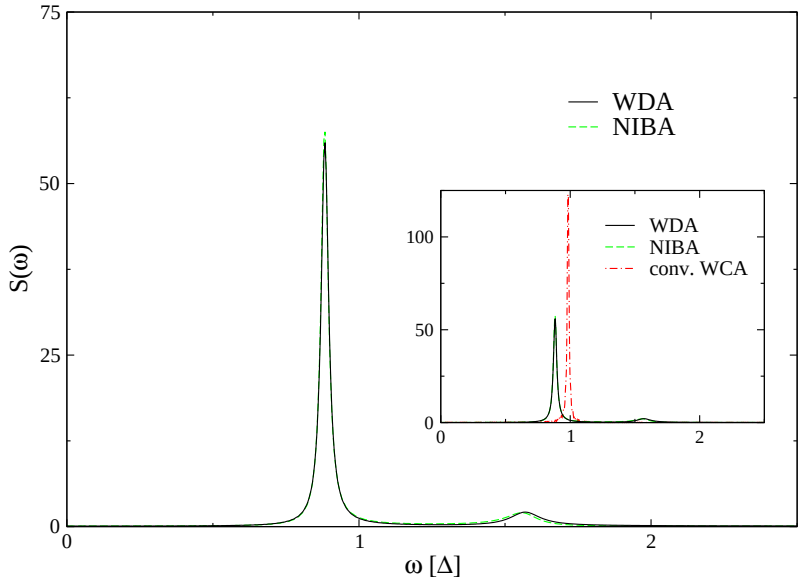

Figure 4.6: Spectral function of $P(t)$ for the NIBA and the analytical WDA (same parameters as in the previous Fig. 4.5). The oscillation frequencies of WDA and NIBA coincide, whereas in the inset one can at first glance see the appearance of a single peak concerning the Fourier Transform of the conventional WCA.

eters. Then, in order to obtain an analytical form for the dynamical population difference $P(t)$, for small enough temperatures (i.e. $k_{\mathrm{B}}T \lesssim \hbar\Omega$) and small coupling strength between detector and environment, we approximated the NIBA kernels within a weak-damping approach, whose details are explained in Sec. 4.3. The agreement of our analytical solution for $P(t)$ valid at *arbitrary* detuning $|\Delta - \Omega| \neq 0$ with the numerical NIBA is striking. The former one is able to reproduce the two oscillation frequencies which are related to the tunneling and the detection frequency, respectively, as predicted by *ab-initio* numerical schemes like QUAPI [88]. Our results are of interest for the understanding of dephasing in qubits strongly coupled to a broadened harmonic mode as e.g. flux qubits [5, 19] or cavity QED qubits [85].

I offer you peace.
I offer you love.
I offer you friendship.
I see your beauty.
I hear your need.
I feel your feelings.
My wisdom flows from the Highest Source.
I salute that Source in you.
Let us work together for unity and love.

Mohandas Karamchand "Mahatma" Gandhi

Chapter 5

Coherence and tunneling in a dissipative bistable potential

In this Chapter, we wish to release the constraint of reducing the Hilbert space to the lowest two levels and take into account in the dynamics higher-lying energy eigenstates which could be eventually populated. In many experimental situations, the temperature is not low enough and the spacing between the energy levels is so small that higher energy levels are in fact populated [22, 23, 24, 25, 26, 27, 28, 29, 30, 31, 32]. We generalize in this Chapter the results of Refs. [28, 29], where an approximated treatment of the particle dynamics was provided, being valid for large enough damping and/or temperatures of the order of the classical oscillation frequency in a well. In this regime, the particle dynamics is fully incoherent and well described within the so-called *generalized Non Interacting Cluster Approximation* (gNICA), an approximation analogous to the NIBA for a generic M-level system. In the regime where the typical vibrational relaxation frequency, i.e. the transition between the doublets, is larger than the temperature, gNICA fails. Therefore, in the following we investigate the nontrivial parameter regime $\hbar\Delta_i^{\mathcal{E}} \lesssim k_{\rm B}T < \hbar\omega_0$, where the bath induced correlations among tunneling path elements can still be treated within the gNICA, but bath-induced correlation among vibrational relaxation events must be fully retained.

By starting from the general formulation of Chapter 2 in terms of path-integrals, we derive an approximation for describing the more complex dynamics in a generic dissipative bistable potential in the presence of a static external bias. The assumption of a static external driving can be easily released to include a time dependence, see e.g. [62]. We also observe that the formalism developed in this Chapter for a bistable potential can be soon generalized to the case of a dissipative multilevel system. The steps followed to

develop our approximation are explained in detail in Sec. 5.1. We obtain in Sec. 5.1.2 a generalized master equation for the diagonal elements of the reduced density matrix, where the dynamics *intra*-well is separated by the *inter*-well transitions. Finally, in Sec. 5.2 we derive the so-called *Weakly Interacting VR-Blip Approximation* which constitutes our main finding of the present Chapter.

Throughout this Chapter, we choose an Ohmic spectral density with an exponential cut-off, i.e.

$$J(\omega) = \eta\,\omega\,\mathrm{e}^{-|\omega|/\omega_c}, \tag{5.1}$$

where $\eta = \mathcal{M}\gamma$, with the viscosity coefficient γ being the coupling strength to the bath, and the cut-off frequency $\omega_c \gg (\omega_0, \Delta_i^{\mathcal{E}}, \gamma)$ is taken to be the largest frequency in the model.

In particular, for the Ohmic spectral function given in Eq. (5.1), the bath correlation function (2.16) takes the form

$$S(t) = \frac{\eta}{\pi\hbar}\left\{-\ln\left|\frac{\Gamma(1+\frac{1}{\hbar\beta\omega_c}+\frac{it}{\hbar\beta})}{\Gamma(1+\frac{1}{\hbar\beta\omega_c})}\right|^2 + \frac{1}{2}\ln(1+\omega_c^2t^2)\right\}, \tag{5.2a}$$

$$R(t) = \frac{\eta}{\pi\hbar}\arctan(\omega_c t)\,. \tag{5.2b}$$

In the following we assume that the condition $\hbar\omega_c\beta \gg 1$ is verified. Hence, by noticing that $\Gamma(1+iy)\Gamma(1-iy) = \pi y/\sinh(\pi y)$, the real part $S(t)$ of the bath correlation function $Q(t)$ can also be rewritten as follows:

$$S(t) = \frac{\eta}{\pi\hbar}\left\{-\ln\left[\frac{\pi t}{\hbar\beta\sinh(\pi t/\hbar\beta)}\right] + \frac{1}{2}\ln(1+\omega_c^2t^2)\right\}. \tag{5.3}$$

In the so-called *scaling limit*, namely at long times $\omega_c t \to \infty$ the function $S(t)$ behaves like

$$S_{\text{s.l.}}(t) \overset{\omega_c t\to\infty}{\longrightarrow} \frac{\eta}{\pi\hbar}\ln\left(\frac{\hbar\beta\omega_c}{\pi}\sinh\frac{\pi t}{\hbar\beta}\right) \tag{5.4}$$

$$\approx \frac{\eta}{\pi}\left\{\frac{\pi t}{\hbar\beta} + \ln\left(\frac{\hbar\beta\omega_c}{2\pi}\right)\right\}, \qquad \omega_c t \gg \hbar\omega_c\beta\,, \tag{5.5}$$

which shows a linear behavior. This illustrates that the correlations between the paths are damped out exponentially at long times for a low temperature Ohmic bath. For long times $\omega_c t \to \infty$, the arctan-function in the imaginary part $R(t)$ approaches 1 or -1, depending on

the sign of the argument, i.e.,

$$R(t) \overset{\omega_c t\to\infty}{\longrightarrow} \frac{\eta}{2\hbar}\mathrm{sign}(t)\,, \tag{5.6}$$

so that the imaginary part $R(t)$ becomes a constant function for all times t.

5.1 Separation of time scales and dynamics

In this section we want to introduce some approximations to (2.25) which are justified in the regime of moderate to high temperatures and/or moderate to strong damping. They exploit the *separation of time scales* between tunneling events among DVR-states located in different wells and vibrational relaxation (VR) transitions.

5.1.1 Which simplifications are allowed due to the separation of time scales?

`Simplification (1).` The first approximation we do is to consider only paths in the summation (2.25) which return to a diagonal state after a VR or tunneling transition. Namely, every second time interval is a sojourn. This assumption relies on the fact that these paths give the major contribution to the summation, since the more a path travels off-diagonal, the more damped every out-of-diagonal excursion is. Hence, the expression for the occupation probabilities becomes ($t > t_0$)

$$\rho_{\mu_N\mu_N}(t) = \langle q_{\mu_N}|\boldsymbol{\rho}(t)|q_{\mu_N}\rangle = \sum_{\mu_0=1}^{M}\rho_{\mu_0\mu_0}\Bigg[\delta_{\mu_N\mu_0} \tag{5.7}$$

$$+\sum_{n=1}^{\infty}\int_{t_0}^{t}\mathcal{D}\{t_j\}\sum_{\{\mu_j\nu_j\}}B_n\,(-1)^n\prod_{j=0}^{n-1}(-1)^{\varsigma_{2j}}\frac{\Delta_{2j+1}^2}{2^2}\,F_n\,G_n\,\tilde{H}_n\Bigg]\,, \tag{5.8}$$

where

$$B_n \equiv \exp\left\{-\mathrm{i}\sum_{j=1}^{n}\epsilon_{\mu_{2j-1}\nu_{2j-1}}\tau_j\right\}\,, \tag{5.9}$$

$$F_n \equiv \exp\left\{-\sum_{l=1}^{n}\xi_{2l-1}^2 S_{2l,2l-1}\right\}\,, \tag{5.10}$$

$$G_n \equiv \exp\left\{-\sum_{l=2}^{n}\sum_{j=1}^{l-1}\xi_{2l-1}\Lambda_{l,j}\xi_{2j-1}\right\}, \tag{5.11}$$

$$\tilde{H}_n \equiv \exp\left\{-i\sum_{l=1}^{n}\sum_{j=0}^{l-1}\xi_{2l-1}\ \ _{l,j}\right\} \tag{5.12}$$

and $n = N/2$ (which counts the number of blips). Moreover, $\varsigma_{2j} \equiv \delta_{2j} + \delta_{2j+1}$, $S_{j,k} \equiv S(t_j - t_k)$ and analogously for R. The functions $\Lambda_{j,k}$, $X_{j,k}$ and $_{l,j}$ are defined as

$$\Lambda_{j,k} = -S_{2j,2k} + S_{2j,2k-1} - S_{2j-1,2k-1} + S_{2j-1,2k}\,, \tag{5.13}$$

$$X_{j,k} = +R_{2j,k} - R_{2j-1,k}\,, \tag{5.14}$$

$$_{j,k} = X_{j,2k}\chi_{2k} + X_{j,2k+1}\chi_{2k+1}\,, \tag{5.15}$$

such that $\Lambda_{j,k}$ describes blip-blip correlations, while $_{j,k}$ accounts for blip-sojourn interactions. In particular, when $t_0 \to -\infty$, the term $_{j,0}$ reduces to $X_{j,1}\chi_1$ only and $\tilde{H}_n$ becomes:

$$H_n \equiv \lim_{t_0\to-\infty}\tilde{H}_n = I_n \exp\left\{-i\sum_{l=2}^{n}\xi_{2l-1}X_{l,1}\chi_1\right\}\exp\left\{-i\sum_{l=2}^{n}\sum_{j=2}^{2(l-1)}\xi_{2l-1}X_{l,j}\chi_j\right\}, \tag{5.16}$$

where

$$I_n \equiv \exp\left\{-i\sum_{l=1}^{n}\xi_{2l-1}R_{2l,2l-1}\chi_{2l-1}\right\} \tag{5.17}$$

accounts for the interaction of a blip with its preceeding sojourn.

In the case $M = 2$, it holds $\chi_{2k+1} = -\chi_{2k}$ and this allows some simplifications: The function $_{j,k}$ simplifies as $+\tilde{X}_{j,k}\chi_{2k}$, with $\tilde{X}_{j,k} = X_{j,2k} - X_{j,2k+1}$, $k > 1$, ($\tilde{X}_{j,0} = -X_{j,1}$) and there our notation can be mapped into the notation introduced in Sec. 3.2 for the spin-boson problem by identifying $\xi_{2j-1} = \xi_j^{[\text{Sec.3.2}]}$ and $\chi_{2j} = \chi_j^{[\text{Sec.3.2}]}$.

`Simplification (2).` This approximation consists in neglecting interactions among the so-called *tunneling*-blips (T-blips) as well as among tunneling and VR events. This is justified by the fact that tunneling events are rare on the scale of VR, and hence bath-induced correlations are exponentially suppressed. Consistently, we also neglect interactions between two VR events interrupted by a tunneling event. These assumptions allow us then to completely separate the intra-well dynamics i.e. among states lying in the same well

from the inter-well dynamics.

Notice that correlations between VR events in the same well, occurring between two successive tunneling transitions, are retained in our approximation.

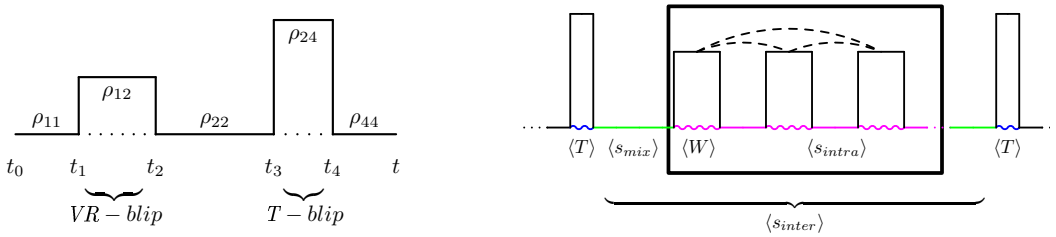

(a) Allowed path from simplification (1)

(b) Allowed inter-blip interactions

Figure 5.1: [Panel (a)] Generic path in an M-level system according to approximation (1): Only paths which return to diagonal states after two VR- or T-transitions are retained. Hence, such paths can be viewed as a sequence of sojourns interrupted by VR-blips and T-blips. [Panel (b)] Retained bath-induced correlations according to approximation (2). Wiggled lines denote intra-blip interactions and dashed lines inter-VR-interactions. Blip-sojourn interactions are omitted for the sake of clarity. Due to the time-scale separation between tunneling and vibrational relaxation events, *tunneling*-blips (blue) are rare with respect to VR-blips (magenta). We indicated here with $\langle T\rangle$ and $\langle W\rangle$ the average T-blip and VR-blip time intervals, respectively.

In Fig. 5.1(a) a generic path is depicted, as allowed by simplification (1), where the system is back to a diagonal state of the RDM after two steps (see in contrast Fig. 2.1(b)). In Fig. 5.1(b) the blip-blip correlations among VR-blips, as kept in simplification (2), are shown. The different heights mean that the path travels out of diagonal reaching further (T-blips) or closer (VR-blips) out-of-diagonal RDM states. We isolate with a box all transitions taking place within the same well (magenta) from those connecting one well to the other (blue).The influence of the bath is to couple each blip with all preceeding sojourns and blips, as well as to induce intra-blip interactions.

In Fig. 5.1(b), we also indicate the different time scales associated to the various tunneling and VR-processes. In particular, we call $\langle T\rangle$ the average time interval spent in a T-blip (blue) and $\langle W\rangle$ the average time spent in a VR-blip (magenta). The typical length of a sojourn in the box is $\langle s_{intra}\rangle \propto \Delta_{intra}^{-1} \sim \omega_0^{-1}$ and that of a "*tunneling*-sojourn" (which is of the order of the time interval between two tunneling events) is $\langle s_{inter}\rangle \propto \Delta_{inter}^{-1}$. Finally, we denote with $\langle s_{mix}\rangle$ the average time spent between the last VR-transition and a tunneling

event.

The bath interactions within a blip of length τ which connects the sojourns (ν,ν) with (μ,μ) are proportional to $\exp[-\xi^2_{\mu\nu}S(\tau)]$, which becomes for long times $\exp[-\frac{\eta}{\hbar^2}(q_\mu - q_\nu)^2 k_{\rm B}T\tau]$, as follows from Eq. (5.5). For a T-blip it holds $q_\mu - q_\nu \approx q_0$, such that we can define (in analogy with the *spin-boson* case) the dimensionless parameter $\alpha \equiv \eta\, q_0^2/2\pi\hbar$ – the so-called *Kondo parameter* – and say that a typical T-blip length is $\langle T\rangle \sim \hbar/\alpha k_{\rm B}T$. Following this analogy, we could also define an "effective" coupling constant as $\alpha^{\mu\nu}_{intra} = \eta\,(q_\mu - q_\nu)^2/2\pi\hbar$ for the blips inside the box and correspondingly we obtain $\langle W\rangle \sim \hbar/\alpha^{\mu\nu}_{intra}k_{\rm B}T$, which in general will be much larger than $\langle T\rangle$, since the DVR-states inside a well are closer to each other than two generic states lying in different wells.

We could here then reformulate the limit of validity of the approximation given in [29], where all inter-blip correlations are neglected. This is justified at high temperature and/or large damping where $\langle W\rangle \ll \langle s_{intra}\rangle$, or equivalently $\hbar\omega_0/\alpha_{intra}k_{\rm B}T \ll 1$.

In order to extend the analysis in [29] to lower temperatures, we consider now the parameter regime, see Fig. 5.1(b), where interactions among T-blips as well as between the adjacent T-blips and the VR-blips are neglected. However, intra-T-blip interactions are retained, as well as among VR-blips which are not interrupted by a T-blip. For this to happen, the condition to be satisfied is:

$$\langle s_{inter}\rangle \geq \langle s_{mix}\rangle \gg \langle T\rangle\,, \tag{5.18}$$

i.e. the distance $\langle s_{mix}\rangle$ between two generic adjacent T- and VR-blips should be large enough to be able to neglect the interaction among them. This results in the possibility to also neglect the T-blips interactions, since $\langle s_{inter}\rangle$ is always larger than or comparable to $\langle s_{mix}\rangle$. The reason for condition (5.18) is that the interaction between a VR-blip and an adjacent T-blip is proportional to

$$\Lambda_{mix} \approx -S(\langle s_{mix}\rangle + \langle W\rangle) + S(\langle T\rangle + \langle s_{mix}\rangle + \langle W\rangle) - S(\langle T\rangle + \langle s_{mix}\rangle) + S(\langle s_{mix}\rangle).$$

This means that, when the interval $\langle s_{mix}\rangle$ is sufficiently large with respect to the average T-blip and VR-blip lengths, Eq. (5.5) can be used yielding $\Lambda_{mix} \approx 0$. Hence, we can consider all T-blips as non-interacting.

In other words, when the temperature and the coupling constant between bath and system are such that the condition of Eq. (5.18) is satisfied, we can perform a sort of Non-Interacting Blip Approximation (NIBA) [3, 12] for the T-blips. However, *all* interactions

among the paths inside the wells must be retained if at the same time $\langle W \rangle \approx \langle s_{intra} \rangle$. Notice that since in our approach the ratio $\langle W \rangle / \langle s_{intra} \rangle$ is not constrained, our model also can describe the situation in [29], as soon as $\langle s_{intra} \rangle \gg \langle W \rangle$. The convenience of our generalization is that we don't suppose necessarily a large damping or high temperature, since the inter-T-blips interactions can be neglected because the many inter-well events well separate the T-blips.

`Simplification (3).` Having separated the tunneling from the vibrational relaxation dynamics, we have still to solve the quite intricated problem of an ensamble of *interacting* VR-blips. In the following, we shall assume that the interaction among VR-blips is weak enough that its effects can be treated to the lowest order. Hence, we call this the *Weakly-Interacting VR-blip Approximation* (VR-WIBA). Its consequences are described in more detail below in Sec. 5.2.

5.1.2 Generalized master equation (GME)

The approximations (1) and (2) allow us to separate inter- and intra-well dynamics. Hence, the irreducible kernels for tunneling and vibrational relaxation, $T_{\mu\nu}$ and $\tilde{W}_{\mu\nu}$ respectively, can be identified and a generalized master equation (GME) for the populations can be derived. This procedure is explained in detail in App. E. It reads ($t \geq t_0$)

$$\dot{\rho}_{\mu\mu}(t) = \sum_{\substack{\nu \notin \{\mu\} \\ \nu = \mu}} \int_{t_0}^{t} dt' T_{\mu\nu}(t-t') \rho_{\nu\nu}(t') + \sum_{\nu \in \{\mu\}} \int_{t_0}^{t} dt' \tilde{W}_{\mu\nu}(t-t') \rho_{\nu\nu}(t') \,, \tag{5.19}$$

where the notation

$$\sum_{\nu \in \{\mu\}}$$

means (from now on) that the sum runs over all states which lie in the same well as μ. Here irreducibility means that the paths associated to a given kernel cannot be cut into uncorrelated pieces at an intermediate sojourn without removing the bath correlations across such a sojourn [12]. Due to our assumption that interactions between T-blips are neglected, as well as between T-blips and VR-blips, the irreducible T-kernel $T_{\mu\nu}$ ($\mu \neq \nu$) is of second order in $\Delta_{\mu\nu}^2$ and reads

$$\begin{aligned} T_{\mu\nu}(t-t') = \frac{\Delta_{\mu\nu}^2}{2} \exp\left\{-(q_\mu - q_\nu)^2 S(t-t')\right\} \\ \times \cos\left\{\epsilon_{\nu\mu}(t-t') - (q_\mu - q_\nu)^2 R(t-t')\right\} (1 - \delta_{\nu \in \{\mu\}}) \,. \end{aligned} \tag{5.20}$$

Here, the factor $(1-\delta_{\nu\in\{\mu\}})$ ensures that μ and ν refer to DVR-states in different wells.

The construction of the irreducible VR-kernels $\tilde{W}_{\mu\nu}$ is more intricated, since correlations between VR transitions must be retained if one is interested in moderate damping strengths and/or intermediate temperatures $\hbar\Delta_{inter} \lesssim k_{\rm B}T \lesssim \hbar\Delta_{intra}$. In particular, one finds that

$$\tilde{W}_{\mu\nu} = W^{(2)}_{\mu\nu} + \Sigma'_{\mu\nu}, \tag{5.21}$$

where we separated the contribution of the second-order kernel (with respect to $\Delta^2_{\mu\nu}$)

$$W^{(2)}_{\mu\nu}(\tau) = \frac{\Delta^2_{\mu\nu}}{2}\exp\left\{-(q_\mu-q_\nu)^2 S(\tau)\right\}\cos\left\{\epsilon_{\nu\mu}\tau-(q_\mu-q_\nu)^2 R(\tau)\right\}\delta_{\nu\in\{\mu\}} \tag{5.22}$$

from the higher order contribution $\Sigma'_{\mu\nu}$, of which we refrain from giving the exact expression here. Notice that retaining only Eq. (5.22) and discarding higher order terms amounts precisely to the approximation discussed in [29], when only lowest order T- and VR-kernels were retained.

Rather, in the following Section we discuss how to perform the approximation (3) on the irreducible kernel $\Sigma'_{\mu\nu}$ valid for Ohmic damping.

5.2 The Weakly Interacting *VR*-Blip Approximation (*VR*-WIBA)

Within the approximation scheme (3), we treat the VR-blips as weakly interacting objects, with blip-blip and blip-sojourn interactions described by Eqs. (5.13) and (5.14), respectively (Weakly-Interacting VR-Blip Approximation or VR-WIBA). Hence, we expand G_n and H_n up to linear order in $\Lambda_{j,k}$ and $X_{j,k}$, respectively, to find for the beyond-second-order contribution $\Sigma'_{\mu\nu} \approx \Sigma^{VR-\rm WIBA}_{\mu\nu} \equiv \Sigma_{\mu\nu}$, with (here $\xi \equiv t-t'$)

$$\begin{aligned}\Sigma_{\mu\nu}(\xi) = \sum_{n=2}^{\infty}\int_{t'}^{t}\mathcal{D}\{t_j\}\sum_{\kappa_j^{(2)}\in\{\mu\}} B_n\,\delta_{\kappa_0^{(1)},\nu}\,\delta_{\kappa_{n-1}^{(2)},\mu}\,\delta_{\kappa_j^{(2)},\kappa_{j+1}^{(1)}}\,(-1)^n\prod_{j=0}^{n-1}(-1)^{\varsigma_{2j}}\frac{\Delta^2_{\kappa_j^{(2)}\kappa_j^{(1)}}}{2^2}\,F_n \\ \times I_n\left[1-\sum_{l=2}^{n}\sum_{j=1}^{l-1}\xi_{2l-1}\Lambda_{l,j}\xi_{2j-1} - i\sum_{l=2}^{n}\xi_{2l-1}X_{l,1}\chi_1 - i\sum_{l=2}^{n}\sum_{j=2}^{2(l-1)}\xi_{2l-1}X_{l,j}\chi_j\right] \\ -\text{ reducible graphs}\,,\end{aligned} \tag{5.23}$$

where, as shown in E.1, products of reducible graphs of lower order must be subtracted in order to obtain the irreducible kernel $\Sigma_{\mu\nu}$. In particular, $\kappa_j^{(1)}$ denotes the coordinate which changes its value into $\kappa_j^{(2)}$ during the j-th transition, $\Delta_{\kappa_j^{(2)}\kappa_j^{(1)}} \equiv 0$ when $\kappa_j^{(2)} = \kappa_j^{(1)}$. Let us clarify it with an example: During the transition $\mu\nu \to \mu'\nu$, we mean $\kappa^{(1)} \equiv \mu$ and $\kappa^{(2)} \equiv \mu'$. The delta functions fix the initial and the final states of the paths. Despite its intricate appearance, $\Sigma_{\mu\nu}$ can be recast into the compact form (see proof in E.1)

$$\Sigma_{\mu\nu}(\xi) = + \int_0^{\xi} d\tau_{f-1} \int_0^{\xi-\tau_{f-1}} d\tau_1 \Big[K(\tau_{f-1})\, p(s) \left(K(\tau_1)\, \Lambda_{f-1,1} + A(\tau_1)\, X_{f-1,1} \right) \Big]_{\mu\nu}^{\in\{\mu\}}, \quad (5.24)$$

which constitutes together with Eqs. (5.19), (5.20) and (5.22) one main result of this Chapter. Here, τ_1 and $\tau_{f-1} = t_f - t_{f-1} = t - t_{f-1}$ indicate the initial and the final blip time intervals, respectively, and $s = t - t' - \tau_1 - \tau_{f-1}$. The superscript nearby the bracket, $\in \{\mu\}$, means that every jump must be performed inside the same well which q_μ belongs to, as soon as one looks at the matrix elements. The transition matrices have the form

$$K_{\mu\nu}(\tau) \equiv \frac{\Delta_{\mu\nu}^2}{2} \exp\left\{-(q_\mu - q_\nu)^2 S(\tau)\right\} \sin\left[\epsilon_{\nu\mu}\tau - (q_\mu - q_\nu)^2 R(\tau)\right] (q_\nu - q_\mu)\,, \quad (5.25a)$$

$$A_{\mu\nu}(\tau) \equiv \frac{\Delta_{\mu\nu}^2}{2} \exp\left\{-(q_\mu - q_\nu)^2 S(\tau)\right\} \cos\left[\epsilon_{\nu\mu}\tau - (q_\mu - q_\nu)^2 R(\tau)\right] (q_\nu - q_\mu)\,, \quad (5.25b)$$

the corresponding sum-rules being

$$K_{\nu\nu}(\tau) = - \sum_{\substack{\kappa\in\{\nu\} \\ \kappa\neq\nu}} K_{\kappa\nu}(\tau)\,, \quad (5.26a)$$

$$A_{\nu\nu}(\tau) = - \sum_{\substack{\kappa\in\{\nu\} \\ \kappa\neq\nu}} A_{\kappa\nu}(\tau)\,. \quad (5.26b)$$

It is worth noticing that in Eq. (5.25a) the factor $q_\nu - q_\mu$ comes from ξ_1 or ξ_{f-1}, whereas in Eq. (5.25b) it comes from χ_1.

Finally, the function p accounts for all intermediate *VR*-transitions occurring between the initial and the final blip time intervals. To be definite, $p_{\mu\nu}(t - t') \equiv \rho_{\mu\mu}(t; \nu\nu, t')$ is the probability to be in the state $(\mu\mu)$ at time t, being in the diagonal state $(\nu\nu)$ at time t'. Since the functions $\Lambda_{f-1,1}$ and $X_{f-1,1}$ induce correlations between the initial and final blips, the internal transitions describe a gas of non-interacting *VR*-blips where the *intra*-blip

correlations are fully retained. Hence, $p_{\mu\nu}(t)$ obeys the differential equation ($t \geq t_0$)

$$\dot{p}_{\mu\nu}(t) = \sum_{\kappa\in\{\mu\}} \int_{t_0}^{t} dt' W^{(2)}_{\mu\kappa}(t-t') p_{\kappa\nu}(t') \,, \tag{5.27}$$

with $p_{\mu\nu}(t_0) = \delta_{\mu,\nu}$.

5.2.1 The four-state system

We wish here to evaluate the beyond-NIBA contribution $\Sigma_{\mu\nu}(\xi)$ in the simplest situation of a four-level system (see Fig. 5.2). In this case, let us consider for example the generic two DVR-states inside the left well and let us label them 1 and 2. After introducing $p_{\rm N} \equiv p_{22} - p_{21} = p_{11} - p_{12}$ (where $p_{\rm N}$ is the symmetric part of the expectation value for the left well of σ_z with $p_{\mu\nu}$ obtained by solving Eq. (5.27) with NIBA kernels) and using Eq. (5.26), one finds for the kernel Σ_{21}:

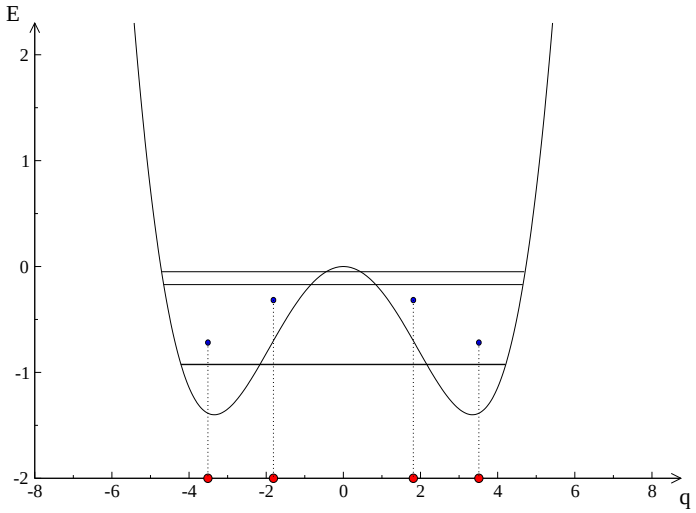

Figure 5.2: Energy vs position coordinate is shown for a four-state system. On the x-axis, the position of the DVR-eigenstates (red dots) and their corresponding on-site energies (blue dots) for the parameters $\Delta U = 1.4$, $\varepsilon = 0$ (in units of ω_0) are shown. Notice that the lowest two states are not resolved on this scale.

$$\begin{aligned}\Sigma_{21}(\xi) = \int_0^{\xi} d\tau_{f-1} \int_0^{\xi-\tau_{f-1}} d\tau_1 \Big[& + K_{21}(\tau_{f-1})\, p_{12}(s) \left(K_{21}(\tau_1)\, \Lambda_{f-1,1} + A_{21}(\tau_1)\, X_{f-1,1} \right) \\ & + K_{21}(\tau_{f-1})\, p_{11}(s) \left(K_{11}(\tau_1)\, \Lambda_{f-1,1} + A_{11}(\tau_1)\, X_{f-1,1} \right) \\ & + K_{22}(\tau_{f-1})\, p_{22}(s) \left(K_{21}(\tau_1)\, \Lambda_{f-1,1} + A_{21}(\tau_1)\, X_{f-1,1} \right) \\ & + K_{22}(\tau_{f-1})\, p_{21}(s) \left(K_{11}(\tau_1)\, \Lambda_{f-1,1} + A_{11}(\tau_1)\, X_{f-1,1} \right) \Big]\end{aligned} \tag{5.28}$$

$$\begin{aligned}= - \int_0^{\xi} d\tau_{f-1} \int_0^{\xi-\tau_{f-1}} d\tau_1 \; & \left[K_{21}(\tau_{f-1}) + K_{12}(\tau_{f-1}) \right] \\ & \times p_{\mathrm{N}}(s) \left[K_{21}(\tau_1)\, \Lambda_{f-1,1} + A_{21}(\tau_1)\, X_{f-1,1} \right] .\end{aligned} \tag{5.29}$$

An analogue expression is found for the kernel $\Sigma_{12}(\xi)$.

Once we define the symmetric kernel $K^s_{\mathrm{W}} \equiv W^{(2)}_{RL} + W^{(2)}_{LR} + \Sigma_{RL} + \Sigma_{LR}$ and the antisymmetric kernel $K^a_{\mathrm{W}} \equiv W^{(2)}_{RL} - W^{(2)}_{LR} + \Sigma_{RL} - \Sigma_{LR}$, we obtain a similar expression for the symmetric and antisymmetric WIBA kernels (3.66) and (3.64), respectively, although some differences occur due to the approximation $X_{l,2(l-1)} = 0$ performed to obtain the *VR*-WIBA kernels (see App. E). Moreover, there remains a basic difference in the interpretation of the kernels, since in the "pure" TLS the irreducible kernels account for the *tunneling* through the potential barrier whereas in the four-state system they relate states which lie in the same well, i.e. vibrational relaxation events.

5.3 Conclusions

In conclusion, we discussed a novel approximate treatment (called Weakly Interacting *VR*-Blip Approximation) of the dynamics in a driven dissipative bistable potential. It exploits a separation of time scales between tunneling and vibrational relaxation events in certain regimes of temperatures and coupling, i.e. $\hbar\Delta_i^{\mathcal{E}} \lesssim k_{\mathrm{B}}T < \hbar\omega_0$ and $\gamma < \omega_0$. We were able to derive an analytical expression for the kernels which govern the *intra*- and *inter*-well dynamics. The Weakly Interacting *VR*-Blip Approximation is supposed to work in the mentioned regime of parameters and to smoothly reproduce the gNICA predictions in the incoherent regime. However, the limits of validity of this approximation are still to be tested, since no clear regime of validity can be analytical predicted, due to the intricated relationships between the diverse effective coupling constants. Hence, further improvements to the theory are needed, adequate numerical simulations lacking because of numerical difficulties.

I CARE.

Don Milani

Chapter 6

Conclusions and perspectives

In this PhD thesis we have been concerned with dissipative and decoherence processes which take place specifically for quantum systems in a dissipative bistable potential. This potential describes a Hamiltonian system whose spectrum is composed by a ladder of levels, grouped as doublets under the potential barrier and being almost equally spaced above it. The system interacts with a thermal environment, which in this work has been chosen to be composed by an ensemble of harmonic oscillators, which is a common approach in the literature [12, 13, 84]. The dynamical quantity we looked at is the so-called reduced density matrix (RDM), obtained by tracing out the full density matrix the environmental degrees of freedom. The Feynman-Vernon real-time path-integral technique [11] is illustrated in Chapter 2, where the matrix elements for the RDM are exactly evaluated. Depending on which regime of parameters we are interested in, i.e. temperature and coupling strength with the reservoir, a few or several energy levels contribute to the dynamics. In particular, in Chapters 3 and 4 a two-level system (TLS) is analyzed. This corresponds to the regime where only the lowest doublet is energetically accessible. The environment enters the dynamics via the bath-correlation function, expressed as an integral over the so-called bath spectral density, which fully characterizes the bath spectrum.

In Chapter 3, a wide class of spectral densities is considered. In particular, the case of Ohmic and super-Ohmic spectral densities is discussed and analytical results for the kernels governing the dynamics of the population difference are obtained. Our theory, called Weakly-Interacting Blip Approximation (WIBA), is developed by using the real-time path-integral technique illustrated in Chapter 2. Starting from the exact path-integral solution for the spin-boson reduced density matrix, effective intra-blip correlations are fully included and inter-blip and blip-sojourn interactions are considered up to linear order, being

the *sojourn* the time spent in a diagonal state of the RDM and *blip* the time spent in an off-diagonal state. The WIBA is nonperturbative in the coupling strength as well as in the tunneling frequency and gives reliable results over a wide range of temperatures and coupling strength to the thermal environment. In specific regimes, the WIBA fully agrees with conventional perturbative approximations in the tunneling matrix element, like the so-called Non-Interacting Blip Approximation (NIBA) [12, 13], or in the system-bath coupling strength [14, 15, 16]. In an intermediate regime of parameters, a good agreement with the *ab-initio* numerical scheme Quasi-Adiabatic Path-Integral Propagator (QUAPI) [17] is found.

In Chapter 4, the TLS is assumed to be coupled with an external detector, like a dc-SQUID, the latter being coupled to an Ohmic environment. This model describes a more realistic qubit, as frequently discussed in the literature [5, 18, 19, 20, 21, 85]. In [64], it has been shown that such a system can be exactly mapped onto a TLS interacting with a structured environment. Up to now, the latter model has been used to investigate the decoherence properties of a qubit within a perturbative approach in the spectral density [86, 87]. However, when the qubit and detector frequencies become comparable or in a regime of strong coupling between qubit and detector, such a perturbative scheme breaks down [88, 89]. In the mentioned Chapter, we showed how to investigate in a correct way the dynamics of a spin-boson system with a structured environment in the case of strong coupling between a symmetric TLS and a detector. The dynamics was evaluated upon starting from the NIBA and approximating the NIBA kernels up to first order in the detector-bath coupling strength. Analytical results, valid also at finite detuning, were obtained and we showed that our theory correctly reproduces the onset of multiple oscillation frequencies in the dynamics due to the entanglement between TLS and detector.

Finally, in Chapter 5 we discussed the more general case of an M-level system coupled with an Ohmic environment. This situation describes the case of a bistable potential where the temperature is high enough that higher-lying energy levels are being populated and the system cannot be reduced to a simple TLS. Many are the experimental situations [22, 23, 24, 25, 26, 27, 28, 29, 30, 31, 32] which can be described by our theory. We developed a novel approximation called Weakly Interacting VR-Blip Approximation (VR-WIBA) for the dynamics in a driven dissipative bistable potential. In the regimes of low to moderate temperatures and coupling strengths, we exploited a separation of time scales between tunneling and vibrational relaxation events and we could derive analytical kernels for the *intra*- and *inter*-well dynamics. The VR-WIBA generalizes the theory put forward in [28, 29] called gNICA where the tunneling and VR-dynamics are fully incoherent. Unfortunately,

we did not have enough time to test our theory on existing approximation schemes, but we expect the *VR*-WIBA is able to correctly reproduce the gNICA or weak-coupling approximations in the appropriate regimes of parameters. We hope this will be done by someone else soon!

With the present work, we believe to have made important progresses in the proper understanding of the decoherence processes which take place in two- and multi-level systems. Control of decoherence is one foremost challenge for the realization of working quantum computers.

May this PhD thesis be precious for important future investigations in the field of driven dissipative quantum systems.

Appendix A

Derivation of the NIBA kernels

In the non-interacting blip approximation, as already mentioned in the Sec. 3.3, one neglects all blip-blip correlations and blip-sojourns interactions in Eq. (3.14), i.e. $\Phi_{\rm inter}^{(n)} = 0$. The blip-preceeding-sojourn interactions are neglected as well ($\Phi_{\rm bps}^{(n)} = 0$), i.e. one sets $X_{j,j-1} \approx R_{2j,2j-1}$. As a consequence, the influence function (3.10) factorizes into individual influence factors depending only on the dipole length $\tau_j := t_{2j} - t_{2j-1}$. Following an analogous procedure as in Sec. 3.3.1, the NIBA series expression can be derived, and the corresponding GME, of the same form as in Eq. (3.33), is obtained. The kernels finally read

$$K_{\rm N}^{s}(t) = \Delta^2 {\rm e}^{-S(t)} \cos(\varepsilon t) \cos[R(t)]\,, \tag{A.1a}$$

$$K_{\rm N}^{a}(t) = \Delta^2 {\rm e}^{-S(t)} \sin(\varepsilon t) \sin[R(t)]\,, \tag{A.1b}$$

$$K_{0,{\rm N}}^{s}(t) = \Delta^2 {\rm e}^{-S(t)} \cos(\varepsilon t) \cos[R(t)]\,, \tag{A.1c}$$

$$W_{\rm N}(t) \equiv K_{\rm N}^{s}(t) - K_{0,{\rm N}}^{s}(t) = 0\,. \tag{A.1d}$$

The kernels are of lowest order in the tunneling matrix Δ but are *non*-perturbative in δ_s. The NIBA is expected to be a good approximation whenever the average time spent in a blip is much larger than the time spent in a sojourn.

In general, the inter-dipole interaction can be safely neglected for all temperatures for sub-Ohmic damping $s < 1$, and the TLS is expected to exhibit incoherent dynamics even for very small coupling δ_s. For Ohmic and super-Ohmic damping, NIBA is expected to be a good approximation at high enough temperature and/or strong damping. In particular, spectral densities of the Ohmic form reach for large temperatures faster the asymptotic behavior $S(t) \propto t$ at long times, implying that the correlations in $\Lambda_{j,k}$ cancel out exactly. The

NIBA is known to fail, as said, at low temperatures and weak coupling for an asymmetric TLS because the dipole-dipole correlations $\Lambda_{j,k}$ contribute already to terms which depend linearly on the spectral density $G(\omega)$.

Appendix B

Evaluation of the WIBA kernels

In this Appendix, the prescription (3.63) to evaluate the WIBA kernels in the time domain is illustrated. Let us consider, to fix the ideas, $\Sigma_{0,a}(\xi) = \sum_l \Sigma_{0,a}^{(l)}(\xi)$. The kernel $\Sigma_{0,a}^{(l)}$, given in Eq. (3.53), is reported here for clarity:

$$\begin{aligned}\Sigma_{0,a}^{(l)}(\xi) \equiv \int_0^{\xi} d\xi_1 \int_0^{\xi-\xi_1} d\xi_l \gamma_{\bar{h}_l}(\xi_l) f(\xi-\xi_1-\xi_l) \\ \times \left[\gamma_{g_1}(\xi_1) X_{l,0} - \gamma_{\bar{g}_1}(\xi_1)\Lambda_{l,1}\right] ,\end{aligned} \tag{B.1}$$

with $X_{l,0} = R(\xi-\xi_1+\tau_1) - R(\xi-\xi_1+\tau_1-\tau_l)$. Notice that the operators γ's depend on the functions $g/\bar{g}$ $(h/\bar{h})$ defined in Eqs. (3.43) and (3.44).

In the function $f(s)$ which appears in the expression for the kernel (see Eq. (3.49)), the first derivative of the conditional probability $\dot{p}_{\rm eN}^{(l-2)}(s)$ is present. Then, it could be integrated out by parts, obtaining

$$\begin{aligned}\Sigma_{0,a}^{(l)}(\xi) = \int_0^{\xi} d\xi_1 \int_0^{\xi-\xi_1} d\xi_l \, \dot{\gamma}_{\bar{h}_l}(\xi_l) \\ \times p_{\rm eN}^{(l-2)}(\xi-\xi_1-\xi_l) \left[\gamma_{g_1}(\xi_1) X_{l,0} - \gamma_{\bar{g}_1}(\xi_1)\Lambda_{l,1}\right] .\end{aligned} \tag{B.2}$$

Here, the first derivative of the operator $\gamma_{\bar{h}_l}(\xi_l)$ acts on the functions $X_{l,0} = R(\xi-\xi_1+\tau_1) - R(\xi-\xi_1+\tau_1-\tau_l)$ and $\Lambda_{l,1} = S(\xi-\xi_1+\tau_1) + S(\xi-\xi_1-\tau_l) - S(\xi-\xi_1) - S(\xi-\xi_1+\tau_1-\tau_l)$

as

$$\begin{aligned}
&\dot{\gamma}_{\bar{h}}(\xi_l)X_{l,0} \\
&= \partial_{\xi_l}\int_0^{\xi_l} d\tau_l\, \bar{h}(\tau_l,\xi_l-\tau_l)X_{l,0} \\
&\approx \partial_{\xi_l}\int_0^{\xi_l} d\tau_l\, \bar{\bar{h}}(\tau_l,\xi_l)X_{l,0} \\
&= \bar{h}_{\rm eN}(\xi_l)\left[R(\xi-\xi_1+\tau_1)-R(\xi-\xi_1+\tau_1-\xi_l)\right],
\end{aligned} \tag{B.3}$$

and

$$\begin{aligned}
&\dot{\gamma}_{\bar{h}}(\xi_l)\Lambda_{l,1} \\
&= \partial_{\xi_l}\int_0^{\xi_l} d\tau_l\, \bar{h}(\tau_l,\xi_l-\tau_l)\Lambda_{l,1} \\
&\approx \partial_{\xi_l}\int_0^{\xi_l} d\tau_l\, \bar{\bar{h}}(\tau_l,\xi_l)\Lambda_{l,1} \\
&= \bar{h}_{\rm eN}(\xi_l)\left[S(\xi-\xi_1+\tau_1)+S(\xi-\xi_1-\xi_l)\right. \\
&\left.-S(\xi-\xi_1)-S(\xi-\xi_1+\tau_1-\xi_l)\right].
\end{aligned} \tag{B.4}$$

As already observed when calculating the *extended*-NIBA kernels, the explicit dependence of the integrand of Eq. (B.3) on ξ_l yields an integral form for $\dot{\gamma}_{\bar{h}}(\xi_l)X_{l,0}$. An approximate form is obtained if we apply the same prescription (3.35) as for the *extended*-NIBA. Namely, one approximates the bath correlation differences in $Y_{j,j-1}$ with the first derivative of $R(t)$. Hence, for g and h Eq. (3.36) holds, whereas for $\bar{g}$ and $\bar{h}$ it follows ($l>1$)

$$\begin{aligned}
\bar{g}(\tau_l,\xi_l-\tau_l) &\approx \bar{\bar{g}}(\tau_l,\xi_l) \\
&= \Delta^2 \mathrm{e}^{-S(\tau_l)}\cos(\varepsilon\tau_l)\sin[R(\tau_l)-\tau_l\dot{R}(\xi_l)]\,, \\
\bar{h}(\tau_l,\xi_l-\tau_l) &\approx \bar{\bar{h}}(\tau_l,\xi_l) \\
&= \Delta^2 \mathrm{e}^{-S(\tau_l)}\sin(\varepsilon\tau_l)\cos[R(\tau_l)-\tau_l\dot{R}(\xi_l)]\,,
\end{aligned} \tag{B.5}$$

the corrections being of order $\mathcal{O}[\tau_l^2\ddot{R}(\xi_l)]$. We define $\bar{g}_{\rm eN}(\xi_l)\equiv\bar{\bar{g}}(\xi_l,\xi_l)$ and $\bar{h}_{\rm eN}(\xi_l)\equiv\bar{\bar{h}}(\xi_l,\xi_l)$.

In order to evaluate the antisymmetric WIBA kernel $K^a_{\rm WIBA}$ from the prescription (3.63), one sees that the previous expression must be derived with respect to ξ. After substituting

$u \equiv \xi - \xi_1$ in the Eq. (B.2), we get

$$\begin{aligned}\Sigma_{0,a}^{(l)}(\xi) = &\int_0^{\xi} du \int_0^{u} d\xi_l \, \bar{h}_{\mathrm{eN}}(\xi_l) \\ &\times p_{\mathrm{eN}}^{(l-2)}(u-\xi_l)\left[\gamma_{g_1}(\xi-u)X_{l,0} - \gamma_{\bar{g}_1}(\xi-u)\Lambda_{l,1}\right],\end{aligned} \tag{B.6}$$

with $X_{l,0} = R(u+\tau_1) - R(u+\tau_1-\xi_l)$ and $\Lambda_{l,1} = S(u+\tau_1) + S(u-\xi_l) - S(u) - S(u+\tau_1-\xi_l)$.

Then, in order to get the derivative of $\Sigma_{0,a}^{(l)}(\xi)$ with respect to ξ, it is enough to evaluate

$$\begin{aligned}&\partial_\xi \left[\gamma_{g_1}(\xi-u)X_{l,0} - \gamma_{\bar{g}_1}(\xi-u)\Lambda_{l,1}\right] \\ &= \partial_\xi \int_0^{\xi-u} d\tau_1 \left[g_1(\tau_1, s_0 \to \infty)X_{l,0} - \bar{g}_1(\tau_1, s_0 \to \infty)\Lambda_{l,1}\right] \\ &= g_{\mathrm{N}}(\xi-u)X_{l,0} - \bar{g}_{\mathrm{N}}(\xi-u)\Lambda_{l,1}\,,\end{aligned} \tag{B.7}$$

where now $X_{l,0} = R(\xi) - R(\xi-\xi_l)$ and $\Lambda_{l,1} = S(\xi) + S(\xi-\xi_1-\xi_l) - S(\xi-\xi_1) - S(\xi-\xi_l)$.

Hence, we obtain for the l-th order (after the derivative, we substitute back $\xi_1 \equiv \xi - u$)

$$\begin{aligned}&\partial_\xi \Sigma_{0,a}^{(l)}(\xi) \\ &= \int_0^{\xi} d\xi_1 \int_0^{\xi-\xi_1} d\xi_l \, \bar{h}_{\mathrm{eN}}(\xi_l) p_{\mathrm{eN}}^{(l-2)}(\xi-\xi_1-\xi_l) \\ &\times \left[g_{\mathrm{N}}(\xi_1)X_{l,0} - \bar{g}_{\mathrm{N}}(\xi_1)\Lambda_{l,1}\right].\end{aligned} \tag{B.8}$$

In the end, the antisymmetric WIBA kernel reads

$$\begin{aligned}K_{\mathrm{WIBA}}^{a}(\xi) &\equiv K_{\mathrm{eN}}^{a}(\xi) - \sum_{\sigma=2}^{\infty} K_{\mathrm{WIBA}}^{a\,(\sigma)}(\xi) \\ &= K_{\mathrm{eN}}^{a}(\xi) \\ &- \int_0^{\xi} d\xi_1 \int_0^{\xi-\xi_1} d\xi_f \, \bar{h}_{\mathrm{eN}}(\xi_f)\, p_{\mathrm{eN}}(\xi-\xi_1-\xi_f) \\ &\times \left[g_{\mathrm{N}}(\xi_1)X_{f,0} - \bar{g}_{\mathrm{N}}(\xi_1)\Lambda_{f,1}\right],\end{aligned} \tag{B.9}$$

where we introduced $p_{\mathrm{eN}}(t) \equiv \sum_{\sigma=2}^{\infty} p_{\mathrm{eN}}^{(\sigma-2)}(t)$. Following similar lines, we obtain for the

symmetric WIBA kernels:

$$\begin{aligned} K^s{}_{0,\mathrm{WIBA}}(\xi) &\equiv K^s_{0,\mathrm{eN}}(\xi) - \sum_{\sigma=2}^{\infty} K^s_{0,\mathrm{WIBA}}{}^{(\sigma)}(\xi) \\ &= K^s_{0,\mathrm{eN}}(\xi) \\ &- \int_0^{\xi} d\xi_1 \int_0^{\xi-\xi_1} d\xi_f \, \bar{h}_{\mathrm{eN}}(\xi_f)\, p_{\mathrm{eN}}(\xi - \xi_1 - \xi_f) \\ &\times \left[h_{\mathrm{N}}(\xi_1) X_{f,0} + \bar{h}_{\mathrm{N}}(\xi_1) \Lambda_{f,1} \right] , \end{aligned} \tag{B.10}$$

and

$$\begin{aligned} K^s_{\mathrm{WIBA}}(\xi) &\equiv K^s_{\mathrm{eN}}(\xi) - \sum_{\sigma=2}^{\infty} K^s_{\mathrm{WIBA}}{}^{(\sigma)}(\xi) \\ &= K^s_{\mathrm{eN}}(\xi) \\ &- \int_0^{\xi} d\xi_1 \int_0^{\xi-\xi_1} d\xi_f \, \bar{h}_{\mathrm{eN}}(\xi_f)\, p_{\mathrm{eN}}(\xi - \xi_1 - \xi_f) \\ &\times \left[\bar{h}_{\mathrm{eN}}(\xi_1) \Lambda_{f,1} \right] . \end{aligned} \tag{B.11}$$

We identified in all equations the last time interval with τ_f and correspondingly ξ_f. In this last equation, we also identified the first time interval τ_k with τ_1 (therefore ξ_k with ξ_1) and $\Lambda_{f,k}$ with $\Lambda_{f,1}$.

In Eqs. (B.9) and (B.10), is $X_{f,0} = R(\xi) - R(\xi - \xi_f)$, and for all the three kernels $\Lambda_{f,1} = S(\xi) + S(\xi - \xi_1 - \xi_f) - S(\xi - \xi_1) - S(\xi - \xi_f)$. In Eq. (B.11), the term proportional to $X_{f,0}$ is absent because it vanishes after the integration by parts and the derivative, since it does not depend on s_0.

Appendix C

Calculation of the parameter x

Here we are interested in finding out the correct value for x which comes in the formulas after we make the expansion in Bessel functions. We refer here to the Eq. (4.37), which we rewrite for clarity.

$$K^s(\lambda) = \Delta^2 \int_0^\infty \mathrm{d}\tau e^{-\lambda\tau}\, e^{-Q_0'(\tau)} \left\{ \cos\left(Q_0''(\tau)\right) \left[1 - Q_1'(\tau)\right] - \sin\left(Q_0''(\tau)\right) Q_1''(\tau) \right\}. \tag{C.1}$$

Let us examine, to fix the ideas, the term $\exp\{-Q_0'(\tau)\}\cos\left(Q_0''(\tau)\right)$:

$$\begin{aligned} e^{-Q_0'(\tau)} \cos\left(Q_0''(\tau)\right) &\equiv e^Y \mathfrak{Re}\left\{ e^{-Y\cos\Omega\tau} e^{+\mathrm{i}W\sin\Omega\tau} \right\} && \text{(C.2)} \\ &= e^Y \mathfrak{Re}\left\{ e^{\mathrm{i}[\mathrm{i}Y\cos\Omega\tau + W\sin\Omega\tau]} \right\} && \text{(C.3)} \\ &= e^Y \mathfrak{Re}\left\{ e^{\mathrm{i}\sqrt{W^2-Y^2}\left[\frac{\mathrm{i}Y}{\sqrt{W^2-Y^2}}\cos\Omega\tau + \frac{W}{\sqrt{W^2-Y^2}}\sin\Omega\tau\right]} \right\}. && \text{(C.4)} \end{aligned}$$

It could be now convenient to interprete

$$\begin{cases} \cos x \equiv \dfrac{\mathrm{i}Y}{\sqrt{W^2-Y^2}} = +\dfrac{Y}{\sqrt{Y^2-W^2}} & \text{(C.5a)} \\ \sin x \equiv \dfrac{-W}{\sqrt{W^2-Y^2}} = +\dfrac{\mathrm{i}W}{\sqrt{Y^2-W^2}}\ , & \text{(C.5b)} \end{cases}$$

so that the exponent can be rewritten as

$$e^{-Q_0'(\tau)} \cos\left(Q_0''(\tau)\right) = e^Y \mathfrak{Re}\left\{ e^{\mathrm{i}\sqrt{W^2-Y^2}\cos\left(\Omega\tau + x\right)} \right\}. \tag{C.6}$$

At this point we can use the Jacobi-Anger expansion (4.24) to expand the exponent in series of Bessel functions. Then we get

$$K^s(\lambda) = \Delta^2 e^Y \int_0^\infty \mathrm{d}\tau e^{-\lambda\tau} \left\{ \left[J_0(u_0) + 2\sum_{n=1}^{+\infty} (-\mathrm{i})^n J_n(u_0) \cos(n\Omega\tau) \cosh\left(n\frac{\beta\Omega}{2}\right) \right] \times \left[1 - Q_1'(\tau)\right] + 2\sum_{n=1}^{+\infty} (-\mathrm{i})^n J_n(u_0) \sin(n\Omega\tau) \sinh\left(n\frac{\beta\Omega}{2}\right) Q_1''(\tau) \right\}, \tag{C.7}$$

which coincides with Eq. (4.49), once we introduce the amplitudes. Here, u_0 is given by

$$u_0 \equiv \sqrt{W^2 - Y^2} = \mathrm{i}\sqrt{Y^2 - W^2} = \mathrm{i}\frac{4g^2}{\Omega^2} \frac{1}{\sinh\left(\frac{\beta\Omega}{2}\right)}, \tag{C.8}$$

since $Y \equiv -W\coth(\frac{\beta\Omega}{2})$, hence $|Y| \geq |W|$ (note that $W > 0$ and hence $Y < 0$). One notices that the argument of the Bessel functions is small, whenever $\beta\hbar\Omega/2 \gtrsim 1$ and $g \lesssim \Omega$, i.e. in the regime we are interested in.

Now we would like to obtain the exact value of x.

From Eq. (C.5), we rewrite the tangent as

$$\tan x = \frac{+\mathrm{i}W}{Y} = -\mathrm{i}\tanh(\frac{\beta\Omega}{2}) = \tan(-\mathrm{i}\frac{\beta\Omega}{2}) \tag{C.9}$$

We assume x to be complex, therefore we write it as $x = a + \mathrm{i}b$. In general, it holds

$$\cos(a + \mathrm{i}b) = \cos a \cosh b - \mathrm{i}\sin a \sinh b \tag{C.10}$$

$$\sin(a + \mathrm{i}b) = \sin a \cosh b + \mathrm{i}\cos a \sinh b\,. \tag{C.11}$$

From (C.10), in order to have $\cos(a + \mathrm{i}b) = +Y/\sqrt{Y^2 - W^2}$, namely a real number, it must be

$$a = n\pi\,. \tag{C.12}$$

From Eqs. (C.10) and (C.11), we can write the tangent as

$$\tan(a + \mathrm{i}b) = \frac{\tan a + \mathrm{i}\tanh b}{1 - \mathrm{i}\tan a \tanh b} \xrightarrow[a=n\pi]{} +\mathrm{i}\tanh b \equiv +\mathrm{i}\frac{W}{Y}, \tag{C.13}$$

as we get by calculating the tangent from Eq. (C.5). Hence,

$$\tanh b = \frac{W}{Y}. \tag{C.14}$$

We can eventually write x as

$$x \equiv a + \mathrm{i}b = n\pi + \mathrm{i}\,\mathrm{arctanh}\frac{W}{Y} = n\pi - \mathrm{i}\frac{\beta\Omega}{2}\,. \tag{C.15}$$

In order to decide, whether to assume $n = 0$ or $n = 1$, one must look at the cosine or sine:

$$\cos x \xrightarrow[a=n\pi]{\text{Eq.(C.10)}} (-1)^n \frac{1}{\sqrt{1-\tanh^2 b}} = (-1)^n \frac{1}{\sqrt{1-\dfrac{W^2}{Y^2}}} = (-1)^n \frac{|Y|}{\sqrt{Y^2-W^2}} \tag{C.16}$$

$$\equiv \frac{+Y}{\sqrt{Y^2-W^2}} < 0 \qquad \Longmapsto n = 1 \tag{C.17}$$

or, equivalently,

$$\sin x \xrightarrow[a=n\pi]{\text{Eq.(C.11)}} \mathrm{i}(-1)^n \frac{\tanh b}{\sqrt{1-\tanh^2 b}} = \mathrm{i}(-1)^n \frac{\dfrac{W}{Y}}{\sqrt{1-\dfrac{W^2}{Y^2}}} \tag{C.18}$$

$$= \mathrm{i}(-1)^n \frac{\dfrac{W}{Y}|Y|}{\sqrt{Y^2-W^2}} = -\mathrm{i}(-1)^n \frac{W}{\sqrt{Y^2-W^2}} \equiv \frac{+\mathrm{i}W}{\sqrt{Y^2-W^2}} \qquad \Longmapsto n = 1\,. \tag{C.19}$$

Appendix D

Explicit form for the decay rate γ_p

In this Appendix we wish to give the analytical result for the decay rate $\gamma_p(\lambda_p)$ as function of the solution λ_p of the undamped pole equation Eq. (4.52):

$$\gamma_p(\lambda_p) = \frac{1}{\kappa}\frac{1}{2\lambda_p^2\left[(\lambda_p^2+\Omega^2)^2+\Delta_{1_{(c)}}^2\Omega^2\right]}\Bigg[\lambda_p^2\left(p+q\Delta_{1_{(c)}}^2+t\Delta_{1_{(s)}}^2+u\Delta_{1_{(c)}}^2\Delta_{1_{(s)}}^2+r\Delta_{1_{(c)}}^4\right) + \Omega^2\left(s+w\Delta_{1_{(c)}}^2+t\Delta_{1_{(s)}}^2\right)+\lambda_p^2\left(\Delta_{1_{(c)}}^2 g(\lambda_p)+\Delta_{1_{(s)}}^2 h(\lambda_p)\right)\Bigg], \tag{D.1}$$

with

$$\begin{aligned}
p &\equiv (2A-B)\Omega^2\Delta_0^2+(B-D)\Delta_0^4, && \text{(D.2)}\\
q &\equiv \Delta_0^2(\frac{A}{2}+2B-D)+\Omega^2(2B-\frac{A}{2}), && \text{(D.3)}\\
t &\equiv -\frac{V\Omega}{4}(\Omega^2+3\Delta_0^2), && \text{(D.4)}\\
u &\equiv -3\frac{V\Omega}{4}, && \text{(D.5)}\\
r &\equiv \frac{A}{2}+B, && \text{(D.6)}\\
s &\equiv -\Omega^2\Delta_0^2 B+\Delta_0^4(B-D), && \text{(D.7)}\\
w &\equiv \Delta_0^2(\frac{A}{2}+B)-\Omega^2\frac{A}{2} && \text{(D.8)}
\end{aligned}$$

and

$$g(\lambda_p) \equiv \frac{(\lambda_p^2+\Omega^2)^2}{\lambda_p^2+4\Omega^2}\left(C\Omega+\frac{A}{2}\frac{\lambda_p^2-4\Omega^2}{\lambda_p^2+4\Omega^2}\right), \tag{D.9}$$

$$h(\lambda_p) \equiv \frac{(\lambda_p^2+\Omega^2)^2}{\lambda_p^2+4\Omega^2}\frac{V\Omega}{4}\frac{3\lambda_p^2+20\Omega^2}{\lambda_p^2+4\Omega^2}. \tag{D.10}$$

As already seen, the physical poles are $\lambda^2 = -\lambda_{1,2}^2 \equiv \lambda_\pm^2$. Correspondingly, the decay rates $\gamma_\pm = \gamma(\lambda_\pm)$ follow according to Eq. (D.1).

Appendix E

Derivation of the GME within the *VR*-WIBA

In order to get the general expression for the GME, once the Eq. (5.18) is verified, let us consider the case $M = 4$. We shall generalize the results to a generic M-level system.

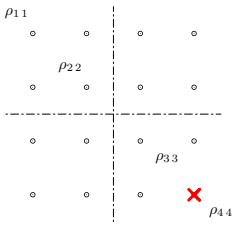

Figure E.1: Schematic representation of the RDM for a $M = 4$ level system. We suppose $\rho_{\mu\mu}(t) = \rho_{44}$ (marked as a red cross).

In the spirit of the NIBA, where also the blip-preceeding sojourn interactions $Y_{j,j-1}$ are neglected, cf. App. A, we approximate the complicate structure of the function H_n defined in Eq. (5.16) by setting $X_{l,2(l-1)} = 0$.

Let us first focus on the case ρ_{44} (the red cross in Fig. E.1) and suppose that the initial condition is a right-well state, say $\rho_{\mu_0\mu_0} = \rho_{33}$ or $\rho_{\mu_0\mu_0} = \rho_{44}$. We then classify a generic path in terms of the number of tunneling transitions. It is much more convenient to work in the Laplace space (we neglect for simplicity the hats above all quantities).

Looking at Eq. (5.8) in the Laplace space, we can make a table of all paths which connect the states ρ_{33} and ρ_{44} to the final one (see Table E.1).

$\rho_{\mu_0\mu_0}$	ρ_{33}	ρ_{44}
T^0	$\frac{1}{\lambda}\frac{W_{43}}{\lambda}$	$\frac{1}{\lambda}\left(1+\frac{W_{44}}{\lambda}\right)$
T^1	$\frac{1}{\lambda}\left(1+\frac{W_{44}}{\lambda}\right)\frac{T_{44}}{\lambda}\frac{W_{43}}{\lambda}$ $\frac{1}{\lambda}\frac{W_{43}}{\lambda}\frac{T_{33}}{\lambda}\left(1+\frac{W_{33}}{\lambda}\right)$	$\frac{1}{\lambda}\left(1+\frac{W_{44}}{\lambda}\right)\frac{T_{44}}{\lambda}\left(1+\frac{W_{44}}{\lambda}\right)$ $\frac{1}{\lambda}\frac{W_{43}}{\lambda}\frac{T_{33}}{\lambda}\frac{W_{33}}{\lambda}$
...	...	...

Table E.1: Contributions at different orders in T of the paths in the RDM to the master equation for ρ_{44}.

Specifically, the zeroth order in T is given by

$$\rho_{44}^{(0)} = \sum_{\mu_0\in R}\frac{1}{\lambda}\left(\delta_{4\mu_0}+\frac{W_{4\mu_0}}{\lambda}\right)\mathrm{e}^{-\lambda t_0}\rho_{\mu_0\mu_0}\,, \tag{E.1}$$

where the exponential appears there because of the causality. Notice that each free sojourn contributes with a factor $1/\lambda$ to (E.1). For a generic final RDM state $(\mu\mu)$, one finds

$$\rho_{\mu\mu}^{(0)} = \sum_{\mu_0\in R}\frac{1}{\lambda}\left(\delta_{\mu\mu_0}+\frac{W_{\mu\mu_0}}{\lambda}\right)\mathrm{e}^{-\lambda t_0}\rho_{\mu_0\mu_0}\,. \tag{E.2}$$

In Eqs. (E.1), (E.2) we defined ($\mu\neq\nu$, $\xi=t-t'$)

$$\begin{aligned} W_{\mu\nu} = \sum_{n=1}^{\infty}\int_0^\infty d\xi \mathrm{e}^{-\lambda\xi}\int_{t'}^{t}\mathcal{D}\{t_j\}\sum_{\kappa_j^{(2)}\in\{\mu\}}B_n \\ \times\,\delta_{\kappa_0^{(1)},\nu}\,\delta_{\kappa_{n-1}^{(2)},\mu}\,\delta_{\kappa_j^{(2)},\kappa_{j+1}^{(1)}}(-1)^n\prod_{j=0}^{n-1}(-1)^{\varsigma_{2j}}\frac{\Delta^2_{\kappa_j^{(2)}\kappa_j^{(1)}}}{2^2}\,F_n\,G_n\,H_n\Bigg]. \end{aligned} \tag{E.3}$$

This kernel accounts for all transitions within two states $(\nu\nu)$ and $(\mu\mu)$ lying in the same well. For $W_{\mu\mu}$ it holds the sum-rule

$$W_{\nu\nu} = -\sum_{\substack{\kappa\in\{\nu\}\\ \kappa\neq\nu}}W_{\kappa\nu}\,. \tag{E.4}$$

To first order in T we can identify two possibilities, each depending on the initial state

$\mu_0\mu_0$ (see Table E.1):

$$\rho^{(1)}_{\mu\mu} = \sum_{\substack{\mu_0\in R\\ \alpha,\beta\in R}} \frac{1}{\lambda}\left(\delta_{\mu\alpha}+\frac{W_{\mu\alpha}}{\lambda}\right)\frac{T_{\alpha\beta}}{\lambda}\left(\delta_{\beta\mu_0}+\frac{W_{\beta\mu_0}}{\lambda}\right)\mathrm{e}^{-\lambda t_0}\rho_{\mu_0\mu_0}\,. \tag{E.5}$$

Since $T_{\alpha\beta}$ can only connect states in the same well which are identical, for $\alpha\in R$ and $\beta\in R$, $\alpha\neq\beta$, it holds $T_{\alpha\beta}=0$.

We now define

$$\Gamma_{\alpha\beta} \equiv \sum_{\sigma\in\{\beta\}} \frac{T_{\alpha\sigma}}{\lambda}\left(\delta_{\sigma\beta}+\frac{W_{\sigma\beta}}{\lambda}\right) \tag{E.6}$$

as the element which accounts for intra-well vibrational relaxations followed by one *tunneling* event, which can either bring the particle to the other well ($\alpha\notin\{\sigma\}$) or just come back to the well from which it left ($\alpha=\sigma$).

We can hence generalize Eq. (E.5) to higher orders in T and include also the possibility to start from a generic left state. For a RDM diagonal state (μ,μ) lying in one of the two wells, we can then write in the Laplace space

$$\rho_{\mu\mu} = \sum_{n=0}^{\infty}\rho^{(n)}_{\mu\mu} \tag{E.7}$$

$$= \sum_{\mu_0}\sum_{\alpha\in\{\mu\}}\frac{1}{\lambda}\left(\delta_{\mu\alpha}+\frac{W_{\mu\alpha}}{\lambda}\right)\left[\delta_{\alpha\mu_0}+\Gamma_{\alpha\mu_0}+\sum_{\gamma}\Gamma_{\alpha\gamma}\Gamma_{\gamma\mu_0}+\dots\right]\mathrm{e}^{-\lambda t_0}\rho_{\mu_0\mu_0} \tag{E.8}$$

$$= \sum_{\mu_0}\sum_{\alpha\in\{\mu\}}\frac{1}{\lambda}\left(\delta_{\mu\alpha}+\frac{W_{\mu\alpha}}{\lambda}\right)\sum_{p=0}^{\infty}(\Gamma^p)_{\alpha\mu_0}\,\mathrm{e}^{-\lambda t_0}\rho_{\mu_0\mu_0} \tag{E.9}$$

$$= \sum_{\mu_0}\sum_{\alpha\in\{\mu\}}\frac{1}{\lambda}\left(\delta_{\mu\alpha}+\frac{W_{\mu\alpha}}{\lambda}\right)\left[\frac{1}{\mathbb{1}-\Gamma}\right]_{\alpha\mu_0}\mathrm{e}^{-\lambda t_0}\rho_{\mu_0\mu_0}\,, \tag{E.10}$$

which can also be rewritten in matricial form:

$$\vec{\rho}(\lambda) = \left(\mathbb{1}+\frac{W}{\lambda}\right)\frac{1}{\lambda-T\left(\mathbb{1}+\frac{W}{\lambda}\right)}\mathrm{e}^{-\lambda t_0}\vec{\rho}_0\,. \tag{E.11}$$

To this conclusion we came by starting from an analysis order by order in the *tunneling* kernel T. We would have come to the same result also beginning from a detailed description of all contributions order by order in Δ^2 (including in this latter case all possible combinations of Δ_{inter} and Δ_{intra}).

It can be proved for each order in Δ^2 (see below) that the series entering Eq. (E.8) can

be recast in a more convenient way:

$$\frac{1}{\lambda}\left(+ \frac{W}{\lambda}\right) \sum_{p=0}^{\infty} \left[\frac{T}{\lambda} \left(+ \frac{W}{\lambda}\right)\right]^p \equiv \frac{1}{\lambda} \sum_{p=0}^{\infty} \left(\frac{T+\tilde{W}}{\lambda}\right)^p , \tag{E.12}$$

where $\tilde{W}$ is the sum of all *irreducible* graphs. Irreducibility means that the graph cannot be cut into two uncorrelated pieces at an intermediate sojourn without removing the bath correlations across such a sojourn [12]. We show here the proof only for the case Δ^6, which is the first non-trivial case, refraining to give the proof here for the other orders. From the left-hand side of Eq. (E.12) we isolate all at most sixth-order contributions:

$$\left(+ \frac{W^{(2)}}{\lambda} + \frac{W^{(4)}}{\lambda} + \frac{W^{(6)}}{\lambda}\right) \left[+ \frac{T}{\lambda} \left(+ \frac{W^{(2)}}{\lambda} + \frac{W^{(4)}}{\lambda}\right) + \frac{T^2}{\lambda^2} \left(+ \frac{W^{(2)}}{\lambda}\right)^2 + \frac{T^3}{\lambda^3}\right] , \tag{E.13}$$

which at the sixth-order read

$$\frac{T^3}{\lambda^3} + \frac{W^{(6)}}{\lambda} + 3\frac{T^2}{\lambda^2}\frac{W^{(2)}}{\lambda} + 2\frac{T}{\lambda}\frac{W^{(4)}}{\lambda} + \frac{T}{\lambda}\frac{{W^{(2)}}^2}{\lambda} + \left[\Delta^8\right] . \tag{E.14}$$

From the right-hand side we also isolate all at most sixth-order terms

$$\left(\frac{T+W^{(2)}}{\lambda}\right)^3 + \left(\frac{T+W^{(2)}+\tilde{W}^{(4)}}{\lambda}\right)^2 + \frac{\tilde{W}^{(6)}}{\lambda} \tag{E.15}$$

and obtain for the sixth-order contributions

$$\frac{T^3}{\lambda^3} + \frac{W^{(6)}}{\lambda} + 3\frac{T^2}{\lambda^2}\frac{W^{(2)}}{\lambda} + 2\frac{T}{\lambda}\frac{W^{(4)}}{\lambda} + \frac{T}{\lambda}\frac{{W^{(2)}}^2}{\lambda} + \left[\Delta^8\right] , \tag{E.16}$$

namely the same result as in Eq. (E.14).

Here we used the formal definition of irreducible graphs [12], i.e.

$$\tilde{W}^{(2n)} \equiv W^{(2n)} - \sum_{j=2}^{n} (-1)^j \sum_{\substack{m_1 \dots m_j \\ \{m_j \text{even}\}}} W^{(m_1)} \dots W^{(m_j)} \delta_{m_1+\dots+m_j,2n} . \tag{E.17}$$

Notice also that with the symbol $W^{(2n)}$ ($\tilde{W}^{(2n)}$) we mean the contribution of W ($\tilde{W}$) at the $2n$-th order, n counting the number of blips.

This allows us to get the final form for the general master equation. It follows in fact

from Eq. (E.12)

$$\rho_{\mu\mu} = \sum_{\mu_0} \frac{1}{\lambda} \left[\sum_{p=0}^{\infty} \left(\frac{T+\tilde{W}}{\lambda} \right)^p \right]_{\mu\mu_0} \mathrm{e}^{-\lambda t_0} \rho_{\mu_0\mu_0} \tag{E.18}$$

$$= \sum_{\mu_0} \left[\frac{1}{\lambda - \left(T+\tilde{W}\right)} \right]_{\mu\mu_0} \mathrm{e}^{-\lambda t_0} \rho_{\mu_0\mu_0} \,. \tag{E.19}$$

By multiplying from the left hand side both sides of Eq. (E.19) by the quantity $\left[\lambda - \left(T+\tilde{W}\right)\right]_{\sigma\mu}$ and summing over μ, one gets

$$\lambda \sum_{\mu} \delta_{\sigma\mu}\rho_{\mu\mu} - \sum_{\mu} \left(T+\tilde{W}\right)_{\sigma\mu} \rho_{\mu\mu} = \sum_{\mu_0} \delta_{\sigma\mu_0} \mathrm{e}^{-\lambda t_0} \rho_{\mu_0\mu_0} \,, \tag{E.20}$$

or

$$\lambda\rho_{\sigma\sigma} - \sum_{\mu_0} \delta_{\sigma\mu_0} \mathrm{e}^{-\lambda t_0} \rho_{\mu_0\mu_0} = \sum_{\mu} \left(T+\tilde{W}\right)_{\sigma\mu} \rho_{\mu\mu} \tag{E.21}$$

where one can easily identify on the left-hand side the Laplace Transform of the first derivative of ρ with respect of time. By sending $\sigma \to \mu$ and $\mu \to \nu$ and transforming back to the time space, we finally obtain the GME for a generic DVR-state (μ,μ)

$$\dot{\rho_{\mu\mu}}(t)\theta(t-t_0) = \sum_{\substack{\nu\notin\{\mu\} \\ \nu=\mu}} \int_{t_0}^{t} dt' T_{\mu\nu}(t-t')\rho_{\nu\nu}(t') + \sum_{\nu\in\{\mu\}} \int_{t_0}^{t} dt' \tilde{W}_{\mu\nu}(t-t')\rho_{\nu\nu}(t') \,, \tag{E.22}$$

where the sums run over such indexes according to the definitions of T and $\tilde{W}$.

E.1 Summation to all orders in Δ^2 in the intra-well kernel

In this Appendix we would like to discuss how to arrive at Eq. (5.24). The idea is to isolate all the contributions that give rise to the p's which build up between the initial and the final blips.

Let us consider the kernel $\Sigma_{\mu\nu}$ relating the initial and final RDM states $(\nu\nu)$ and $(\mu\mu)$, respectively, with *at least* two visits to off-diagonal states. Hence, the lowest order in Δ of $\Sigma_{\mu\nu}$ is the 4-th order term $\Sigma^{(4)}_{\mu\nu}$. To proceed, we must distinguish four cases, depending on the states the path can reach after the first and before the last blips (see Fig. E.2).

Let's focus first on $\Sigma^{(4)}_{\mu\nu}(\xi)$, $\mu \neq \nu$ (remind that $\xi = t - t'$). In this case – sketched in Fig. E.3 – there are only three possibilities for the sojourn spanning the time interval $t_3 - t_2$.

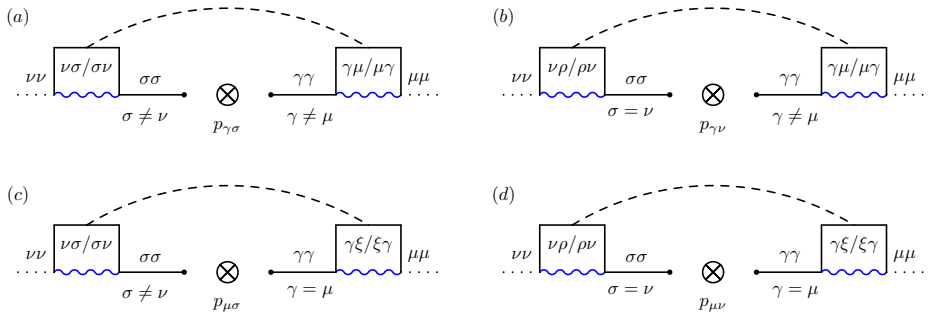

Figure E.2: Generic paths which contribute to the beyond-NIBA kernel: We must sum all these four possible different cases. With the bubble we represent the conditional probability p calculated from Eq. (5.27), i.e. for a gas of non-interacting blips. The dashed line denotes the interaction between the first and the last blip.

Hence (overall here we define $\tau_i \equiv t_{2i} - t_{2i-1}$):

$$\Sigma^{(4)}_{\mu\nu}(\xi) = \left\{ \overset{(a)}{+} \sum_{\sigma\gamma\in\{\mu\}} \sum_{\substack{(\mu_1\nu_1)=\{\nu\sigma/\sigma\nu\}\\(\mu_3\nu_3)=\{\gamma\mu/\mu\gamma\}}} \overset{(b)}{-} \sum_{\rho\gamma\in\{\mu\}} \sum_{\substack{(\mu_1\nu_1)=\{\nu\rho/\rho\nu\}\\(\mu_3\nu_3)=\{\gamma\mu/\mu\gamma\}}} \overset{(c)}{-} \sum_{\sigma\xi\in\{\mu\}} \sum_{\substack{(\mu_1\nu_1)=\{\nu\sigma/\sigma\nu\}\\(\mu_3\nu_3)=\{\gamma\xi/\xi\gamma\}}} \right\}$$
$$\int_0^\xi d\tau_3 \int_0^{\xi-\tau_3} d\tau_1 \frac{\Delta_1^2}{2^2}\frac{\Delta_3^2}{2^2} \mathrm{e}^{-\mathrm{i}\epsilon_{\mu_1\nu_1}\tau_1} \mathrm{e}^{-\mathrm{i}\epsilon_{\mu_3\nu_3}\tau_3} \delta_{\sigma\gamma} \tag{E.23}$$
$$\times \exp\left\{-\xi_1^2 S_{2,1}\right\} \exp\left\{-\xi_3^2 S_{4,3}\right\} \exp\left\{-i\xi_1 R_{2,1}\chi_1\right\} \exp\left\{-i\xi_3 R_{4,3}\chi_3\right\}$$
$$\times \left[1 - \xi_3\Lambda_{2,1}\xi_1 - i\xi_3 X_{2,1}\chi_1 - i\xi_3 X_{2,2}\chi_2\right]$$
$$- \text{reducible graphs}$$
$$= \left\{ \overset{(a)}{+} \sum_{\sigma\gamma\in\{\mu\}} \sum_{\substack{(\mu_1\nu_1)=\{\nu\sigma/\sigma\nu\}\\(\mu_3\nu_3)=\{\gamma\mu/\mu\gamma\}}} \overset{(b)}{-} \sum_{\rho\gamma\in\{\mu\}} \sum_{\substack{(\mu_1\nu_1)=\{\nu\rho/\rho\nu\}\\(\mu_3\nu_3)=\{\gamma\mu/\mu\gamma\}}} \overset{(c)}{-} \sum_{\sigma\xi\in\{\mu\}} \sum_{\substack{(\mu_1\nu_1)=\{\nu\sigma/\sigma\nu\}\\(\mu_3\nu_3)=\{\gamma\xi/\xi\gamma\}}} \right\}$$
$$\int_0^\xi d\tau_3 \int_0^{\xi-\tau_3} d\tau_1 \frac{\Delta_1^2}{2^2}\frac{\Delta_3^2}{2^2} \mathrm{e}^{-\mathrm{i}\epsilon_{\mu_1\nu_1}\tau_1} \mathrm{e}^{-\mathrm{i}\epsilon_{\mu_3\nu_3}\tau_3} \delta_{\sigma\gamma} \tag{E.24}$$
$$\times \exp\left\{-\xi_1^2 S_{2,1}\right\} \exp\left\{-\xi_3^2 S_{4,3}\right\} \exp\left\{-i\xi_1 R_{2,1}\chi_1\right\} \exp\left\{-i\xi_3 R_{4,3}\chi_3\right\}$$
$$\times \left[-\xi_3\Lambda_{2,1}\xi_1 - i\xi_3 X_{2,1}\chi_1\right] ,$$

where the summations between brackets at the beginning mean that we should sum up the two contributions, with intermediate states given by those specified in the summations.

Analogously in Fig. E.4 we show a generic path of 6-th order in Δ^2. This time the summations run over the four cases shown in Fig. E.2 and we obtain for the $\Sigma^{(6)}_{\mu\nu}(\xi)$:

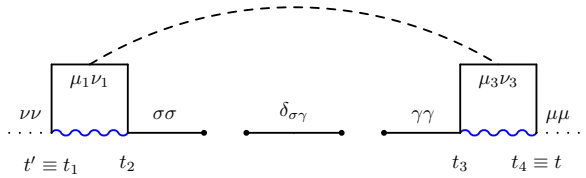

Figure E.3: Generic path which contributes to the 4-th order beyond-NIBA intra-well kernel $\Sigma_{\mu\nu}$. The dashed line denotes the inter-blip interaction.

$$
\begin{aligned}
\Sigma^{(6)}_{\mu\nu}(\xi) = \Bigg\{ & \overset{(a)}{+} \sum_{\sigma\gamma\,\in\{\mu\}} \sum_{\substack{(\mu_1\nu_1)=\{\nu\sigma/\sigma\nu\} \\ (\mu_5\nu_5)=\{\gamma\mu/\mu\gamma\}}} \overset{(b)}{-} \sum_{\rho\gamma\,\in\{\mu\}} \sum_{\substack{(\mu_1\nu_1)=\{\nu\rho/\rho\nu\} \\ (\mu_5\nu_5)=\{\gamma\mu/\mu\gamma\}}} \\
& \overset{(c)}{-} \sum_{\sigma\xi\,\in\{\mu\}} \sum_{\substack{(\mu_1\nu_1)=\{\nu\sigma/\sigma\nu\} \\ (\mu_5\nu_5)=\{\gamma\xi/\xi\gamma\}}} \overset{(d)}{+} \sum_{\rho\xi\,\in\{\mu\}} \sum_{\substack{(\mu_1\nu_1)=\{\nu\rho/\rho\nu\} \\ (\mu_5\nu_5)=\{\gamma\xi/\xi\gamma\}}} \Bigg\} \sum_{(\mu_3\nu_3)\,\in\{\mu\}} (-1)^{\varsigma_2+1} \\
& \int_0^{\xi} d\tau_5 \int_0^{\xi-\tau_5} d\tau_1 \int_0^{\xi-\tau_5-\tau_1} d\tau_2 \int_0^{\xi-\tau_5-\tau_1-\tau_2} d\tau_3 \frac{\Delta_1^2}{2^2}\frac{\Delta_3^2}{2^2}\frac{\Delta_5^2}{2^2} \mathrm{e}^{-\mathrm{i}\epsilon_{\mu_1\nu_1}\tau_1} \mathrm{e}^{-\mathrm{i}\epsilon_{\mu_3\nu_3}\tau_3} \mathrm{e}^{-\mathrm{i}\epsilon_{\mu_5\nu_5}\tau_5} \\
& \times \exp\left\{-\xi_1^2 S_{2,1}\right\} \exp\left\{-\xi_3^2 S_{4,3}\right\} \exp\left\{-\xi_5^2 S_{6,5}\right\} \exp\left\{-i\xi_1 R_{2,1}\chi_1\right\} \\
& \times \exp\left\{-i\xi_3 R_{4,3}\chi_3\right\} \exp\left\{-i\xi_5 R_{6,5}\chi_5\right\} \left[1 - \xi_3\Lambda_{2,1}\xi_1 - \xi_5\Lambda_{3,1}\xi_1 - \xi_5\Lambda_{3,2}\xi_3\right. \\
& \left. - i\xi_3 X_{2,1}\chi_1 - i\xi_5 X_{3,1}\chi_1 - i\xi_3 X_{2,2}\chi_2 - i\xi_5\left(X_{3,2}\chi_2 + X_{3,3}\chi_3 + X_{3,4}\chi_4\right)\right] \\
& - \text{reducible graphs}
\end{aligned}
\tag{E.25}
$$

$$
\begin{aligned}
= \Bigg\{ & \overset{(a)}{+} \sum_{\sigma\gamma\,\in\{\mu\}} \sum_{\substack{(\mu_1\nu_1)=\{\nu\sigma/\sigma\nu\} \\ (\mu_5\nu_5)=\{\gamma\mu/\mu\gamma\}}} \overset{(b)}{-} \sum_{\rho\gamma\,\in\{\mu\}} \sum_{\substack{(\mu_1\nu_1)=\{\nu\rho/\rho\nu\} \\ (\mu_5\nu_5)=\{\gamma\mu/\mu\gamma\}}} \\
& \overset{(c)}{-} \sum_{\sigma\xi\,\in\{\mu\}} \sum_{\substack{(\mu_1\nu_1)=\{\nu\sigma/\sigma\nu\} \\ (\mu_5\nu_5)=\{\gamma\xi/\xi\gamma\}}} \overset{(d)}{+} \sum_{\rho\xi\,\in\{\mu\}} \sum_{\substack{(\mu_1\nu_1)=\{\nu\rho/\rho\nu\} \\ (\mu_5\nu_5)=\{\gamma\xi/\xi\gamma\}}} \Bigg\} \sum_{(\mu_3\nu_3)\,\in\{\mu\}} (-1)^{\varsigma_2+1} \\
& \int_0^{\xi} d\tau_5 \int_0^{\xi-\tau_5} d\tau_1 \int_0^{\xi-\tau_5-\tau_1} d\tau_2 \int_0^{\xi-\tau_5-\tau_1-\tau_2} d\tau_3 \frac{\Delta_1^2}{2^2}\frac{\Delta_3^2}{2^2}\frac{\Delta_5^2}{2^2} \mathrm{e}^{-\mathrm{i}\epsilon_{\mu_1\nu_1}\tau_1} \mathrm{e}^{-\mathrm{i}\epsilon_{\mu_3\nu_3}\tau_3} \mathrm{e}^{-\mathrm{i}\epsilon_{\mu_5\nu_5}\tau_5} \\
& \times \exp\left\{-\xi_1^2 S_{2,1}\right\} \exp\left\{-\xi_3^2 S_{4,3}\right\} \exp\left\{-\xi_5^2 S_{6,5}\right\} \exp\left\{-i\xi_1 R_{2,1}\chi_1\right\} \\
& \times \exp\left\{-i\xi_3 R_{4,3}\chi_3\right\} \exp\left\{-i\xi_5 R_{6,5}\chi_5\right\} \left[-\xi_5\Lambda_{3,1}\xi_1 - i\xi_5 X_{3,1}\chi_1\right] ,
\end{aligned}
\tag{E.26}
$$

where one can notice that only the interactions among the first and the last blips survive, as emphasized by the Fig. E.4.

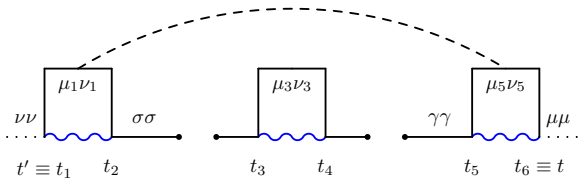

Figure E.4: Generic path which contributes to the 6-th order beyond-NIBA intra-well kernel.

It is useful to isolate the terms in the kernels which are not correlated to the other integrands, and hence define

$$g^{(0)}_{\gamma\sigma}(\xi - \tau_1 - \tau_3) \equiv \delta_{\sigma\gamma} \tag{E.27}$$

for the 4-th order kernel (E.24),

$$g^{(1)}_{\gamma\sigma}(\xi - \tau_1 - \tau_5) \equiv \sum_{(\mu_3\nu_3)\in\{\mu\}} \int_0^{\xi-\tau_5-\tau_1} d\tau_2 \int_0^{\xi-\tau_5-\tau_1-\tau_2} d\tau_3\, (-1)^{\varsigma_2+1} \frac{\Delta_3^2}{2^2}\, \mathrm{e}^{-\mathrm{i}\epsilon_{\mu_3\nu_3}\tau_3}\, \mathrm{e}^{-\xi_3^2 S_{4,3}}\, \mathrm{e}^{-i\xi_3 R_{4,3}\chi_3} \tag{E.28}$$

for the 6-th order (E.26) and analogue for higher orders.

Once we substitute the above expressions into the kernels, we can notice that the only integrals which survive are those over the initial and the final blip time intervals (τ_1 and $\tau_{f-1} = t_f - t_{f-1} = t - t_{f-1}$, respectively). The sum over higher order kernels transforms into a sum over higher orders of g: After summing up all contributions $g^{(j)}(s)$, it is easy to proof that (here $s \equiv \xi - \tau_1 - \tau_{f-1}$)

$$\sum_{j=0}^{\infty} g^{(j)}_{\gamma\sigma}(s) = p_{\gamma\sigma}(s)\,, \tag{E.29}$$

which we indicate with p for simplicity.

Thus, the kernel finally reads

$$\Sigma_{\mu\nu}(\xi) = \sum_{n=1}^{\infty} \Sigma^{(2n)}_{\mu\nu}(\xi) \tag{E.30}$$

which amounts to be

$$
\begin{aligned}
&\overset{(a)}{+} \sum_{\sigma\gamma\,\in\{\mu\}} \sum_{\substack{(\mu_i\nu_i)=\{\nu\sigma/\sigma\nu\}\\(\mu_f\nu_f)=\{\gamma\mu/\mu\gamma\}}} \int_0^{\xi} d\tau_{f-1} \int_0^{\xi-\tau_{f-1}} d\tau_1 \frac{\Delta_1^2}{2^2}\frac{\Delta_{f-1}^2}{2^2} \mathrm{e}^{-\mathrm{i}\epsilon_{\mu_1\nu_1}\tau_1}\ \mathrm{e}^{-\mathrm{i}\epsilon_{\mu_{f-1}\nu_{f-1}}\tau_{f-1}}\ p_{\gamma\sigma}(s) \\
&\times \mathrm{e}^{-\xi_1^2 S_{2,1}}\ \mathrm{e}^{-\xi_{f-1}^2 S_{f,f-1}}\ \mathrm{e}^{-i\xi_1 R_{2,1}\chi_1}\ \mathrm{e}^{-i\xi_{f-1}R_{f,f-1}\chi_{f-1}}\ [-\xi_{f-1}\Lambda_{f-1,1}\xi_1 - i\xi_{f-1}X_{f-1,1}\chi_1] \\
&\overset{(b)}{-} \sum_{\rho\gamma\,\in\{\mu\}} \sum_{\substack{(\mu_i\nu_i)=\{\nu\rho/\rho\nu\}\\(\mu_f\nu_f)=\{\gamma\mu/\mu\gamma\}}} \int_0^{\xi} d\tau_{f-1} \int_0^{\xi-\tau_{f-1}} d\tau_1 \frac{\Delta_1^2}{2^2}\frac{\Delta_{f-1}^2}{2^2} \mathrm{e}^{-\mathrm{i}\epsilon_{\mu_1\nu_1}\tau_1}\ \mathrm{e}^{-\mathrm{i}\epsilon_{\mu_{f-1}\nu_{f-1}}\tau_{f-1}}\ p_{\gamma\nu}(s) \\
&\times \mathrm{e}^{-\xi_1^2 S_{2,1}}\ \mathrm{e}^{-\xi_{f-1}^2 S_{f,f-1}}\ \mathrm{e}^{-i\xi_1 R_{2,1}\chi_1}\ \mathrm{e}^{-i\xi_{f-1}R_{f,f-1}\chi_{f-1}}\ [-\xi_{f-1}\Lambda_{f-1,1}\xi_1 - i\xi_{f-1}X_{f-1,1}\chi_1] \\
&\overset{(c)}{-} \sum_{\sigma\xi\,\in\{\mu\}} \sum_{\substack{(\mu_i\nu_i)=\{\nu\sigma/\sigma\nu\}\\(\mu_f\nu_f)=\{\gamma\xi/\xi\gamma\}}} \int_0^{\xi} d\tau_{f-1} \int_0^{\xi-\tau_{f-1}} d\tau_1 \frac{\Delta_1^2}{2^2}\frac{\Delta_{f-1}^2}{2^2} \mathrm{e}^{-\mathrm{i}\epsilon_{\mu_1\nu_1}\tau_1}\ \mathrm{e}^{-\mathrm{i}\epsilon_{\mu_{f-1}\nu_{f-1}}\tau_{f-1}}\ p_{\mu\sigma}(s) \\
&\times \mathrm{e}^{-\xi_1^2 S_{2,1}}\ \mathrm{e}^{-\xi_{f-1}^2 S_{f,f-1}}\ \mathrm{e}^{-i\xi_1 R_{2,1}\chi_1}\ \mathrm{e}^{-i\xi_{f-1}R_{f,f-1}\chi_{f-1}}\ [-\xi_{f-1}\Lambda_{f-1,1}\xi_1 - i\xi_{f-1}X_{f-1,1}\chi_1] \\
&\overset{(d)}{+} \sum_{\rho\xi\,\in\{\mu\}} \sum_{\substack{(\mu_i\nu_i)=\{\nu\rho/\rho\nu\}\\(\mu_f\nu_f)=\{\gamma\xi/\xi\gamma\}}} \int_0^{\xi} d\tau_{f-1} \int_0^{\xi-\tau_{f-1}} d\tau_1 \frac{\Delta_1^2}{2^2}\frac{\Delta_{f-1}^2}{2^2} \mathrm{e}^{-\mathrm{i}\epsilon_{\mu_1\nu_1}\tau_1}\ \mathrm{e}^{-\mathrm{i}\epsilon_{\mu_{f-1}\nu_{f-1}}\tau_{f-1}}\ p_{\mu\nu}(s) \\
&\times \mathrm{e}^{-\xi_1^2 S_{2,1}}\ \mathrm{e}^{-\xi_{f-1}^2 S_{f,f-1}}\ \mathrm{e}^{-i\xi_1 R_{2,1}\chi_1}\ \mathrm{e}^{-i\xi_{f-1}R_{f,f-1}\chi_{f-1}}\ [-\xi_{f-1}\Lambda_{f-1,1}\xi_1 - i\xi_{f-1}X_{f-1,1}\chi_1]\ ,
\end{aligned}
\tag{E.31}
$$

where with ξ_{f-1} and χ_{f-1} we mean the blip and the sojourn before the last ones.

After introducing the notations used in Eqs. (5.25a) and (5.25b) with the sum-rules (5.26), the kernel (E.31) assumes the compact form

$$
\Sigma_{\mu\nu}(\xi) = + \int_0^{\xi} d\tau_{f-1} \int_0^{\xi-\tau_{f-1}} d\tau_1 \Big[K(\tau_{f-1})\, p(s) \left(K(\tau_1)\, \Lambda_{f-1,1} + A(\tau_1)\, X_{f-1,1} \right) \Big]_{\mu\nu}^{\in\{\mu\}}\ ,
\tag{E.32}
$$

where the superscript nearby the bracket means that every jump must be performed inside the same well which q_μ belongs to.

E.2 Kernels in the Laplace space

Everything takes a very compact form in the Laplace space, where it holds

$$
\int_0^{\infty} d\xi\ \mathrm{e}^{-\lambda\xi} \int_0^{\xi} d\tau_{f-1} \int_0^{\xi-\tau_{f-1}} d\tau_1 = \int_0^{\infty} d\tau_1\ \mathrm{e}^{-\lambda\tau_1} \int_0^{\infty} ds\ \mathrm{e}^{-\lambda s} \int_0^{\infty} d\tau_{f-1}\ \mathrm{e}^{-\lambda\tau_{f-1}}\ .
\tag{E.33}
$$

Since $\Sigma_{\mu\nu}$ depends linearly on $\Lambda_{f-1,1}$ and $X_{f-1,1}$, it is convenient to remember Eqs. (3.15a) and (3.15b) and to explicitly write the bath correlation functions as integrals over frequency, i.e.

$$S(\tau) = \frac{1}{\pi\hbar}\int_0^\infty d\omega \frac{J(\omega)}{\omega^2}\coth\left(\frac{\hbar\omega\beta}{2}\right)(1-\cos\omega\tau) \tag{E.34a}$$

$$= \frac{1}{2\pi\hbar}\int_{-\infty}^\infty d\omega \frac{J(\omega)}{\omega^2}\coth\left(\frac{\hbar\omega\beta}{2}\right)\left(1-\mathrm{e}^{i\omega\tau}\right), \tag{E.34b}$$

$$R(\tau) = \frac{1}{\pi\hbar}\int_0^\infty d\omega \frac{J(\omega)}{\omega^2}\sin\omega\tau = -i\frac{1}{2\pi\hbar}\int_{-\infty}^\infty d\omega \frac{J(\omega)}{\omega^2}\mathrm{e}^{i\omega\tau}, \tag{E.34c}$$

where we used the fact that the bath spectral density $J(\omega)$ is odd in ω.

In particular, Λ and X become

$$\begin{aligned}\Lambda_{f-1,1} &\equiv -S(s+\tau_{f-1}) + S(\tau_1+s+\tau_{f-1}) - S(\tau_1+s) + S(s)\\ &= -\frac{1}{2\pi\hbar}\int_{-\infty}^\infty d\omega \frac{J(\omega)}{\omega^2}\coth\left(\frac{\hbar\omega\beta}{2}\right)\mathrm{e}^{i\omega s}\left(1-\mathrm{e}^{i\omega\tau_1}\right)\left(1-\mathrm{e}^{i\omega\tau_{f-1}}\right), \end{aligned}\tag{E.35}$$

$$\begin{aligned}X_{f-1,1} &\equiv +R(\tau_1+s+\tau_{f-1}) - R(\tau_1+s)\\ &= i\frac{1}{2\pi\hbar}\int_{-\infty}^\infty d\omega \frac{J(\omega)}{\omega^2}\coth\left(\frac{\hbar\omega\beta}{2}\right)\mathrm{e}^{i\omega s}\,\mathrm{e}^{i\omega\tau_1}\left(1-\mathrm{e}^{i\omega\tau_{f-1}}\right), \end{aligned}\tag{E.36}$$

and the Eq. (5.24) reads finally

$$\hat{\Sigma}_{\mu\nu}(\lambda) = \frac{1}{2\pi\hbar}\int_{-\infty}^\infty d\omega \frac{J(\omega)}{\omega^2}\left\{\hat{\ }(\lambda)\,\hat{p}(\lambda-i\omega)\left[-\coth\left(\frac{\hbar\omega\beta}{2}\right)\hat{\ }(\lambda) + i\,\hat{A}(\lambda-i\omega)\right]\right\}_{\mu\nu}^{\in\{\mu\}}, \tag{E.37}$$

where

$$_{\mu\nu}(\tau) \equiv K_{\mu\nu}(\tau)\left(1-\mathrm{e}^{i\omega\tau}\right). \tag{E.38}$$

Clearly, also $_{\mu\nu}(\tau)$ follows the sum-rule (5.26a).

Analogously, in the case of a $M=4$ level system, in the limit where the tunneling kernel $T_{\mu\nu}$ approaches zero, we can proceed as we did so far, specializing our interest to the left well. The kernel Σ_{21} in the case of two uncorrelated two-level system reads in the Laplace space (as it follows from Eq. (5.29)):

$$\hat{\Sigma}_{21}(\lambda) = -\frac{1}{2\pi\hbar}\int_{-\infty}^\infty d\omega \frac{J(\omega)}{\omega^2}\left[\hat{\ }_{21}(\lambda) + \hat{\ }_{12}(\lambda)\right] \tag{E.39}$$

$$\times\,\hat{p}_{\mathrm{N}}(\lambda-i\omega)\left[-\coth\left(\frac{\hbar\omega\beta}{2}\right)\hat{\ }_{21}(\lambda) + i\,\hat{A}_{21}(\lambda-i\omega)\right]. \tag{E.40}$$

Once we neglect the tunneling between the two two-level systems, the only second-order kernel which contribute to the GME is $W^{(2)}$.

Bibliography

[1] A. Leggett, Contemp. Phys. **25**, 583 (1984); A. Leggett and A. Garg, Phys. Rev. Lett. **54**, 857 (1985).

[2] A. Caldeira and A. Leggett, Ann. Phys. (N. Y.) **149**, 374 (1983).

[3] A. O. Caldeira and A. J. Leggett, Phys. Rev. Lett. **46**, 211 (1981); A. J. Leggett, S. Chakravarty, A. T. Dorsey, M. Fisher, A. Garg, and W. Zwerger, Rev. Mod. Phys. **59**, 1 (1987); **67**, 725 (E) (1995).

[4] S. Han, J. Lapointe and J. E. Lukens, Phys. Rev. Lett. **66**, 810 (1991); Phys. Rev. B **46**, 6338 (1992).

[5] I. Chiorescu, Y. Nakamura, C. Harmans and J.E. Mooij, Science **299**, 1869 (2003).

[6] Y. Nakamura, Yu. A. Pashin and J.S. Tsai, Nature **398**, 786 (1999).

[7] D. Vion *et al.*, Science **296**, 886 (2002).

[8] Yu. Makhlin, G. Schön, and A. Shnirman, Rev. Mod. Phys. **73**, 357 (2001).

[9] P. Ullersma, Physica (Utrecht) **32**, 27, 56, 74, 90 (1966).

[10] R. Zwanzig, J. Stat. Phys. **9**, 215 (1973).

[11] R. P. Feynman and F. L. Vernon, Jr., Ann. Phys. (N.Y.) **24**, 118 (1963).

[12] U. Weiss, *Quantum Dissipative Systems* (World Scientific, Singapore, 1993; 2nd edition 1999).

[13] A.J. Leggett *et al.*, Rev. Mod. Phys. **59**, 1 (1987); **67**, 725 (E) (1995).

[14] M. Grifoni, E. Paladino and U. Weiss, Eur. Phys. J. B **10**, 719 (1999).

[15] R. Görlich, M. Sassetti and U. Weiss, Europhys. Lett. **10** (6), 507 (1989).

[16] P.N. Argyres and P.L. Kelley, Phys. Rev. **134**, A98 (1964).

[17] N. Makri, *Real time path integrals with quasi-adiabatic propagators: Quantum Dynamics of a system coupled to a harmonic bath*, in *Time-Dependent Quantum Molecular Dynamics*, Proceedings of a NATO Advanced Research Workshop 1992 in Snowbird, Utah, NATO ASI Series B: Physics, Vol. 299, edited by J. Broeckhove and L. Lathouwers (Plenum Press, New York, 1992); D. E. Makarov and N. Makri, Chem. Phys. Lett. **221**, 482 (1994); N. Makri, J. Math. Phys. **36** 2430 (1995); N. Makri and D. E. Makarov, J. Chem. Phys. **102**, 4600 (1995); **102**, 4611 (1995); D. E. Makarov and N. Makri, Phys. Rev. B **52**, R2257 (1995); Phys. Rev. E **52**, 5863 (1995).

[18] C. van der Wal *et al.*, Science **290**, 773 (2000).

[19] I. Chiorescu *et al.*, Nature **431**, 159 (2004).

[20] L. Tian, S. Lloyd, T.P. Orlando, Phys. Rev. B **65**, 144516 (2002).

[21] C.H. van der Wal, F.K. Wilhelm, C.J.P.M. Harmans and J.E. Mooij, Eur. Phys. J. B **31**, 111 (2003).

[22] J. R. Friedman, M. P. Sarachik, J. Tejada, and R. Ziolo, Phys. Rev. Lett. **76**, 3830 (1996); J. M. Hernández, X. X. Zhang, F. Luis, J. Bartolomé, J. Tejada, and R. Ziolo, Europhys. Lett. **35**, 301 (1996); L. Thomas, F. Lionti, R. Ballou, D. Gatteschi, R. Sessoli, and B. Barbara, Nature **383**, 145 (1996); E. M. Chudnovsky, Science **274**, 938 (1996); J. M. Hernández, X. X. Zhang, F. Luis, J. Tejada, J. R. Friedman, M. P. Sarachik, and R. Ziolo, Phys. Rev. B **55**, 5858 (1997); J. A. A. J. Perenboom, J. S. Brooks, S. Hill, T. Hathaway, and N. S. Dalal, Phys. Rev. Lett. **58**, 330 (1998); G. Bellessa, N. Vernier, B. Barbara, and D. Gatteschi, Phys. Rev. Lett. **83**, 416 (1999); W. Wernsdorfer, R. Sessoli, and D. Gatteschi, Europhys. Lett. **42**, 254 (1999).

[23] C. Sangregorio, T. Ohm, C. Paulsen, R. Sessoli, and D. Gatteschi, Phys. Rev. Lett. **78**, 4645 (1997); J. Tejada, X. X. Zhang, E. del Barco, J. M. Hernández, and E. M. Chudnovsky, Phys. Rev. Lett. **79**, 1754 (1997); W. Wernsdorfer and R. Sessoli, Science **284**, 133 (1999); W. Wernsdorfer, T. Ohm, C. Sangregorio, R. Sessoli, D. Mailly, and C. Paulsen, Phys. Rev. Lett. **82**, 3903 (1999); W. Wernsdorfer, I. Chiorescu, R. Sessoli, D. Gatteschi, and D. Mailly, Physica B: Cond. Mat. **284 – 288**, 1231 (2000).

[24] W. Wernsdorfer, R. Sessoli, A. Caneschi, D. Gatteschi, and A. Cornia, Europhys. Lett. **50** (4), 552 (2000).

[25] M. Thorwart and P. Jung, Phys. Rev. Lett. **78**, 2503 (1997).

[26] R. I. Cukier, C. Denk, and M. Morillo, K. Chun and N. O. Birge, Phys. Rev. B **51**, 13767 (1995); M. Morillo and R. I. Cukier, Phys. Rev. B **54**, 13962 (1996); M. Morillo, C. Denk, and R. I. Cukier, Chem. Phys. **212**, 157 (1996); R. I. Cukier, C. Denk, and M. Morillo, Chem. Phys. **217**, 179 (1997).

[27] H. Dekker, Phys. Rev. A **44**, 2314 (1991); Physica A **175**, 485 (1991); **176**, 220 (1991); **178**, 289 (1991); **179**, 81 (1991); **210**, 507 (E) (1994).

[28] M. Thorwart, M. Grifoni, and P. Hänggi, Phys. Rev. Lett. **85**, 860 (2000).

[29] M. Thorwart, M. Grifoni, and P. Hänggi, Annals of Physics **293**, 15-66 (2001).

[30] K. Chun and N. O. Birge, Phys. Rev. B **48**, R11500 (1993).

[31] R. I. Cukier, M. Morillo, K. Chun, and N. O. Birge, Phys. Rev. B **51**, 13767 (1995).

[32] B. H. Meier, F. Graf, and R. R. Ernst, J. Chem. Phys. **76**, 767 (1982); S. Nagaoka, T. Terao, F. Imashiro, A. Saika, and N. Hirota, J. Chem. Phys. **79**, 4694 (1983); A. Stoeckli, A. Furrer, Ch. Schoenenberger, B. H. Meier, R. R. Ernst, and I. Anderson, Physica B **136**, 161 (1986); A. Stöckli, B. H. Meier, R. Kreis, R. Meyer, and R. R. Ernst, J. Chem. Phys. **93**, 1502 (1990); A. J. Horsewill, P. J. McDonald, and D. Vijayaraghavan, J. Chem. Phys. **100**, 1889 (1994); A. J. Horsewill and A. Ikram, Physica B **226**, 202 (1996).

[33] A. Barenco, A. Berthiaume, D. Deutsch, A. Ekert, R. Jozsa, and C. Macchiavello, SIAM J. Comp. **26**, 1541 (1997).

[34] P. Zanardi and M. Rasetti, Mod. Phys. Lett. B **11**, 1085 (1997).

[35] G. M. Palma, K.-A. Suominen and A. K. Ekert, Proc. R. Soc. London Sect. A 452, 567 (1996); L.-M Duan and G.-C. Guo, Phys. Rev. Lett. **79**, 1953 (1997); L.-M Duan and G.-C. Guo, Phys. Rev. A **57**, 737 (1998); P. Zanardi, Phys. Rev. A **56**, 4445 (1997).

[36] P. Zanardi and M. Rasetti, Phys. Rev. Lett. **79**, 3306 (1997).

[37] D. A. Lidar, I. L. Chuang, K. B. Whaley, Phys. Rev. Lett. **81**, 2594 (1998).

[38] M. J. Storcz, J. Vala, K. R. Brown, J. Kempe, F. K. Wilhelm and K. B. Whaley, Phys. Rev. B **72**, 064511 (2005).

[39] D.P. DiVincenzo and D. Loss, Phys. Rev. B **71**, 035318 (2005).

[40] S. Braunstein, and H.-K. Lo (eds.) *Experimental Proposals for Quantum Computation* (Wiley, Berlin, volume 48, 2000), Special Focus Issue of Fortschritte der Physik.

[41] G. Burkard, in *Handbook of Theoretical and Computational Nanotechnology*, ed. by M. Rieth and W. Schommers (American Scientific Publishers, New York, 2005), cond-mat/0409626.

[42] W. J. Elion *et al.*, Nature **371**, 594 (1994).

[43] J. M. Martinis et al. , PRB 35, 4682 (1987)

[44] J. Clarke, A. N. Cleland, M. H. Devoret, D. Estève, and J. M. Martinis, Science **239**, 992 (1988).

[45] S. Han, J. Lapointe, and J. E. Lukens, Phys. Rev. Lett. **66**, 810 (1991).

[46] R. Rouse, S. Han, and J. E. Lukens, Phys. Rev. Lett. **75**, 1614 (1995).

[47] S. Han, R. Rouse, and J. E. Lukens, Phys. Rev. Lett. **76**, 3404 (1996).

[48] P. Silvestrini, V. G. Palmieri, B. Ruggiero, and M. Russo, Phys. Rev. Lett. **79**, 3046 (1997).

[49] S. Han, R. Rouse, and J. E. Lukens, Phys. Rev. Lett. **84**, 1300 (2000).

[50] J. R. Friedmann, V. Patel, W. Chen, S. K. Tolpygo, and J. E. Lukens, Nature **406**, 43 (2000); G. Blatter; *ibid.* **406**, 25 (2000).

[51] J. E. Mooij, T. P. Orlando, L. Levitov, L. Tian, C. H. van der Waal and S. Lloyd, Science **285**, 1036 (1999); T. P. Orlando, J. E. Mooij, L. Tian, C. H. van der Waal, L. Levitov, S. Lloyd and J. J. Mazo, Phys. Rev. B **60**, 15398 (1999).

[52] C. H. van der Wal, A. C. ter Haar, F. K. Wilhelm, R. N. Schouten, C. J. P. M. Harmans, T. P. Orlando, S. Lloyd and J. E. Mooij, Science **290**, 773 (2000).

[53] T. Sleator and H. Weinfurter, Phys. Rev. Lett. **74**, 4087 (1995); D. P. DiVincenzo, Phys. Rev. A **51**, 1015 (1995).

[54] F. Schmidt-Kaler, H. Häffner, M. Riebe, S. Gulde, G. P. T. Lancaster, T. Deuschle, C. Becher, C. F. Roos, J. Eschner and R. Blatt, Nature **422**, 408 (2003).

[55] S. Gasparoni, J.W. Pan, P. Walther, T. Rudolph and A. Zeilinger, Phys.Rev.Lett. **93** 020504 (2004).

[56] J. H. Plantenberg, P. C. de Groot, C. J. P. M. Harmans and J. E. Mooij, Nature **447**, 836 (2007).

[57] *Quantum Tunneling of Magnetization*, Proceedings of the NATO Advanced Research Workshop 1994 in Grenoble, France, NATO ASI Series E: Applied Sciences, Vol. 301, edited by L. Gunther and B. Barbara (Kluwer, Dordrecht, 1995).

[58] J. L. van Hemmen and A. Sütő, Europhys. Lett. **1**, 481 (1986); Physica B **141**, 37 (1986).

[59] P. Hänggi, P. Talkner, and M. Borkovec, Rev. Mod. Phys. **62**, 251 (1990).

[60] Th. Dittrich, P. Hänggi, G.-L. Ingold, B. Kramer, G. Schön, and W. Zwerger, *Quantum Transport and Dissipation* (Wiley-VCH, Weinheim, 1998).

[61] D. O. Harris, G. G. Engerholm, and W. D. Gwinn, J. Chem. Phys. **43**, 1515 (1965).

[62] M. Grifoni and P. Hänggi, Phys. Rep. **304**, 230 (1998).

[63] M. Grifoni and P. Hänggi, Phys. Rep. **304**, 229 (1998).

[64] A. Garg, J.N. Onuchic and V. Ambegaokar, J. Chem. Phys. **83**, 4491(1985).

[65] R.P. Bell, *The Tunnel Effect in Chemistry* (Chapman and Hall, London, 1980).

[66] B. Golding, N. M. Zimmerman, and S. N. Coppersmith, Phys. Rev. Lett. **68**, 998 (1992).

[67] C. Tannoudji, C. Dupont-Roc and J. Grynberg, *Atom Photon Interaction: Basic Processes and Applications* (Wiley, New York, 1992).

[68] Blips/sojourns are time intervals spent in off-diagonal and diagonal elements of the reduced density matrix, respectively. In the NIBA, the correlations among them are fully neglected.

[69] C. Aslangul, N. Pottier and D. Saint-James, J. Phys. (Paris) **47**, 757 (1986).

[70] Yu. Dakhnovskii, Phys. Rev. B **49**, 4649 (1994).

[71] I.A. Goychuk, E.G. Petrov and V. May, Phys. Rev. E **52**, 2392 (1995).

[72] A. Würger, Phys. Rev. Lett **78**, 1759 (1997); Phys. Rev. B **57**, 347 (1998).

[73] M. Winterstetter and U. Weiss, Chem. Phys. **217**, 155 (1997).

[74] R. Görlich and U. Weiss, Phys. Rev. B **38**, 5254 (1988).

[75] L. Hartmann, I.A. Goychuk, M. Grifoni and P. Hänggi, Phys. Rev. E **61**, R4690 (2000).

[76] R. Egger and U. Weiss, Z. Phys. B **89**, 97 (1992).

[77] J.T. Stockburger, Phys. Rev. E **59**, R4709 (1999).

[78] M.C. Goorden, M. Thorwart and M. Grifoni, Phys. Rev. Lett. **93**, 267005 (2004).

[79] S. Kehrein and A. Mielke, Ann. Phys. (Leipzig) **6**, 90 (1997)

[80] R. D. Coalson, D. G. Evans and A. Nitzan, J. Chem. Phys. **101**, 436 (1994); A. Lucke, C. H. Mak, R. Egger, J. Ankerhold, J. Stockburger and H. Grabert, J. Chem. Phys. **107**, 8397 (1997).

[81] I.S. Gradshteyn and I.M. Ryzhik, *Tables of Integrals, Series and Products* (Academic Press, London, 1965).

[82] S. Vorojtsov, E. R. Mucciolo and H. U. Baranger, Phys. Rev. B **71**, 205322 (2005); M. Thorwart, J. Eckel and E. R. Mucciolo, Phys. Rev. B **72**, 235320 (2005).

[83] J.T. Stockburger, M. Grifoni, M. Sassetti and U. Weiss, Z. Phys. B **94**, 447 (1994).

[84] M. Grifoni and P. Hänggi, Phys. Rep. **304**, 229 (1998).

[85] A. Wallraff *et al.*, Nature **431**, 162 (2004).

[86] M. Thorwart, L. Hartmann, I. Goychuk, and P. Hänggi, J. Mod. Opt. **47**, 2905 (2000).

[87] A. Yu. Smirnov, Phys. Rev. B **67**, 155104 (2003).

[88] M. Thorwart, E. Paladino and M. Grifoni, Chem. Phys. **296**, 333 (2004).

[89] F. K. Wilhelm, S. Kleff and J. von Delft, Chem. Phys. **296**, 345 (2004).

[90] M. C. Goorden and F. K. Wilhelm, Phys. Rev. B **68**, 012508 (2003).

[91] M.C. Goorden, M. Thorwart and M. Grifoni, Phys. Rev. Lett. **93**, 267005 (2004); Eur. Phys. J. B **45**, 405 (2005).